TECHNISCHE UNIVERSITÄT
ILMENAU

14th German Ferrofluid Workshop

March 17th - 19th, 2014
Ilmenau

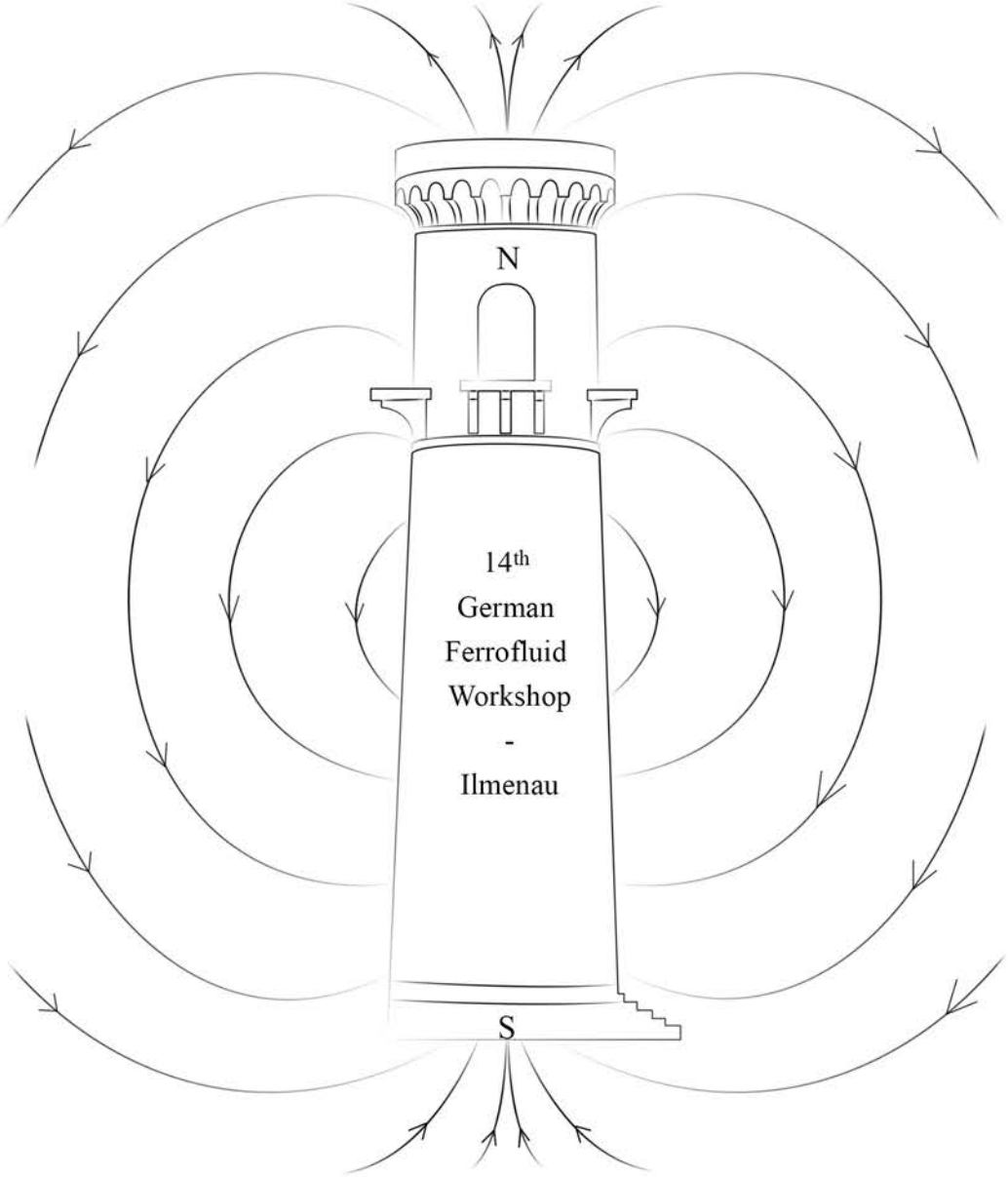

Book of Abstracts

Program of the

14th German Ferrofluid Workshop

Ilmenau, 17.03.-19.03.2014

Monday, March 17th, 2014

Opening

13:00 – 13:30	P. Scharff (Rector of the TU Ilmenau), K. Zimmermann, S. Odenbach		

Lecture Session 1 (Chair: J.H. Clement)

13:35 – 14:20	***I. Hilger***	***Keynote Presentation***	
14:20 – 14:45	J. Schotter, S. Schrittwieser, F. Ludwig, J. Dieckhoff, K. Soulantika, S.L. Mozo, B. Pelaz, W. Parak	*Homogeneous breast cancer biomarker detection by optically measuring the rotational dynamics of magnetic nanorods*	S.1
14:45 – 15:10	N. Pömpner, M. Stapf, I. Hilger	*Cytotoxicity and uptake levels of methotrexate coupled magnetic nanoparticles in different breast cancer cell lines for multimodal treatment*	S.3
15:10 – 15:35	P. Tripal, J. Zaloga, R.P. Friedrich, E. Schreiber, B. Weigel, R. Tietze, J. Nowak, S. Odenbach, S. Lyer, C. Alexiou	*Magnetically controlled cell seeding for vascular tissue engineering using endothelial cells loaded with iron oxide nanoparticles*	S.5
15:35 – 16:15	**Coffee Break**		

Lecture Session 2 (Chair: K. Zimmermann)

16:15 – 16:40	N. Buske	*Tailored Magnetic Dispersions for Spectacular Applications*	S.7
16:40 – 17:05	P. Cremer, A.M. Menzel, H. Löwen	*Finite-element simulation of ferrogels: Magneto-mechanical coupling and stress-strain behaviour*	S.9
17:05 – 17:30	P.A. Sánchez, J.J. Cerdá, T. Sintes, S.S. Kantorovich	*Supramolecular magnetic filaments: fundamental physics and potential applications*	S.11
17:30 – 18:15	***O. Mollenhauer***	***Keynote Presentation***	
18:30 – 19:30	**Poster Session 1**		

Tuesday, March 18th, 2014

Lecture Session 3 (Chair: S. Dutz)

09:00 – 09:45	***T.M. Buzug***	***Keynote Presentation***	
09:45 – 10:10	F. Wiekhorst, N. Löwa, S. Metzkow, W. Poller, A. Ludwig, L. Trahms	*Magnetic Particle Spectroscopy detecting changes during cellular uptake of magnetic nanoparticles*	S.13
10:10 – 10:35	S. Disch, P. Bender, M. Kundt, D. Honecker, A.M. Schmidt	*Field-induced reorientation of shape anisotropic magnetic nanoparticles*	S.15
10:35 – 11:00	C. Kuhlmann, T. Wawrzik, M. Schilling, F. Ludwig	*Concept for a 10MHz ac susceptometer with adjustable sample temperature*	S.17

11:00 – 11:30 **Coffee Break – Poster Session 2**

Lecture Session 4 (Chair: A.M. Schmidt)

11:30 – 11:55	I. Appel, R. Müller, S. Behrens	*Synthesis and properties of catalytically active and magnetic Co@SiO_2 and Co@ZSM-5 nanoparticles*	S.19
11:55 – 12:20	C. Stötzel, H.D. Kurland, J. Grabow, S. Dutz, E. Müller, M. Sierka, F.A. Müller	*Control of the Crystal Phase Composition of Fe_xO_y Nanopowders prepared by CO_2 Laser Vaporization*	S.21
12:20 – 12:45	P. Quiroz, B. Halbedel	*Kinetic study of crystallization titanium substituted barium hexaferrite in a glassy matrix of the system BaO-Fe_2O_3-TiO_2-B_2O_3*	S.23

12:45 – 14:00 **Lunch**

Lecture Session 5 (Chair: D. Baumgarten)

14:00 – 14:45	***D. Fischer***	***Keynote Presentation***	
14:45 – 15:10	R. Müller, O. Stranik, F. Schlenk, S. Werner, D. Malsch, D. Fischer, W. Fritzsche	*Optical detection of nanoparticle aggregation in a living system under the influence of a magnetic field*	S.24
15:10 – 15:35	J. Zaloga, J. Nowak, C. Janko, R. Tietze, R.P. Friedrich, S. Odenbach, S. Lyer, G. Lee, C. Alexiou	*Developing a fatty acid - protein coated SPION system with enhanced biocompatibility for drug delivery*	S.26

15:45 – 17:15	**Guided Tour in Ilmenau**	
17:30 – 18:30	**General Assembly of the Ferrofluidverein Deutschland e.V.**	
	Poster Session 3	
18:45 –	**"Thuringian Evening"**	

Wednesday, March 19th, 2014

Lecture Session 6 (Chair: R. Richter)

09:00 – 09:30	***J. Schumacher***	***Keynote Presentation***	
09:30 – 09:55	T.I. Volkova, V.A. Turkov, K. Zimmermann, V.A. Naletova	*Ferrofluid Volume between Plates in the Field of an Electromagnetic Coil*	S.28
09:55 – 10:20	A. Attaran, J. Brummund, T. Wallmersperger	*A contribution to the modeling of ferrogels*	S.30
10:20 – 10:45	S. Förster, T. Friedrich, S. Mehdizadeh Taheri, I. Rehberg, S. Rosenfeldt	*How frustrated can 8 dipoles be?*	S.31
10:45 – 11:10	J. Linke, D. Borin, S. Odenbach	*First-order reversal curve (FORC-) analysis of magneto-active materials with mixed magnetic phases*	S.33
11:10 – 11:45	**Coffee Break – Poster Session 4**		

Lecture Session 7 (Chair: S. Odenbach)

11:45 – 12:10	J. Landers, L. Roeder, A. Schmidt, H. Wende	*Measurement of microviscosity in crosslinked polyacrylamide ferrohydrogels by Mössbauer spectroscopy*	S.35
12:10 – 12:35	E. Roeben, S. Teusch, M. Dörfer, M. Effertz, L. Kibkalo, A.M. Schmidt	*Magnetic Particle Nanorheology of Complex Fluids*	S.37
12:35 – 13:00	M. Schümann, S. Odenbach	*The effect of the addition of magnetic micro particles on the mechanical properties of soft polyurethane foams*	S.39
13:00 – 13:15	**Closing (Best Poster Award, best Presentation Award)**		

List of
Further Abstracts
(Posters)

Homogeneous breast cancer biomarker detection by optically measuring the rotational dynamics of magnetic nanorods

J. Schotter[1], S. Schrittwieser[1], F. Ludwig[2], J. Dieckhoff[2], Katerina Soulantika[3], Sergio Lentijo Mozo[3], Beatriz Pelaz[4], Wolfgang Parak[4]

[1] *Molecular Diagnostics, AIT Austrian Institute of Technology, Vienna, Austria*
[2] *Institute of Electrical Measurement and Fundamental Electrical Engineering, TU Braunschweig, Braunschweig, Germany*
[3] *Université de Toulouse, INSA, UPS, LPCNO, and CNRS, LPCNO, Toulouse, France*
[4] *Philipps-Universität Marburg, Germany*

We recently introduced a novel homogeneous biosensor concept that is based on optically observing the rotational dynamics of noble metal coated magnetic nanorods [1, 2]. These nanorods are functionalized by antibodies that specifically bind biomarker molecules present in the sample solution. Due to the small size of the nanorods, such binding events significantly alter their hydrodynamic volumes. Consequently, when the orientation of the nanorods in the solution is continuously altered by applying a rotating magnetic field (RMF), nanorods with bound biomarkers experience a higher hydrodynamic drag and follow the applied rotating magnetic field at a larger phase lag angle. This angle α is measured optically by picking up the nanorod-orientation-dependent transmission of a polarized laser beam shining through the sample dispersion (Fig. 1). Here, we report on the detection of the soluble domain of the breast cancer biomarker (sHER2) by our method using an advanced diagnostic prototype instrument.

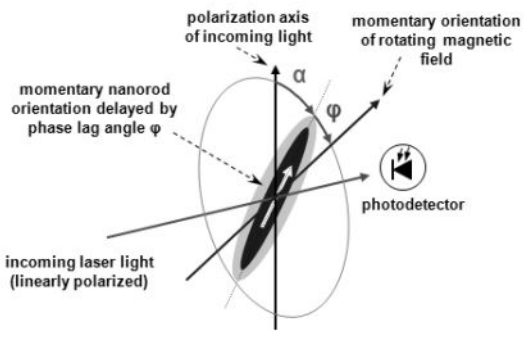

Fig. 1: Concept sketch of nanorod rotation and detection

Nanoprobe synthesis

As base particles, we employ magnetic nanorods synthesized by an organometallic approach which produces single crystalline (hcp) Co-nanorods with a uniform diameter of 6 nm and adjustable length between 40 and 200 nm with narrow size distribution [3]. Next, a noble metal shell is synthesized around the Co-core in order to protect the core from oxidation and to provide amplification of the optical signal. This is accomplished via a thin interlayer and sequential deposition of platinum (Pt) and gold (Au), which provides the best protection of the core against oxidation, resulting in stability periods of aqueous nanorod dispersions of more than ten weeks.
Following synthesis, the nanorods are stabilized with hydrophobic surfactants in organic solvents such as toluene. For transfer into and stabilization in aqueous solutions, we coat the nanorods by an amphiphilic polymer, i.e. a polymer comprising hydrophobic side chains for the linkage to the nanorod surface and a hydrophilic backbone that provides water solubility through charged groups [4]. After water stabilization, the nanorods are functionalized by monoclonal Herceptin® antibodies as recognition agents for HER2 assays by EDC / Sulfo-NHS carboxyl activation.

Diagnostic prototype instrument

The goal for realizing an advanced diagnostic prototype instrument is to improve

on the following properties with regard to the earlier laboratory instrument:

- Compact device that is easily transportable to laboratories at other locations
- Reduction of complexity and costs as compared to the laboratory instrument
- Automated operation (i.e. load sample and press button to measure)
- Improved optical sensitivity (i.e. lower nanoprobe limit of detection, LoD)

Fig. 2: Overview of the realized diagnostic prototype instrument (+ power supply box, not shown)

We have been able to meet those goals by a design comprising a desktop measurement box containing the coil system to generate the rotating magnetic field (RMF) and the optics to measure the dynamic reaction of the nanoprobe dispersions on the RMF (Fig. 2). The entire system is controlled by a laptop computer, and the power supplies and capacitor switches for driving the rotating magnetic field (RMF) are situated in a separate power supply box that can be placed underneath the table. These two boxes and the Laptop computer comprise the entire system, so it can easily be transported to other laboratory locations for preclinical testing. The nanorod LoD of the diagnostic prototype instrument could be improved to about 2 pM.

HER2 assay results

Fig. 3 shows measured phase lag differences in a RMF between Herceptin-functionalized nanorods without added analyte (reference value) and Herceptin-functionalized nanorods with different concentrations of added HER2 along with a logistic fit. The logistic fit indicates a maximum saturation phase lag change of about 11° and a HER2 LoD of about 1 nM. The analyte LoD is substantially better than reported before (20 nM, see FFWS 2013), which is due to the higher RMF magnitude that's applicable by the diagnostic prototype instrument (10 mT vs. 5 mT) as well as its improved nanoprobe LoD. In addition, we also refined the nanorod antibody functionalization procedure by using the smaller blocking molecule ethanolamine (as compared to BSA), which reduces to reference phase lag of functionalized nanorods. These results demonstrate that there is still a lot of room for improvement regarding the analyte LoD for our biosensor concept, and we will continue to enhance its performance.

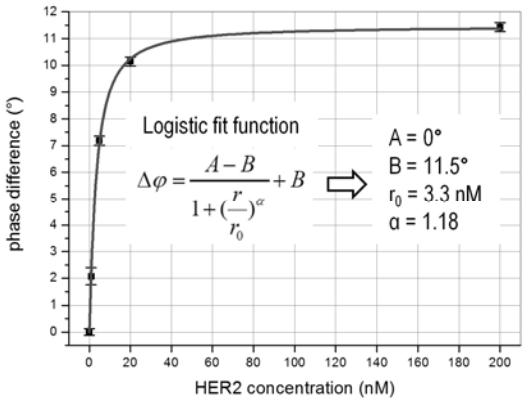

Fig. 3: HER2 assay results using the diagnostic prototype instrument (RMF: 10mT, 1kHz; nanoprobe conc. 48pM)

Acknowledgments

The research leading to these results has received funding from the European Community's 7th Framework Programme under grant agreement n° NMP4-LA-2010-246479.

References

[1] Schrittwieser et al., ACS Nano 6 (2012), 791-801.
[2] Schrittwieser et al., SMALL, (2013) DOI: 10.1002/smll.201300023.
[3] Soulantica et al., Appl. Phys. Lett. 95 (2009), 152504.
[4] Pellegrino et al., Nano Letters 4 (2004), 703-707.

Cytotoxicity and uptake levels of methotrexate coupled magnetic nanoparticles in different breast cancer cell lines for multimodal treatment

N. Pömpner[1], M. Stapf[1], I. Hilger[1]

[1] Jena University Hospital, Institute of Diagnostic and Interventional Radiology, Department of Experimental Radiology

Introduction

Superparamagnetic nanoparticles are a favored tool for anti tumor therapy, particularly in inducing localized magnetic hyperthermia in an alterniering magnetic field and/or a contolled release of chemotherapeutic agents like methotrexate (MTX). Furthermore, MTX functionalized iron oxid nanoparticles can be used for drug and magnetic targeting. MTX is known to be a folic acid analogon. Antifolates like MTX have been recognized to enter tumor cells by three different mechanisms: the reduced folate carrier (RFC), the folate receptor alpha (FRα) and the proton coupled folate transporter (PCFT). It is unclear if the uptake of MTX via these transport mechanism correlates to cytotoxicity. In this work the expression level of FRα and RFC mRNA was analyzed concerning MTX cytotoxicity.

Materials and Methods

Used cell lines
Different breast cancer cell lines, including T47D, BT-474, MDA-MB-231, MCF-7, MX1, AU-565, SK-BR-3 as well as the bladder cancer cell line T24 and the non-tumor cell line HMEC-1 were used.

Coupling of MTX to magnetic material
Amine-groups of the superparamagnetic, polyethylene glycol (PEG) iron oxide nanoparticles were covalently coupled by carbodiimde to the carboxylate groups of Methotrexate (MTX-MNP).

Cytotoxicity of MTX-MNP to breast cancer cells
Various breast cancer cell lines were seeded onto 96-well plates and treated with MTX-MNP in concentrations ranging from 25 to 100 µg MTX-MNP/ml medium. At defined time points, the cells were heated to 44 °C for 1-2 h. Afterwards cell viability was determined by AlamarBlue assay (cellular NADH levels) 48 h and 72 h after MTX exposure and correlated to non-treated controls.

Determination of FRα protein and RCF mRNA level
For protein expression of FRα
RFC mRNA levels whole cell lysates were used and determined by Western blot and qRT-PCR, respectively. For ΔC_P calculation after qRT-PCR, β-2 microglobulin was used as reference gene. The C_P (Crossing Point) describes the PCR cycle where the fluorescence exceeds significantly the background fluorescence and is indirect proportional to the realtive amount of the amplified gene.

Results

Independent from incubation duration and MTX-MNP dosage, a medium to strong decrease of cell viability after hyperthermia was observed in all tested cell lines. T47D, BT-474, MCF-7 and MX1 cells exhibited only a slight decrease of cell viability after 48h and 72h of MTX-MNP treatment (Fig. 1). Cell viability decreased to 46 % of controls cells after MTX-MNP addition to MDA-MB-231 with a recovery thereafter (data not shown). In AU-565 and SK-BR-3, cell viability was reduced with

increasing incubation time from 48 h to 72 h (in AU-565 46% vs. 9% and in SK-BR-3 73% vs. 45 %).

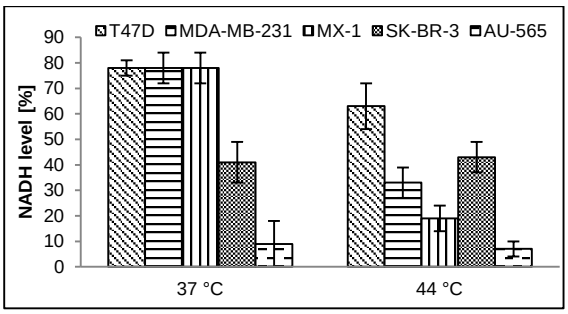

Fig. 1: Cellular viability (relative NADH level) after MTX-MNP exposure. Different breast cancer cell lines were treated with 100 µg/ml of MTX-MNP and subsequently heated to 44 °C for 1 h and normalized to untreated 37 °C control. NADH level was determined 72 h after MTX-MNP addition.

Interestingly, there was a comparatively high and nearly equal mRNA level of RFC transcripts in all tested breast cancer cell lines (4,1-5,2 C_P) except for MDA-MB-231(14,6 C_P). mRNA levels of RFC transcripts in tested breast cancer cell lines were similar to bladder cancer (T24) and non-tumor cell line HMEC-1 (Fig. 2).

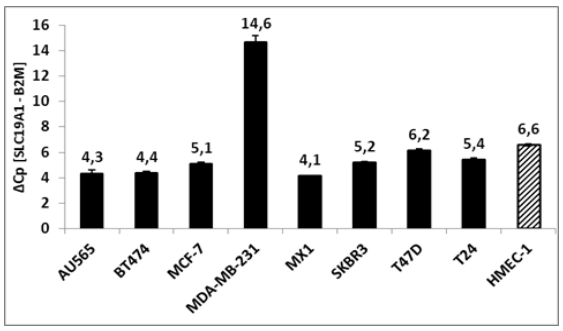

Fig. 2: SLC19A1 expression of different tumor- (filled) and non-tumor (shaded) cell lines. β-2 microglobulin was used as reference gene for ΔC_P calculation.

On the other hand, the FRα protein expression was strongly variable in all tested cell lines and independent from cell viability during the MTX-MNP exposure.

Discussion

As reported in literature, RFC is considered as the major transport route for antifolates like MTX rather than FRα[2]. Furthermore, a significantly higher RFC expression in urothelial carcinomas in comparison to non-urothelial carcinomas was mentioned [1], indicating different expression levels in various cell lines. As our results have shown, there was an almost similar expression of RFC between most tested cell lines including urothelial T24 cells and non-tumor HMEC-1 cells. In contrast MDA-MB-231 cells showed a lower RFC expression (equivalent to larger ΔC_P values), supposing a lower MTX toxicity due to reduced MTX uptake. As observed by AlamarBlue assay cytotoxicity of MTX does not correlate with MTX uptake. Our results indicate that, at least in part, other mechanisms seem to be responsible for MTX cytotoxicity.

Conclusion

A bimodal treatment of hyperthermia and MTX can effectively inactivate certain types cancer cells. In our investigations there was no correlation of the expression level of FRα protein and the RFC mRNA to cytotoxic effects of MTX functionalized iron oxid nanoparticles in all analyzed cell lines. Other mechanism to be discovered are responsible, at least in parts, for MTX related cytotoxicity as free molecule or after functionalization to MNP.

Acknowledgments

This investigation was supported by the German Research Foundation within the composite project PAK-151 under the number HI698/7-4.

References

1. Abdel-Haleem, A.M., et al., *Expression of RFC/SLC19A1 is Associated with Tumor Type in Bladder Cancer Patients.* Plos One, 2011. **6**(7).

Magnetically controlled cell seeding for vascular tissue engineering using endothelial cells loaded with iron oxide nanoparticles

P. Tripal[1], J. Zaloga[1], R. P. Friedrich[1], E. Schreiber[1], B. Weigel[1], R. Tietze[1], J. Nowak[2], S. Odenbach[2], S. Lyer[1], C. Alexiou[1]

[1] Department of Otorhinolaryngology, Head and Neck Surgery, Section for Experimental Oncology and Nanomedicine (SEON), Else Kröner-Fresenius-Stiftung-Professorship, University Hospital Erlangen, Germany.
2 Chair of Magnetofluiddynamics, Measuring and Automation Technology, Technische Universität Dresden, Germany.

Introduction

Progress in tissue engineering is mandatory for the development of modern therapy in the field of regenerative medicine. Nanotechnology offers the potential of circumventing the shortage of available organs and the likelihood of complications caused by chronic immunosuppression as it allows the 3-dimensional growth of autologous tissues by magnetic cell seeding.
We could demonstrate the possibility to colonize a pipe scaffold with primary endothelial cells loaded with in house produced superparamagnetic iron oxid nanoparticles for tissue engineering (SEON-TEPs). Furthermore the experimental results confirm that proliferation and the cytoskeleton of the respective cells were not altered by SEON-TEPs and magnetic seeding. Additionally we could monitor a magnetic seeding of cells already at very low cellular SEON-TEPs concentrations per cell. Finally our results reveal a dramatic reduction of the cellular SEON-TEPs content within seven days upon cultivation, indicating a beneficial dissolution of the particles before a possible transplantation of the tissue.

Results

We could verify that the cellular uptake of SPIONs is depending on the particle coating and the solvent which in turn influence the average size of the SPION agglomerates and the zeta potential in the cell culture media.
To quantify the cellular SEON-TEPs load, we modified a recently published, photometric technique [1] and found a reproducible direct correlation between the absorption at 370 nm and the cellular SEON-TEP amount. We then investigated the cellular uptake of SEON-TEPs and confirmed a direct correlation between SEON-TEPs concentration and incubation time.
Since a prerequisite for magnetic cell seeding and tissue engineering is a low SPION toxicity we monitored the viability of SEON-TEP-loaded cells by measuring cell proliferation and detected a measurable reduction only at very high SEON-TEP concentrations. Additionally there was no observable influence on actin cytoskeleton architecture as shown by immunocytochemistry. We then modified the 3-dimensional cell seeding model [2] with HUVEC cells pre-loaded with SEON-TEPs. As a proof of principle for the production of tubular endothelialized scaffolds we colonized plastic tubes using the Vascucell Endothelizer, which allows magnetically controlled interactions between cells and scaffold matrix. Cells loaded with SEON-TEPs show stable adhesion and colonization of cells to the three dimensional scaffolds and increased cultivation periods caused a more dense coverage of the tubes inner surface and proved the proliferation potential of magnetically seeded cells.
Moreover, cellular SEON-TEPs colocalize with lysosomal markers, suggesting a lysosomal degradation of the nanoparticles, explaining the intracellular decrease of SEON-TEPs upon increased cultivation time.

Conclusion

Magnetic arrangement of autologous, SPION-loaded cells is a valuable tool for the engineering of functional tissues. Our results for three-dimensional colonization of tubes with HUVEC provide encouraging arguments for applying this method on vascular graft fabrication. Even though a tube is a rather simple three-dimensional structure, the data presented here show, that magnetic cell arrangement is very useful new technique. Future advancements, like modulation of the magnetic field and combination with scaffolds or stepwise seeding of different cell layers, could one day enable the engineering of complex structured organs from autologous, differentiated cells.

Acknowledgments

DFG SPP1681 (AL 552/5-1), EFI Projekt FAU Erlangen – Nürnberg.

References

[1] Dadashzadeh, E. R., et al. 2013, Rapid spectrophotometric technique for quantifying iron in cells labeled with superparamagnetic iron oxide nanoparticles: potential translation to the clinic. Contrast Media Mol Imaging 8(1):50-6.

[2] Perea H., et al. 2007, Vascular tissue engineering with magnetic nanoparticles: seeing deeper, J Tissue Eng Regen Med; 1: 318–321.

Tailored Magnetic Dispersions for Spectacular Applications

N. Buske

Magneticfluids, Köpenicker Landstr. 203, 12437 Berlin

Many tailor-made magnetic dispersions were prepared and characterized in our magnetic fluid laboratory, including Magnetic Fluids (MF) and Magnetic Rheological Fluids (MRF). Most of them were used in technical constructions, and nowadays as biocompatible fluids for diagnostics and therapy.

One of the first of our activities was to establish a method of **separating the non-ferrous metals from electronic scrap. The method** is based on the float/sink-separation of in the MF suspended non-magnetic materials in presence of a magnetic field gradient, cf. Fig. 1.

For this application, water based magnetite-MF were developed with saturation polarizations up to 40 mT with the benefit to recover the MF adhered on the material: The particles were magnetically separated by changing the pH, washed and redispersed by changing the pH-value once again. Alternatively, very stable MF were prepared, the low concentrated particles in wash solution could be concentrated by evaporation of the water carrier.

Fig. 1 a suspended golden ring is floating on the surface of a water-based 30mT MF in presence of a Ba-Ferrit permanent magnet.

One of next visions was the construction of an **artificial heart pump** using magnetic fluids of very high saturation polarization and small bulk viscosity. Hydrocarbon based Co-MF up to polarizations of 230 mT, and magnetite petroleum based MF up to 120 mT (close to the theoretical limit) at bulk viscosities < 1 Pa s were used to increase efficiency of the engine model, cf. Fig. 2.

Finally, other constructions without MF were applied.

Fig. 2 Picture of a drive engine model: a couple of electro magnets were filled with magnetic fluids to increase the permeability between the pole shoes.

MF and MRF are used in **machinery** (as **MF-seals, MF-lubricants, MF-dampers**). Our MF and MRF are composed in the outstanding carrier **P**er**F**luorinated **P**oly-**E**ther (PFPE), chemically inert with a very low vapor pressure, not soluble in other fluids, stable against aggressive acids and bases used as lubricant and vacuum pump oil. As an example, 50 mT-magnetite PFPE diffusion pump oil based MF with about 12 vol.% magnetite/maghemite and bulk viscosities < 2 Pa s were prepared and used as functional fluids in **ultrahigh vacuum seals** at GAT-mbH.com in Germany.

Lower viscous carriers, like silicon oils or ionic fluids, are alternatives for PFPE.

MRF compositions containing 1-5 µm Fe-carbonyl particles dispersed in PFPE were tested as functional fluid for **an artificial knee joint**. The bulk viscosity of the MRF could be reversibly increased by switching an external magnetic field on or off, up to four orders. Generally, MRF-particles tend to sediment over the course of time. There-

fore, the reversibility of the MR-effect has to be improved.

In the last years, **biocompatible MF** were prepared for in-vivo use in our lab. as well. magnetite/maghemite cores ranged from 5 up to 10 nm diameter and hydrodynamic diameters from 20 nm, 50 nm, up to some 100 nm. Biocompatible and/or **biofunctional shells** covered the particles. Those polyaspartic shells have as well as $–NH_2$ and –COOH groups which can be separately chemically modified. Bilayer shells of dimercapto-succinic acids can be modified chemically through complexation of radionuclides, and carboxylated cyclodextrin shells can be modified as well as by chemical reaction with -COOH-groups and by inclusion of hydrophobic agents into the holes.
An outlook for further development of cores and shells will be given at the presentation.

The most important property of the dispersions is the high **colloidal stability** of the dispersed particles. The Derjaguin-Landau-Verwey-Overbeek-theory can be used as estimation for the stability of particles in hydrosols, but in organic carriers it is open to explain the particles repulsion.
Therefore, up to today trial and error methods are used to prevent particle´s agglomeration.

Acknowledgments
This work was partly realized in cooperation with Capsulution Pharma AG, Berlin.

Finite-element simulation of ferrogels: Magneto-mechanical coupling and stress-strain behaviour

P. Cremer, A. M. Menzel, H. Löwen

Institut für Theoretische Physik II: Weiche Materie, Heinrich-Heine-Universität Düsseldorf, D-40225 Düsseldorf, Germany

Introduction

Ferrogels are magnetic hybrid materials composed of ferro- or superparamagnetic particles in an elastic polymer matrix [1]. Due to the coupling of elastic and magnetic interactions, the material properties can be dynamically tuned using external magnetic fields. Such magnetoresponsive materials have a wide range of applications including novel damping devices, soft actuators and sensors. Additionally, ferrogels combine the properties of ferrofluids with the convenience of the cross-linked polymer matrix because no container is required to maintain them.

The various realisations of ferrogels differ in the degree of orientational coupling between the magnetic moments of the particles and the surrounding polymer matrix. Systems in which the particles are covalently bound into the matrix so that rotations are hindered by restoring torques show a strong coupling [2]. In other systems the particles are located in mesh pockets that typically only restrict translational motion. Also the particle size plays a role. The magnetic moments of small particles can easily flip with respect to the particle axes while such a relaxation is suppressed for larger particles.

The details of the interaction between magnetic particles and the elastic matrix are of crucial importance for the macroscopic material properties. However, theoretical descriptions for ferrogels relating the structure on the mesoscale to the macroscopic behaviour are rare. Theoretical models are required which provide a unified description spanning the various length scales of the material ranging from the molecular scale of the polymer network to the mesoscopic particle size and up to the macroscopic size of the sample.

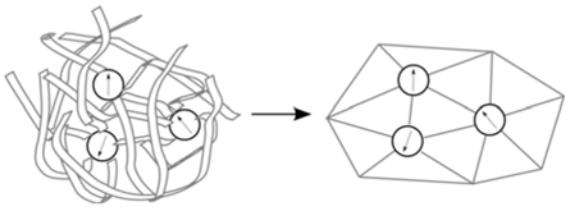

Figure 1: The elastic polymer matrix is simplified to a mesh of finite elements.

Model

We model the system by regarding the interconnecting polymer matrix as an elastic block material and considering embedded particles with magnetic dipole moments. The elastic block material is then discretised into a mesh of triangular (two-dimensions) or tetrahedral (three-dimensions) finite elements. Deformation of a finite element implies an elastic energy cost leading to restoring forces. Not only linear elasticity but also nonlinear, hyperelastic models that are more suitable for cross-linked polymer networks can be implemented.

Ferrogels without orientational coupling can simply be considered by placing freely rotating dipoles at the vertices of the mesh, see Fig. 2 for a sketch. Additionally, we can model systems with strong orientational coupling where particles are cova-

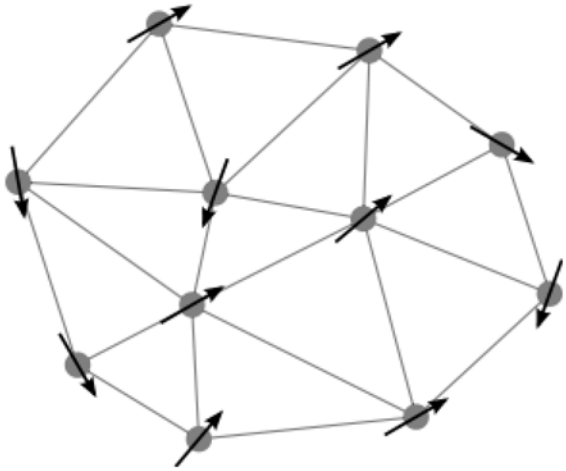

Figure 2: Model sketch for ferrogels without orientational coupling to the elastic matrix.

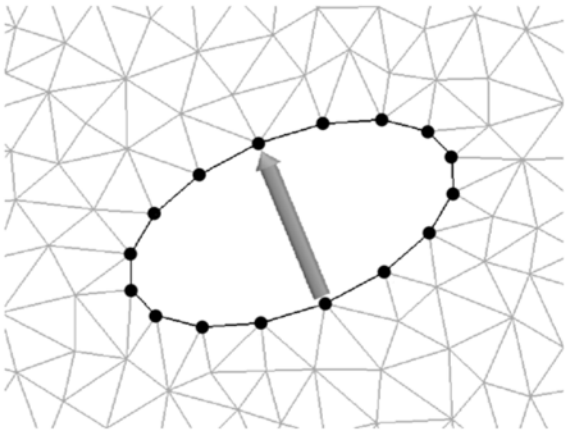

Figure 3: Covalently bound ellipsoidal particle. The particle is orientationally coupled to the polymer matrix since it cannot rotate without deforming the finite elements connected to its surface.

lently bound into the polymer matrix. For this purpose, particles of finite size are inserted explicitly into the mesh and the finite mesh elements are connected to the particle surfaces as shown in Fig. 3. When the particles rotate, they deform the surrounding elastic finite elements leading to restoring torques.
In the future, we also aim to explicitly implement pockets in the polymer matrix where the particles are embedded. This allows to describe systems with partial orientational memory that irreversibly rearrange when an external magnetic field is applied.

Simulation

Using our numerical implementation, we can perform stress-strain measurements to investigate the influence of various parameters on the behaviour of the material. First results for a ferrogel with strong orientational coupling show, that the magnitude of the magnetic moment has a large influence on the elastic modulus of the material. Whether the modulus drops or rises as a function of the magnitude of the magnetic moments depends on the initial distribution of particle positions and orientations.
As a next step, we will use particle configurations provided by experimental groups as an input for our simulations. Using our numerical approach, we can compare the resulting stress-strain behaviour to the experimental data und simultaneously observe the mesoscopic reaction of the samples to the imposed stress. This will help to explain the macroscopic material behaviour on the basis of a mesoscopic particle picture.

Acknowledgments

Support from the DFG through the SPP 1681 and from the ERC Advanced Grant INTERCOCOS (Grant No. 267499) is gratefully acknowledged.

References

[1] M. Zrínyi, L. Barsi, and A. Büki, *Ferrogel: a new magneto-controlled elastic medium*, Polym. Gels Netw. **5**, 415 (1997).

[2] N. Frickel, R. Messing, and A. M. Schmidt, *Magneto-mechanical coupling in $CoFe_2O_4$-linked PAAm ferrohydrogels*, J. Mater. Chem. **21**, 8466 (2011).

A contribution to the modeling of ferrogels

Abdolhamid Attaran[1], Jörg Brummund[1], Thomas Wallmersperger[1]

[1] *Institut für Festkörpermechanik, Technische Universität Dresden*

Ferrogels consist of a soft polymer matrix usually made up of chemically cross-linked polymer networks and a pore ferrofluid [1]. The pore fluid usually carries magnetic particles of a typical size of 10 nm [2]. In the course of preparation, part of the magnetic particles are adhered to the polymer network. Hence, in the realization of the components in the system the magnetic particles are classified either as fixed to the polymer or mobile.

Based on the preparation method, ferrogels can turn into either isotropic or anisotropic gels [3]. In the case of an isotropic ferrogel, the magnetic particles are randomly dispersed throughout the polymer matrix making them only sensitive to the gradient of a magnetic field [4]. The anisotropic ferrogels, in contrast, have a preferred direction [3] and are, thus, responsive to a homogeneous magnetic field as well.

In the current work a systematic development of the field equations of a ferrogel as a multiphasic, multicomponent medium is presented based on the continuum mechanics of mixtures. As is customary in the continuum mechanics, the development of the model begins by the introduction of the kinematic relations and the balance laws. The balance laws, however, must fulfill the "Truesdell's metaphysical principles" [5]. The balance laws include the balance of mass, momentum, angular momentum, energy and entropy. Additionally, the Maxwell relations have to be considered.

In the process of modeling, thermodynamically consistent constitutive laws are next postulated. The field equations of the ferrogel are obtained by plugging the constitutive relations back into the balance laws. The derived set of field equations complemented by appropriate initial, boundary and transition conditions define an Initial Boundary Value Problem (IBVP).

Owing to its versatility, the finite element method (FEM) is further planned to be used to solve the aforementioned IBVP. This enables one to investigate (1) the influence of the magnetic field on the magnetic particles in the polymer gel, (2) the interaction of the particles with the polymer network, and (3) the resulting mechanical deformation of the gel. Thus, depending on the applied magnetic field, the resulting deformation of the gel, and the attainable restoring forces for example of a ferrogel actuator can be determined.

Acknowledgments

This research has been financially supported by the Deutsche Forschungsgemeinschaft in the framework of Priority Programme: " Feld gesteuerte Partikel - Matrix - Wechselwirkungen: Erzeugung, skalenübergreifende Modellierung und Anwendung magnetischer Hybridmaterialien (SPP 1681) ".

References

[1] M. Zrínyi, L. Barsi, and A. Büki. Deformation of ferrogels induced by nonuniform magnetic felds. *The Journal of Chemical Physics*, 104(21):8750 – 8756, 1996.

[2] M. Zrínyi, L. Barsi, and A. Büki. Ferrogel: a new magneto-controlled elastic medium. *Polymer Gels and Networks*, 5(5):415 – 427, 1997.

[3] S. Bohlius, H. R. Brand, and H. Pleiner. Macroscopic dynamics of uniaxial magneticgels. *Phys. Rev. E*, 70:061411, Dec 2004.

[4] E. Jarkova, H. Pleiner, H.-W. Müller, and H.R. Brand. Hydrodynamics of isotropic ferrogels. *Phys. Rev. E*, 68:041706, Oct 2003.

[5] C. Truesdell. *Rational Thermodynamis*. Springer-Verlag New York, 2nd. edition, 1984.

Magnetic Particle Spectroscopy detecting changes during cellular uptake of magnetic nanoparticles

F. Wiekhorst[1], N. Löwa[1], S. Metzkow[2], W. Poller[2], A. Ludwig[2] L. Trahms[1]

[1] *Physikalisch-Technische Bundesanstalt, Berlin, Germany*
[2] *Charité, University Medicine Berlin, Germany*

With their outstanding biocompatibility and superparamagnetic properties magnetic nanoparticles are used in a brought spectrum of diagnostic and therapeutic applications. Due to their potential to label immune cells in vivo, nanoparticles are intensely investigated to study various infective-, inflammatory- and autoimmune diseases [1]. Electrostatically stabilized citrate-coated very small superparamagnetic iron oxide particles (VSOPs) are a promising class of nanoparticles suitable for cell labeling. VSOPs are supposed to bind to negatively charged glycosaminoglycans on the cell surface before being internalized by the cells [2].

Magnetic Particle Spectroscopy (MPS) has been proven a powerful tool for the sensitive and specific detection of magnetic nanoparticles in biological environment, especially in cells [3]. MPS is based on the nonlinear magnetic susceptibility response of magnetic nanoparticles induced by an oscillating magnetic field and permits the quantification of the magnetic nanoparticle iron content without being affected by tissue or non-particular body iron. Furthermore, the MPS spectra provide information about the magnetic state of the analyzed nanoparticles, especially changes due to the environment can be visualized.

We employed MPS to quantify the cellular VSOP uptake in THP-1 monocytes (THP-Mo) and macrophages (THP-MΦ) cell lines. Additionally our attention was directed to the detection of changes of the magnetic properties of VSOP during the cellular uptake. To assess feasibility and accuracy of VSOP quantification by MPS, we additional used the photometric phenanthroline method (Phen) as an independent analytic gold standard.

Materials and Methods

Citric acid coated VSOP were manufactured following the recipe given by Pilgrimm. The VSOP consist of magnetite single cores with about d_c=6 nm diameter as determined by $M(H)$ measurements (hydrodynamic diameter d_{hydr}=8 nm). The iron concentration of the stock suspension was 0.5 mol/L, but for cell treatments the VSOP were diluted in 1% FCS to avoid interaction with serum proteins down to an iron concentration of 0.75 mmol/L (41 µg/ml) and offered to 10^6 cells for uptake.

THP-1 cells (ATCC, Wesel) were cultured in RPMI medium 1640 (Invitrogen, Karlsruhe) supplemented with 10% fetal calf serum, 100 U/mL penicillin, 100 µg/mL streptomycin. For differentiation into macrophages, THP-1 monocytic cells (THP-Mo) were treated for 72 h with 20 ng/mL phorbol myristate acetate, and washed three times with medium afterwards. After 24 h of rest the resulting macrophages (THP-MΦ) were used for experiments. Cell samples were incubated with VSOP for 30 min, 1 h, 3 h, 6 h, and 24 h duration, respectively.

MPS was used to determine the absolute iron amount in the cell samples. At an excitation magnetic field of 25 mT and frequency f_0 = 25 kHz the MNP generate a characteristic signal spectrum in the Fourier transform of the detected time-dependent signal. Only higher odd harmonics of the excitation frequency f_0 were con-

sidered, because f_0 contains the strong fundamental excitation as well as diamagnetic and paramagnetic contributions of the suspension. The VSOP quantification is obtained by the third harmonic A_3 divided with the specific third harmonic A_3*=1.0(1)·10^{-3} Am^2/(gFe) (A_3 normalized to iron amount) of a corresponding reference sample with known VSOP amount.

As a second parameter we used the ratio of fifth and third harmonics A_5/A_3 to assess changes in the dynamic magnetic behavior of the VSOP due to their environment.

Additionally we employed the phenanthroline based iron assay (Phen) to independently quantify the VSOP uptake in reference and cell samples.

Samples were dissolved in 20 µL (35%) HCl, afterwards filled up with 1 mL distilled water and then (the cell samples were) centrifuged to remove cellular debris. Aliquots of 50 µL of the supernatant were mixed with 50 µL (1.5 mol/L) hydroxylamine hydrochloride and 150 µL (4 mol/L 1,10-phenanthroline hydrochloride, 200 mmol/L acetic acid, and 160 mmol/L sodium acetate). Absorbance of samples was measured using an AnthosIII (Biochrom) microplate reader at 492 nm. Iron concentrations were determined using internal of iron standard absorption curves (all chemicals by Merck, Darmstadt).

Results

We found a match with deviations less than 2% between VSOP iron amounts quantified by MPS ($m(\mathrm{Fe})_{\mathrm{MPS}}$) and Phen ($m(\mathrm{Fe})_{\mathrm{Phen}}$) in a dilution series of (reference) samples without cells. In the lower range of iron amounts below 300 ng the deviations strongly increased, as Phen is approaching the detection limit (about 200 ng), whereas by MPS iron amounts less than 100 ng could be safely detected.

Quantifying the VSOP uptake in cells led to systematic overestimation of the iron amount as determined from the third harmonic A_3 of the MPS signal compared to the corresponding Phen value (up to 50%). However, for both cell types the ratio $m(\mathrm{Fe})_{\mathrm{MPS}}/m(\mathrm{Fe})_{\mathrm{Phen}}$ describing the of this was linearly related to the A_5/A_3 ratio of the MPS spectra as shown in Fig. 1. Interestingly, this behavior was dependent on the incubation time (inset Fig. 1), it was found to be strongest for the shortest time of VSOP incubation (30 min).We attribute this behavior to the interaction of the VSOP with the cells during their uptake.

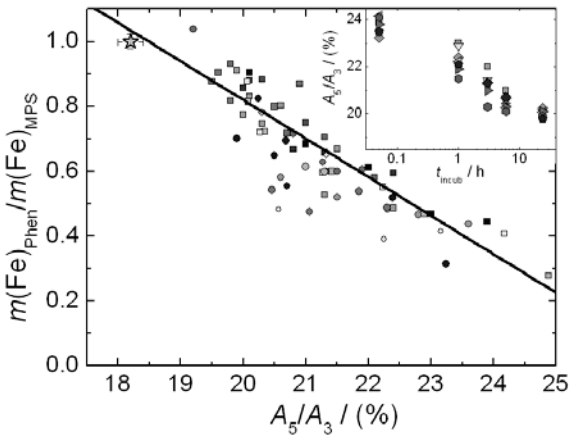

Fig. 1. Correlation between A_5/A_3 ratio and MPS overestimation of cellular VSOP uptake. The star in the upper left marks the A_5/A_3 ratio of fluid stock VSOP. **Inset:** Incubation dependent A_5/A_3 ratio found for VSOP uptake in THP-Mo cells.

Conclusions

MPS in combination with Phen is a powerful tool to analyze cellular uptake of VSOP and allows for detecting changes in magnetic behavior due to interactions of nanoparticles with their biological environment. Using a previously recorded calibration curve the concentration independent A_5/A_3 ratio can be used to reduce uncertainties in further quantification experiments.

Acknowledgments

This work was financially supported by the DFG research units FOR917 and KFO213.

References

[1] S Wagner et al. (2013) Int J Nanomed **8**:767–779

[2] A Ludwig et al. (2013) Basic Res Cardiol **108:**328-1-13

[3] N Löwa et al (2012) IEEE TRANS MAG **49**:1

Field-induced reorientation of shape anisotropic magnetic nanoparticles

S. Disch[1,*], P. Bender[2], M. Kundt[1], D. Honecker[3], A. M. Schmidt[1]

[1]*Department Chemie, Universität zu Köln, Germany*
[2]*Experimentalphysik, Universität des Saarlandes, Saarbrücken, Germany*
[3]*Laboratory for the Physics of Advanced Materials, University of Luxembourg, Luxembourg*

The response of magnetic nanoparticles to applied static and dynamic magnetic fields is the subject of intense research in view of its fundamental technological importance, *e.g.* for medical applications such as imaging and magnetic hyperthermia [1], or sensor applications [2]. The field-assisted self-assembly of shape-anisotropic nanoparticles in dispersions is further desired for liquid crystalline or optically anisotropic materials [3] and as a prerequisite for self-organization into long range ordered arrangements [4]. Our long-term objective is to gain microscopic insight into the orientation dynamics of elongated nanoparticles in order to advance both the self-organization of shape anisotropic nanoparticles and their use as nanoprobes in biomedical applications [5] or to detect the viscoelastic properties of the surrounding matrices [6]. In this contribution, we demonstrate the capability of time-resolved small-angle X-ray scattering (SAXS) techniques for studying the reorientation of elongated magnetic nanoparticles in a dynamic magnetic field.

The weakly ferromagnetic hematite nanoparticles under study are elliptic or spindle-shaped and are known to orient with their principal axis perpendicular to an applied magnetic field [7, 8], leaving two degrees of freedom for particle orientation. In addition to the particle orientation obtained by static SAXS, the time-resolution of our stroboscopic SAXS experiment provides information on the dynamic particle orientation for a given state of an applied alternating or rotating magnetic field (Fig. 1).

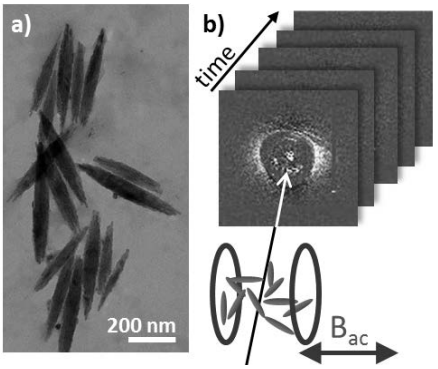

Figure 1: a) TEM of elongated hematite nanoparticles [7] b) schematic of the time-resolved SAXS setup using an alternating magnetic field.

Time-resolved SAXS measurements were carried out using an alternating magnetic field of 10 mT with frequencies between 25 and 300 Hz. In order to enhance the weak anisotropy of the measured SAXS pattern, we subtract the isotropic SAXS measured without magnetic field from each pattern presented in Figure 2. For low frequencies, we clearly observe the time-resolved interplay of isotropic particle orientation and planar particle orientation perpendicular to the inducing field direction in vanishing and maximum applied field, respectively (Fig. 2, left side). With increasing frequency the particle reorientation in the inducing field is delayed, resulting in a quasi-static orientation of the anisotropic particle orientation throughout the entire period, shown exemplarily for 200 Hz in Fig. 2 (right side). The characteristic frequency of particle rotation observed us-

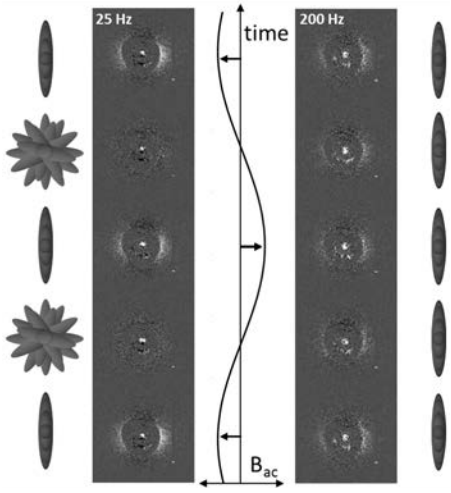

Figure 2: Time-resolved SAXS in alternating magnetic fields. SAXS pattern measured at different states of the applied magnetic field are shown for frequencies of 25 and 200 Hz along with schematics of the nanoparticle orientation.

ing time-resolved SAXS corresponds well to measurements of the rotational diffusion constants using dynamic light scattering and is in good agreement with theoretical estimates [9].
In addition to the planar orientation achieved using alternating magnetic fields, application of rotating fields promises a significantly higher degree of orientation. For frequencies between the characteristic rotational frequencies of the principal and equatorial axes, parallel alignment of the elongated hematite nanoparticles with their principal axis perpendicular to the rotation plane is expected. In our contribution, we give a detailed account of the experimentally observed nanoparticle reorientation behavior in alternating and rotating magnetic fields, with particular emphasis on the varying degree of order obtained with increasing frequencies. Our observations are correlated with complimentary optical transmission measurements.

Acknowledgments

We acknowledge the European Synchrotron Radiation Facility (ESRF), Grenoble, France, for providing the synchrotron radiation facilities at beamline ID13. Dr. M. Burghammer and Dr. M. Sztucki are acknowledged for their support in data acquisition at ID13.

References

[1] Q. A. Pankhurst, J. Connolly, S. K. Johnson, J. Dobson, *J. Phys. D: Appl. Phys.* **36**, R167 (2003).

[2] D. T. N. Chen, Q. Wen, P.A. Janmey, J.C. Crocker, A.G. Yodh, *Annual Review of Condensed Matter Physics* **1**, 301 (2010).

[3] G. M. Whitesides, B. Grzybowski, *Science* **295**, 2418 (2002).

[4] A. Ahniyaz, Y. Sakamoto, L. Bergström, *Proc. Natl. Acad. Sci. U.S.A.* **104**, 17570 (2007).

[5] S. Schrittwieser, F. Ludwig, J. Dieckhoff, A. Tschoepe, A. Guenther, M. Richter, A. Huetten, H. Brueckl, J. Schotter, *Small* **10**, 407 (2014).

[6] P. Bender, A. Tschöpe, R. Birringer, *J. Mag. Mag. Mater.* **346**, 152 (2013).

[7] L. Roeder, P. Bender, A. Tschöpe, R. Birringer, A. M. Schmidt, *J. Polymer Science Part B: Polymer Physics* **50**, 1772 (2012).

[8] C. Märkert, B. Fischer, J. Wagner, *J. Appl. Cryst.* **44**, 441 (2011).

[9] M. M. Tirado, J. G. de la Torre, *J. Chem. Phys.* **71**, 2581 (1979).

Concept for a 10 MHz ac susceptometer with adjustable sample temperature

C. Kuhlmann, T. Wawrzik, M. Schilling, F. Ludwig

Institut für Elektrische Messtechnik und Grundlagen der Elektrotechnik, TU Braunschweig, Hans-Sommer-Str. 66, 38106 Braunschweig

Introduction

AC susceptibility measurements are widely used to determine the magnetic properties of samples. Especially for the investigation of magnetic nanoparticles, they have a wide range of applications [1, 2]. As parameters often depend on temperature, many commercial systems feature temperature control options. While these systems provide very accurate results, they are also very costly. Additionally, few commercial systems provide a frequency range above 100 kHz. In order to obtain temperature dependent measurements in the frequency range up to 10 MHz, a concept for a home-built ac susceptometer with these specifications is presented.

Electrical concept

In order to obtain acceptable field strengths at high frequencies, the inductance of the excitation system should be minimized. Unfortunately, this requirement is in contradiction with a high homogeneity of the excitation field. Another aspect that should be respected for the design of the excitation coil are electrical losses. Due to the skin effect, the resistance of the excitation coil and therefore the thermal losses rise with the square root of frequency. Litz wire should be used to keep these losses minimal. Although theoretical considerations for the optimal number of Litzwire strands exist [3], they do not incorporate single layer coils or homogeneity requirements. Therefore, a magnetic FEM simulation was used to determine the optimal coil geometry and the strand number. Fig. 1 depicts the coil layout and the field distribution after the optimization process. The simulation showed a field inhomogeneity (based on the extrema values within the sample volume) of below 2 percent and a coil inductance of 1.54 µH.

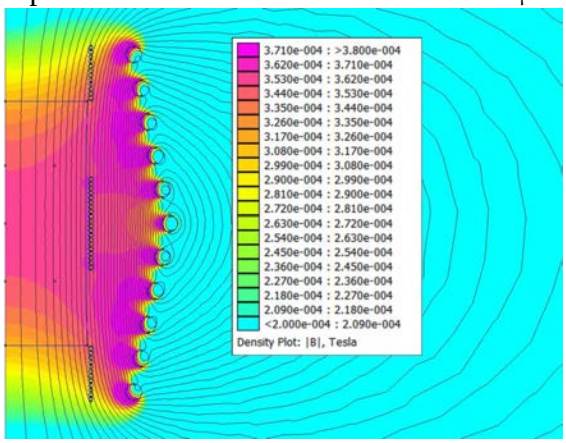

Fig. 1. *Magnetic simulation of the excitation and detection coil system. The left border of the figure is the radial symmetry line.*

Electrical coil losses at 10 MHz with the nominal excitation current of 266 mA are 0.08 W.
The detection of the MNP signal is achieved with a detection coil and a pair of compensation coils that form a symmetric gradiometer.

Thermal concept

Measuring the sample response while a heating system is used to maintain the desired sample temperature requires that the heating does not interfere with the magnetic measurement. For this reason, an electrical

heater cannot be placed in close vicinity to the sample. Due to size constraints, a heat transfer by liquids is not an alternative. Our concept therefore uses an AlN ceramic to transfer the heat to the sample. The ceramic component also acts as a coil former for the detection coils. In order to achieve the desired sample temperature in the presence of an unknown convective heat flux to the environment, two temperature sensors are used to measure the temperature gradient from the heater to the top of the sample enclosure. Assuming a homogenous thermal resistance over the length of the sample enclosure, the temperature at the sample position can be accurately determined. The heater as well as the temperature sensors are positioned outside the active area of the gradiometer so that they do not interfere with the measurement.

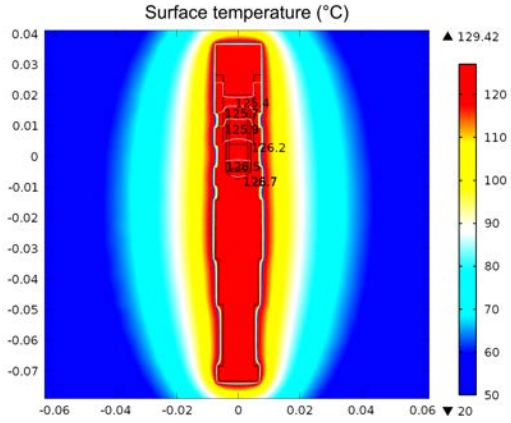

Fig. 2. *Thermal simulation of the heated sample enclosure after 30 minutes of warmup time from room temperature.*

Thermal isolation of the sample enclosure is achieved by Macor^{TM} ceramic parts which also act as the coil former for the excitation coil. The simulation showed that the inhomogeneity of the temperature distribution within the sample area should be below 0.4 °C with 30 minutes of warmup time. The design has a nominal maximum sample temperature of 100 °C. In order to suppress magnetic interference from the environment, the coil system will be shielded by a mu-metal enclosure. This has the additional benefit of reducing temperature variation due to convection.

Signal generation and processing

The generation of the excitation waveform as well as the phase and amplitude measurement of the sample signal is performed by a commercially available lockin amplifier eLockin 205/2 (Anfatec GmbH) with 10 MHz bandwidth. The signal is going to be amplified before being fed into the excitation coil by a homebuilt wideband power amplifier. Temperature control is achieved with a custom built control unit.

Conclusion

We have presented a concept for a ac susceptometer with 10 MHz bandwidth and temperature control for the sample volume up to 100 °C. Necessary compromises and considerations during the design process of electrical and thermal parts have been discussed. Simulations have been used to refine the initial design.

Acknowledgments

Financial support by the DFG via SPP1681 under grant no. LU 800/4-1 is gratefully acknowledged.

References

[1] F. Ludwig et al., Biomedizinische Technik/Biomedical Engineering **58**, 535 (2013).

[2] F. Ludwig, A. Guillaume, M. Schilling, N. Frickel, and A. M. Schmidt, Journal of Applied Physics **108**, 033918 (2010).

[3] C. R. Sullivan, IEEE Transactions on Power Electronics **14**, 283 (1999).

Synthesis and properties of catalytically active and magnetic $Co@SiO_2$ and Co@ZSM-5 nanoparticles

I. Appel[1], R. Müller,[2] S. Behrens[1]

[1]*Institut für Katalyseforschung und-technologie; Karlsruher Institut für Technologie (KIT), Postfach 3640, 76021 Karlsruhe;* [2]*Leibnitz Institut für Photonische Technologien (IPHT), Postfach 100239, 07702 Jena*

Bifunctional catalysts consisting of metal cores and highly porous shells have recently attracted a lot of interest due to their synergetic abilities in consecutive reactions [1]. After chemical reaction at the metallic core, a second reaction takes place directly at neighboring active sites in the shell before the products of the first reaction can leave the particle, thus providing enhanced selectivity for the overall reaction (Figure 1).

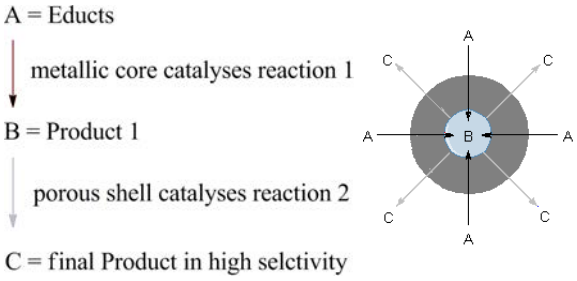

Figure 1: Reaction scheme for a consecutive reaction using core@shell-type particles.

We have developed a novel strategy for the synthesis of bifunctional core@shell-type hybrid nanoparticles combining thermal and chemical stability with catalytic and magnetic properties. Initially, PVP-stabilized Co_3O_4 nanoparticles were prepared via microwave-assisted synthesis. The as-prepared particles were individually coated with an amorphous SiO_2 layer by a modified Stöber synthesis [2]. By this, narrow particle size distributions and adjustable hull thicknesses were achieved (Figure 2).

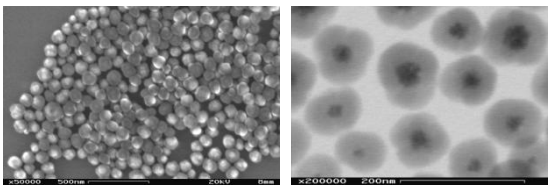

Figure 2: $Co_3O_4@SiO_2$ particles: REM (left) and REM-STEM (right) image.

Finally, the amorphous SiO_2 layer was transformed into a crystalline zeolite (ZSM-5) using our recently developed hydrothermal synthesis procedure. As a result, monodisperse core@shell-type Co_3O_4@ZSM-5 particles with diameters tunable between 70 nm and 100 nm were obtained (Figure 3).

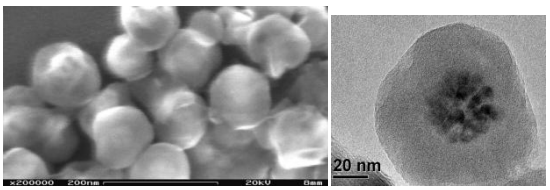

Figure 3: Co_3O_4@ZSM-5 particles: REM (left) and TEM (right) image.

The Co_3O_4 cores of the $Co_3O_4@SiO_2$ and Co_3O_4@ZSM-5 hybrid particles, respectively, were completely reduced to metallic cobalt in a 10 % H_2 in argon stream at 750 °C. The morphology and core@shell structure of the reduced particles was maintained despite the harsh conditions of thermal treatment (Figure 4). They exhibited magnetic properties for several months after exposure to air.

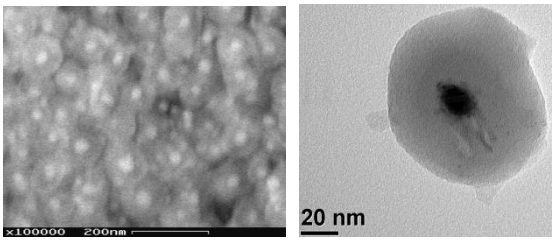

Figure 4: Magnetic Co@H-ZSM-5 particles: REM (left) and TEM (right) image.

The particles were characterized by TEM, REM/EDX, XRD, H_2-TPR, OES-ICP, BET and VSM. Catalytic properties of the Co@H-ZSM-5 nanoparticles were successfully tested for Fischer-Tropsch synthesis.

Outlook

The long-term stability of the reduced particles in different solutions has to be verified and magnetic applications beyond catalysis will be evaluated.

References

[1] J. Bao, J. He, Y. Zhang, Y. Yoneyama, N. Tsubaki, Angewandte Chemie 2008, 120 (2), 359-362.

[2] R. Xie, D. Li, B. Hou, J. Wang, L. Jia, Y. Sun, Catalysis Communications, 2011, 12 (5), 380-383.

Control of the Crystal Phase Composition of Fe_xO_y Nanopowders prepared by CO_2 Laser Vaporization

C. Stötzel[1], H.D. Kurland[1], J. Grabow[1], S. Dutz[2], E. Müller[3], M. Sierka[1], F.A. Müller[1]

[1] *Otto-Schott-Institute of Materials Research (OSIM), Friedrich-Schiller-University Jena, 07743 Jena, Germany*
[2] *Institute of Biomedical Engineering and Informatics, TU Ilmenau, 98693 Ilmenau, Germany*
[3] *Institute of Electronic and Sensor Materials, TU Bergakademie Freiberg, 09599 Freiberg, Germany*

Introduction

Iron oxide (Fe_xO_y) nanoparticles (NP) are conveniently synthesized by wet chemical reactions [1] using additives to control size, shape, and superficial properties. Alternatives are gas phase syntheses including flame spray pyrolysis [2] and plasma synthesis [3]. Here, CO_2 laser vaporization (LAVA) with subsequent gas phase condensation at normal pressure was used for the preparation of Fe_xO_y nanopowders. LAVA stands out because no especially designed precursors are required. Starting materials are coarse powders with the same chemical composition as that of the targeted nanopowders. Basic investigations revealed a close connection between the oxygen (O_2) content of the condensation atmosphere in the LAVA process and the phase composition of the Fe_xO_y nanopowders [4]. In our present work [5] this impact of the O_2 partial pressure on the LAVA prepared Fe_xO_y nanopowders and thus on their physical properties is studied systematically. In depth, morphological, structural, chemical, and magnetic analyses of the obtained Fe_xO_y nanopowders are conducted. Based on the results and on density functional theory (DFT) calculations a model which describes the formation of the initial nucleation stages of iron and oxygen in the vapor phase is proposed. This model elucidates the dependence of the crystal phase composition of the resulting Fe_xO_y nanopowders on the O_2 content of the condensation atmosphere.

Methods

Fe_xO_y nanopowders were prepared from a coarse hematite (α-Fe_2O_3) powder. A continuous high power CO_2 laser beam (wavelength 10.59 µm, radiation power 2 kW) was focused (focus intensity 175 kW cm^{-2}) onto the surface of the raw powder. Absorbing the intense laser radiation the α-Fe_2O_3 powder heated up and vaporized into its atomic components. Expanded and quenched in the flowing process gas clusters formed by homogeneous nucleation. Supersaturation led to the condensation of melt droplets. With further cooling the size of the primary NPs was set by the solidification of the droplets. The O_2 content of the condensation atmosphere was varied (Table 1) applying different combinations of argon, air, and oxygen as the process gas. The Fe_xO_y nanopowders were characterized using X-ray diffraction combined with Rietveld refinement and transmission electron microscopy (TEM). The contents of Fe^{2+} ions were determined by quantitative cerimetric redox titration. Vibrating sample magnetometry was used to determine the magnetic properties of the Fe_xO_y nanopowders. Furthermore, the presence of ozone (O_3) in the zone of condensation was checked using an ultraviolet absorption ozone analyzer.

Results and Discussion

Independent of the process gas composition the LAVA process yielded Fe_xO_y nanopowders with a production rate of 9 g h^{-1}. The obtained NPs are nearly-spherical, faceted and crystalline (Figure 1). Remnant magnetization of the NPs leads to the formation of chain-like agglomerates. The mean diameter of the NPs is 22 nm ± 2 nm independent of the O_2 partial pressure in the condensation atmosphere.

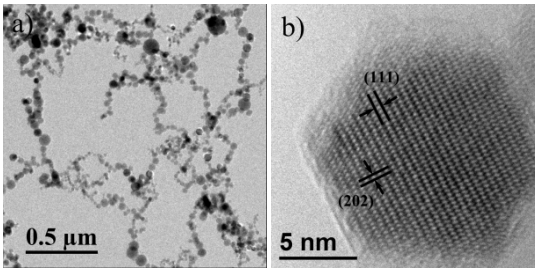

Figure 1: TEM micrographs of LAVA prepared iron oxide NPs: a) typical chain-like agglomerate and b) high resolution micrograph of a γ-Fe_2O_3 NP.

In O_2 depleted condensation atmospheres (Table 1) maghemite (γ-Fe_2O_3) forms as the dominant crystal phase. Increasing the O_2 partial pressure leads to an increasing formation of the Fe_2O_3 polymorph ε-Fe_2O_3. This also results in a change of the magnetic properties of the Fe_xO_y nanopowders since ε-Fe_2O_3 has a small saturation magnetization ($M_S \approx 15$ m^2 kg^{-1} – 15 m^2 kg^{-1}) in combination with a high coercive field (H_C = 1600 kA m^{-1}) [6].

Table 1: O_2 content of the supplied process gas as well as ε-Fe_2O_3 content and saturation magnetization M_S of the obtained Fe_xO_y nanopowders.

O_2 content of the process gas [vol%]	ε-Fe_2O_3 [wt%]	M_S [Am^2 kg^{-1}]
0	0.5±0.1	72.2±2.2
14	2.5±0.8	71.2±2.1
21	10.2±1.9	56.9±1.7
47	36.2±2.1	38.5±1.2
100	43.0±4.3	37.8±1.1

In O_2 enriched process gases O_3 was detected in the vicinity of the laser plasma. DFT calculations reveal that in the presence of O_3 within the zone of condensation a 6-fold coordination of iron with oxygen is facilitated. The crystal structure of ε-Fe_2O_3 differs from the structure of γ-Fe_2O_3 by a higher mean coordination number of iron. Thus, the coordination of iron in the vapor phase predetermines the structure of the crystallizing Fe_xO_y NPs.

Conclusions

Crystaline magnetic iron oxide nanopowders were prepared by the LAVA method. The O_2 partial pressure and thus the O_3 content in the condensation atmosphere of the LAVA process strongly impacts structural and accordingly magnetic characteristics of the prepared Fe_xO_y NPs. Hence, their saturation magnetization and coercive field can be adjusted within certain limits by controlling the O_2 partial pressure during the gas phase condensation of the NPs. The proposed nucleation model for the Fe_xO_y NPs also sheds light on general gas phase nucleation phenomena and facilitates the predetermination of crystal lattice formation by the metal coordination in the vapor phase.

Acknowledgments

This work was supported by the Deutsche Forschungsgemeinschaft (DFG) under grant MU1803/8-2. We thank Professor Peter Schaaf (TU Ilmenau) for very helpful discussions and the Thüringer Landesanstalt für Umwelt und Geologie (TLUG, Jena) for providing the ozone analyzer.

References

[1] Wu, W., et al., *Magnetic Iron Oxide Nanoparticles: Synthesis and Surface Functionalization Strategies.* Nanoscale Res. Lett. 2008, **3**(11), 397-415.

[2] Li, D., et al., *Insight into microstructural and magnetic properties of flame-made gamma-Fe_2O_3 nanoparticles.* J. Mater. Chem. 2007, **17**(46), 4876-4884.

[3] Vollath, D., *Plasma synthesis of nanopowders*. J. Nanopart. Res. 2008, **10**, 39-57.

[4] Kurland, H.D., et al., *Magnetic iron oxide nanopowders produced by CO_2 laser evaporation.* J. Magn. Magn. Mater. 2007, **311**(1), 73-77.

[5] Stötzel, C., et al., *Control of the Crystal Phase Composition of Fe_xO_y Nanopowders Prepared by CO_2 Laser Vaporization.* Cryst. Growth Des. 2013, **13**(11), 4868-4876.

[6] Jin, B., et al., *Giant coercive field of nanometer-sized iron oxide.* Adv. Mater. 2004, **16**(1), 48.

Kinetic study of crystallization titanium substituted barium hexaferrite in a glassy matrix of the system $BaO\text{-}Fe_2O_3\text{-}TiO_2\text{-}B_2O_3$

P. Quiroz, B. Halbedel

Technische Universität Ilmenau, Institute of Materials Engineering - Department Group of Inorganic-Nonmetallic Materials, Ilmenau/Germany.

Titanium ion substitution in the barium hexaferrite is of great interest for use as electromagnetic energy dissipation materials in GHz range. Some currently applications for this powder are electromagnetically absorbing shielding, to reduce radiation exposure to humans or to reduce noise levels of electronic devices [1] and fast bonding/ debonding systems by selective microwave heating [2]..

With the melt substitution and the annealing process it is possible to optimize the electromagnetic absorption of the titanium substituted barium hexaferrite [3]. In this work differential thermal analysis (DSC), X-ray diffraction (XRD) and scanning electron microscopy (SEM) were used to study the crystallization behavior of the rapid cooled melt compositions (mole-%): 40 BaO + 33 B_2O_3 + (27-x) Fe_2O_3 + x TiO_2 with x = 0, 1.8, 3.6, 4.6 and 6.4 mole-% TiO_2 for the production of electromagnetic absorber powders in the microwave range. After annealing of these cooled melts the crystalline phases BaB_2O_4, $BaFe_{12-x}Ti_xO_{19}$ and from melt substitutions of x > 4.6 mole-% TiO_2 a dielectric phase $BaTi_6O_{13}$ were determined by XRD [3]. The Netzsch Thermokinetics® program was used in order to understand the phase transformations through the analysis of the kinetic parameters. Thereby the influence of temperature and heating rate was investigated. Overall activation energy of 311.74 ± 3 kJ mol^{-1} was obtained for the crystallization of barium hexaferrite with the ASTM E698® method [4]. A slightly decreasing tendency in this energy was observed when the TiO_2 content was increased, but it is not a significant variation despite the substitution. In addition, the Friedmann method was used to calculate the activation energy, because it is not constant throughout the crystallization process [4].

Acknowledgments

Financial support for this study was provided by Thuringian State graduate funding, the Niels von Bulow Foundation and the Catholic Academic Exchange Service.

References

[1] S.-P. Ruan, B.-K. Xu, H. Suo, F.-Q. Wu, S.-Q. Xiang, J. Magn. Magn. Mater. 2000, 212, 175-177.

[2] B. Halbedel, J. Hildebrand: Ferrimagnetischer Partikel, Klebstoff und Verfahren zu deren Herstellung. DE 10 2012 213 190.6.

[3] P. Quiroz, B. Halbedel, Mat.-wiss. u. Werkstofftechnik, 2011, 42(8), 731-736.

[4] P. Quiroz, B. Halbedel, High Temperatures-High Pressures, 2013, 42(4), 367-357.

Optical detection of nanoparticle aggregation in a living system under the influence of a magnetic field

R. Müller[1], O. Stranik[1], F. Schlenk[2], S. Werner[2], D. Malsch[1], D. Fischer[2], W. Fritzsche[1]

[1] *Leibniz-Institute for Photonic Technology, Albert-Einstein-Str. 9, 07745 Jena*
[2] *Department of Pharmaceutical Technology, Institute of Pharmacy, Friedrich Schiller University, Jena*

Particles are attracting increasing importance in diagnosis and therapy. Most of the *in vitro* experiments do not mimic the dynamic conditions of the *in vivo* situation. Hence several chicken-based test systems using eggs were employed for research [1]. Blood flow has exceptional rheological properties, especially due to the behaviour of red blood cells. Existing velocimetry studies on chick embryo were performed on candled eggs by means of µPIV (micro particle imaging velocimetry) by [2, 3]. The in-vivo transport of magnetic particles (MP) in rats was observed and transport modes considered assuming a constant size (no agglomerates) [4].
Aim of our work was a first in-vivo observation of MP transport in chicken egg vessels in presence of a magnetic field by single particle tracking. For that we demonstrate the spatial resolution of our observations on a cross section of a vein and a temporal resolution by observation of the cardiac cycle in an artery.

Fertilized chicken eggs were incubated at 37°C and 80% relative humidity for 72 h, were poured into a Petri dish and incubated for further 24 h. Particles (1 µl suspension) were injected intravenously with a glass capillary using a micromanipulator MM33-R (Märzhäuser Wetzlar GmbH, Germany) and a XenoWorks microinjector (BRI217; Sutter Instr. Co., USA). The initial MP concentration was 25 mg/ml. The planar surface of the egg model made the whole blood circuit accessible for investigation and insured the evaluation of toxic effects. Carboxylate-modified polystyrene latex beads (L4530 by Sigma-Aldrich, Germany) with a size of 2 µm and fluorescent-labeled superparamagnetic iron oxide with starch coating with a size of 150nm according to the supplier (nano-screenMAG/R-D by chemicell GmbH, Germany) were used.
Microscopical images were recorded with a AxioImager Z1.m (Carl Zeiss, Jena, Germany) and a PCO Sensicam camera in dark field reflection and fluorescence mode, respectively, with a 5x objective. The picture size is 688/520 pixel. One pixel of the video corresponds with 2.58 µm. Single particle tracking and track analysis is realized with TrackMate, a plugin for the image processing package Fiji [8].

Erythrocyte aggregation by microscopy and UV-Vis spectroscopy and hemolysis (ASTM F756-08) was investigated in order to see possible effects what could alter the transport properties. No aggregation of red blood cells was induced by particles up to 10-fold higher concentration than reached in the embryo model (not shown).
Experiments without a magnetic field were done with the latex beads. In Fig.1 a dark field image (width ≈1.6mm) with a „big“ vein, smaller vessels and red blood cells (top) and a fluorescence image is shown. The data of the inserted frame were used to measure the velocity profile across the vein (inset). Our data (one datapoint = five pixel in y-direction) are an z-average (perpendicular to image plane) over a certain range of the cross section of the vessel what alters the measured velocity profile.
Fig.2 (top) reveals the temporal resolution of the fluorescence images of an artery with tracked objects during systole, i.e. minimum and maximum particle velocity, what is illustrated by the length (20 frames) of the “tails”. The diagramm shows the ve-

locity distribution of the objects inside the dashed frame over a few cardiac cycles. The data during the systole suggest a higher velocity in bigger vessels as expected.

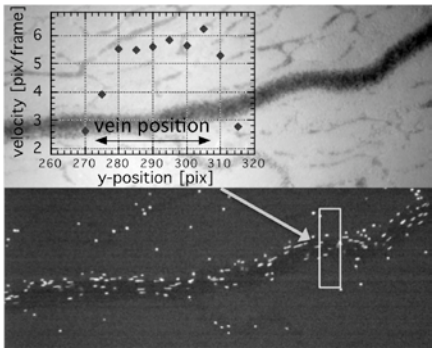

Fig. 1: Dark field (top) and fluorescence image of a vein and velocity profile of particles.

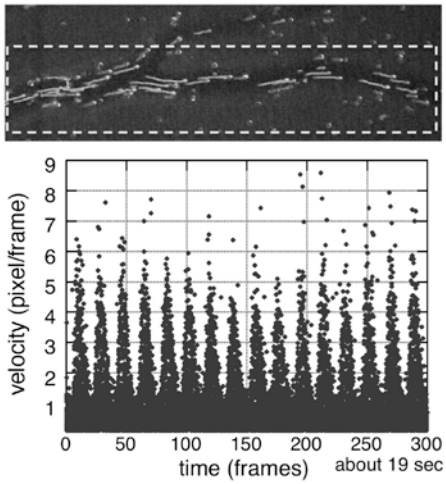

Fig. 2: Fluorescence image of an artery during systole and temporal velocity distribution.

Experiments in presence of a field (by a NdFeB magnet) were done with the magnetic beads. The field parameters at the region of interest were simulated: B ≈ 40 mT and gradB ≈ 5 T/m. In a magnetic field the superparamagnetic beads tend to agglomerate reversilby, i.e. after removing the field the agglomerates should dissolve into single beads again by Brownian motion. A gradient of the field causes a magnetic force, i.e. a movement of particles in direction of the higher field strength. Fig. 3 shows fluorescence images of a vein before applying a field (a), after about 4s (b) and 10s (c) applying a field, respectively, and 8s after removing the field (d). Since the magnetic force doesn't affect parallel to the flow direction (in Fig. 3 slanted to the top) it causes a hydrodynamic resistance what leads to a decreasing velocity or even stopping of the particles near the vascular wall. The images reveal a strong agglomeration caused by the field. After removing the field agglomerates move again or move faster. However they dissolve only partly. The number of tracked objects (inside the dashed frame) stays almost constant (Fig. 4d). One single particle is too small for an observation so that a merging and splitting of objects can't be detected properly. Nevertheless, if we assume superparamagnetic behaviour, the keeping of agglomerates after removing the field could be caused by surface interaction with blood components depending on the coating of the particles. So a testing of the applicability of different particles by our method seems possible.

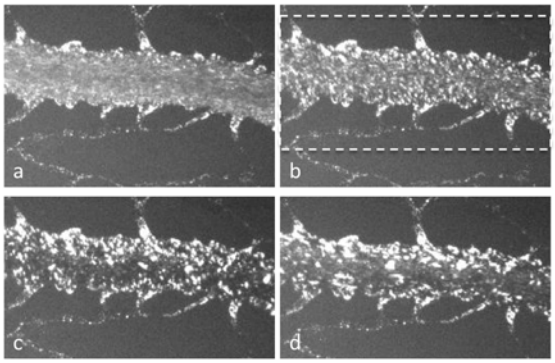

Fig. 3: Formation of agglomerates in a vein under a magnetic field.

Acknowledgments

The authors thank A. Herre for technical assistance and G. Nowak for support with the CAV model.

References

[1] A. Vargas, et al., Adv Drug Deliv Rev, 2007. **59**(11): p. 1162-76.

[2] Vennemann, P., et al., J Biomech, 2006. **39**(7): p. 1191-200.

[3] Poelma, C., et al., PLoS One, 2012. **7**(9): p. e45247.

[4] A. Nacev, et al., Nanomedicine 2010 5(9) 1459-1466

[5] http://fiji.sc/TrackMate; http://fiji.sc/Fiji

Developing a fatty acid - protein coated SPION system with enhanced biocompatibility for drug delivery

Jan Zaloga[1], Johannes Nowak[2], Christina Janko[1], Rainer Tietze[1], Ralf P Friedrich[1], Stefan Odenbach[2], Stefan Lyer[1], Geoffrey Lee[3], Christoph Alexiou[1]

[1] Department of Otorhinolaryngology, Head and Neck Surgery, Section for Experimental Oncology and Nanomedicine (SEON), Else Kröner-Fresenius-Stiftung-Professorship, University Hospital Erlangen, Germany.
[2] Chair of Magnetofluiddynamics, Measuring and Automation Technology, Technische Universität Dresden, Germany.
[3]Division of Pharmaceutics, Friedrich-Alexander Universität Erlangen, Germany

Introduction

Core-shell coated Superparamagnetic Iron Oxide Nanoparticle (SPION) systems have demonstrated very promising properties for biomedical applications [1,2]. However, there are not many approved systems available for clinicians as of yet. The requirements for those systems are high: The ideal core-shell Ferrofluid for biomedical applications is colloidally stable, even in complex media like whole blood, while it retains a sufficient magnetic susceptibility, as well as non-toxic [3]. For drug delivery, the therapeutic efficiency is also a necessary condition. Our workgroup has already demonstrated the great potential of Lauric-acid coated ferrofluids for drug delivery [4,5]. In this present work we developed a system with a surfactant/protein coating and investigated if it fulfils all the basic requirements for drug delivery. We proved the core-shell structure and the pH-dependent surface charge. We demonstrated colloidal stability in blood, magnetic susceptibility and biocompatibility. We coupled the cytotoxic drug Mitoxantrone (MTO) to the particles and demonstrated the therapeutic efficiency of the MTO-particle complex on tumour cells *in vitro*.

Methods

Lauric acid coated magnetite particles were synthetized in one step by a slightly modified method adapted from Bica et al. [6] The solution was purified by dialysis, the pH was adapted and the solution was mixed with an excess of Bovine Serum Albumin (BSA) solution. After Ultrafiltration the resulting Ferrofluids were sterilized either by filtration or autoclaving. The Iron concentrations were determined with an established UV-VIS method and adjusted accordingly. The magnetic properties were characterized with Vibrating Sample Magnetometry (VSM). We used TEM (Philips CM 300 UT) to visualize the magnetite cores and clusters. DLS (Malvern Zetasizer ZS Nano, NICOMP 380 ZLS) was used to characterize surface charge and aggregate sizes. We also investigated the structure of the surface by Fourier-transform infrared spectroscopy (FTIR) and pH – dependent zeta potential measurements. We loaded MTO to the particles and checked the drug content of the colloid with an established HPLC-UV method. The cytotoxicity of the particle systems on Jurkat T-lymphoma cells was analysed with flow cytometry using 4-colour staining and PIT staining. Finally, the stability in EDTA-stabilized whole blood was investigated both macro- and microscopically.

Results

Upon BSA addition to the particles, we first observed a destabilisation of the particles, but at higher protein concentrations the colloid became remarkably stable, with zeta potentials lying below -40 mV. The average diameter of the aggregates was about 80 nm.

TEM images showed particles with a core size of 7,64 ± 1,68 nm. After addition of BSA, we both observe a brittle layer of protein on particle clusters as well as an organic matrix in which all the clusters are located. A pH-dependent eta potential analysis showed that the Point of zero charge (PZC) of the particle system lies around 4,5-5, which is quite consistent with the isoelectric point of BSA. FTIR measurements showed the presence of BSA and iron oxides in the matrix, whereas the lauric acid is only visible after partial removal of the protein corona. At physiological pH, the particles are colloidally stable even in whole blood containing EDTA.

As expected, the samples show superparamagnetic behaviour due to the size of the iron oxide nanoparticles used. The investigations also proved that the addition of the BSA has no major influence on the magnetic properties of the system.

The toxicity of the surfactant-stabilized system is also drastically decreased by the protein coating. The Jurkat cells stay metabolically active, their DNA and their cell membrane stays intact at concentrations up to 100 µg/ml, where surfactant-stabilized particles already show significant toxic effects. When loaded with 300 µg/ml MTO, the protein-coated nanoparticles exhibit excellent cytotoxic effectivity, similar to the one of pure MTO.

Conclusions

Core-shell Lauric acid/BSA coated particles were synthetized by a surface adsorption reaction. The excess BSA forms a matrix in which the agglomerates are located. The synthetized particles exhibit excellent stability, even in complex biorelevant media like whole blood. The magnetic properties are not significantly affected by the artificial protein corona. The BSA coating greatly increases the biotolerability and –compatibility. The loading capacity of the colloid for MTO is very promising, the colloid stays stable even at payloads of 300 µg/ml of drug. The so-prepared system shows excellent toxicity when loaded with MTO, the potency of the drug is not affected by its coupling to the nanoparticles. Thus, we conclude that the prepared core-shell SPIONs exhibit optimal properties for drug delivery purposes and because of its simplicity and reproducibility, is ideal for GMP production.

Acknowledgments

DFG SPP1681 (AL552/5-1), Else Kröner-Fresenius Stiftung (Bad Homburg v. d. H.), Germany;
Bavarian Ministry for Environment and Health (74-U8793-2012/7-35); Margarete Ammon Stiftung, Munich, Germany.

References

[1] A K Gupta, R R Naregalkar, V D Vaidya, M Gupta.: Recent advances on surface engineering of magnetic iron oxide nanoparticles and their biomedical applications; Nanomedicine (Lond). 2007 Feb;2(1):23-39

[2] E Amstad, M Textor, E Reimhult: Stabilization and functionalization of iron oxide nanoparticles for biomedical Applications; Nanoscale. 2011 Jul;3(7):2819- 43. doi: 10.1039/c1nr10173k. Epub 2011 May 31.

[3] I Toth, E Illes, R Bauer, D Nesztor, M Szekeres, I Zupko, E Tombacz: Designed Polyelectrolyte Shell on Magnetite Nanocore for Dilution-Resistant Biocompatible Magnetic Fluids, *Langmuir*, 2012, *28* (48), pp 16638–16646

[4] R Tietze, S Lyer, S Dürr, T Struffert, T Engelhorn, M Schwarz, E Eckert, T Göen, S Vasylyev, W Peukert, F Wiekhorst, L Trahms, A Dörfler, C Alexiou: Efficient drug-delivery using magnetic nanoparticles – biodistribution and therapeutic effects in tumour bearing rabbits, Nanomedicine 9 (2013) pp 961-971

[5] S Dürr, R Tietze, S Lyer, C Janko, E Schreiber, J Mann, R Turcu, K Gitter, S Odenbach, S Vasylyev, M Herrman, W Peukert, C Alexiou: Characterizations of drug carrying magnetic nanoparticles for tumor therapy: biological outcome and first immunological aspects, Magnetohydrodynamics Vol. 49 (2013), No. 2 -4, pp 191-198

[6] D.Bica, L Vekas, M V Avdeev, O Marinica, V Socoliuc, M Balasoiu, V Garamus. Sterically stabilized water based magnetic fluids: Synthesis, structure and properties; JMMM 311 (2007) pp 17–21

Ferrofluid Volume between Plates in the Field of an Electromagnetic Coil

T.I. Volkova[1,2], V.A. Turkov[1], K. Zimmermann[2], and V.A. Naletova[3]

[1]*Lomonosov Moscow State University, Institute of Mechanics, Michurinskii Pr. 1, 119192 Moscow, Russia*
[2]*Faculty of Mechanical Engineering, Technische Universität Ilmenau, PF 100565, 98684 Ilmenau, Germany*
[3]*Faculty of Mechanics and Mathematics, Lomonosov Moscow State University, GSP-1, Leninskie Gory, 119991 Moscow, Russia*

Introduction

The transfer of elastic wave energy from the source to the object of influence is a general challenge in applied acoustics. Magnetic fluid (MF) can be used for the creation of an acoustic duct in the slot gap between the surfaces of these objects [1]. Under an applied alternating magnetic field, the instability of the MF volume can occur, which leads to stepwise changes and hysteresis of the MF surface shape. In [2], the static surface shape of an MF volume between horizontal plates is investigated theoretically. In [3], the MF surface shape between horizontal plates in the field of an electromagnetic coil is calculated numerically.

Formulation of the Problem

In this work, the surface shape of a finite volume of an incompressible MF between horizontal plates is studied both theoretically and experimentally. The MF is surrounded by a nonmagnetic fluid with a smaller density. The magnetic field is generated by a coil with inserted ferrite core, which is positioned above the top plate [3]. The MF magnetization is described by the Langevin's law. The perturbation of the applied magnetic field is neglected. Thus, the MF volume is under the influence of gravitational, magnetic, and capillary forces. The theoretical investigation of the problem was done based on the principle of minimum energy of the system under the condition of the MF volume conservation. Sufficient conditions to determine the surface shapes, on which the energy has a local minimum, were obtained.

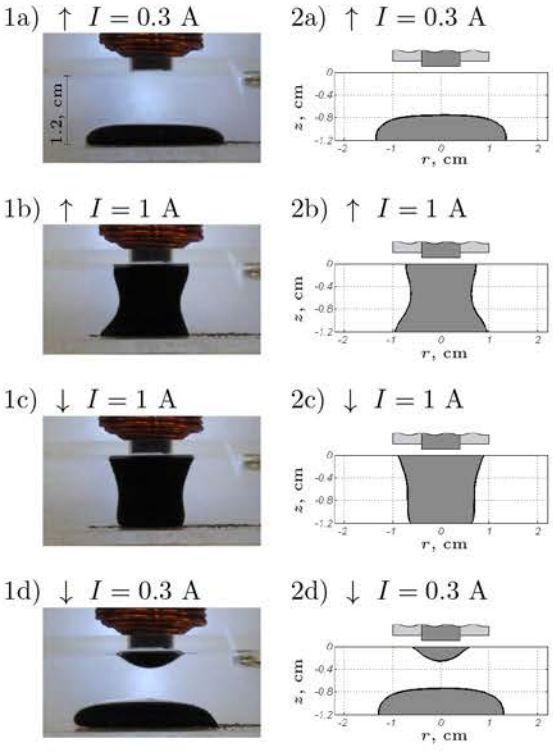

Figure 1: Experimental (1) and numerical (2) results of the surface shape of a MF volume of 2 cm^3, when the current I increases (a,b) and decreases (c,d) quasistatically with a stepsize of ≈ 0.01 A

Experimental and Numerical Results

The applied current range in the experimental setup designed to observe the process of transformation of the MF volume in the field of an electromagnetic coil, is 0–2.6 A. The maximum magnitude of the magnetic field between horizontal plates is up to 655 Oe. The water-based MF ($\rho_{\mathrm{MF}} = 1.1$ g/cm^3, $M_{\mathrm{S}} = 12$ G) surrounded by the polymethylsilicone liquid ($\rho = 0.913$ g/cm^3) was used in the experiments. It was shown that qualitatively different forms of the MF can exist for the same applied current (Fig. 1, 2). There are several different ways of creating the MF bridge between plates. Abrupt and hysteretic behaviours were observed, when the applied magnetic field changed quasistatically (Fig. 2). Additionally the contact angle hysteresis was found in the experiments, which had been taken into account in the numerical calculations (Fig. 1, b,c). The numerical calculations of the static MF surface shape for the given parameters of the problem agree with the experimental data (Fig. 1, 2).

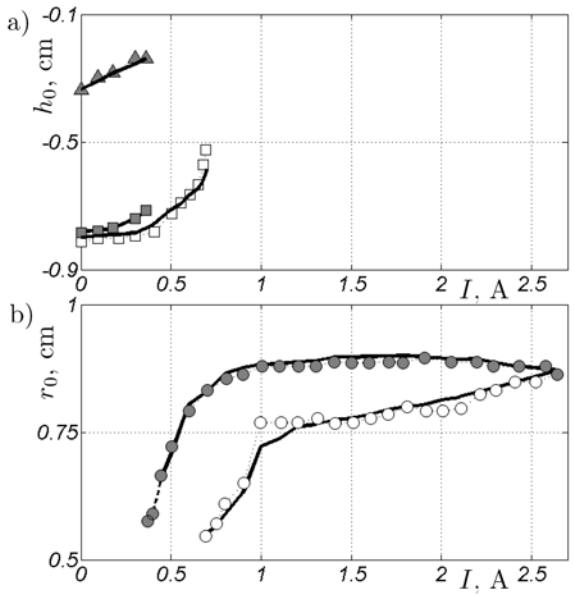

Figure 2: Dependence of the characteristic coordinates h_0 (a) and r_0 (b) on I obtained experimentally (markers) and numerically (solid lines) for an MF volume of 2 cm^3, when the current increases (white markers) and decreases (grey markers) quasistatically: □ – the drop on the lower plate; △ – the drop on the upper plate; ○ – the MF bridge between plates. h_0 is the distance from the top of the drop to the upper plate; r_0 is the radius of the contact spot of the MF bridge with the upper plate

Conclusions

The obtained results of the transformation of the MF volume in non-uniform magnetic field can be used to design systems based on MF (acoustic ducts, seals, valves) in which the alternating magnetic field is used and stepwise changes and hysteresis of the surface shape are possible.

Acknowledgments

This work is supported by the Russian Foundation for Basic Research in the framework of projects Nos. 14-01-31146, 14-01-90003, and 14-01-91330.

References

[1] A.R. Baev, G.E. Konovalov, and A.L. Maiorov. Magnetic Fluids in Technical Acoustics and Non-Destructing Control (Tekhnalogiya, Minsk, 1999) [in Russian].

[2] T.I. Volkova and V.A. Naletova: Instability of the Magnetic Fluid Shape in the Field of a Line Conductor with Current. Fluid Dynamics, Vol. 49, No. 1, 2014, pp. 3–10.

[3] T.I. Volkova, V.A. Naletova and V.A. Turkov: Magnetic Fluid Volume between Horizontal Plates in the Field of an Electromagnetic Coil. Magnetohydrodynamics, Vol. 49, No. 3–4, 2013, pp. 386–390.

Supramolecular magnetic filaments: fundamental physics and potential applications

Pedro A. Sánchez[1], Joan J. Cerdà[2], Tomás Sintes[2], Sofia S. Kantorovich[1,3]

[1]*Compute=rgestütze Physik, Universität Wien, Sensengasse 8/9 1090 Wien, Austria*
[2]*IFISC (CSIC-UIB), Campus Universitat de les Illes Balears E-07122 Palma de Mallorca, Spain*
[3]*Ural Federal University, Lenin av. 51, Ekaterinburg, 620000, Russia*

Artificial magnetic filaments can be obtained by mutually linking magnetic colloids with polymers or other molecules to form a permanent chain. These magnetic chains represent an equivalent of molecular magnetic polymers but at a supramolecular scale. In difference to molecular magnetic polymers, which only manifest their magnetic properties at very low temperatures, supramolecular magnetic filaments retain their magnetic properties at room temperature and zero field. Even though magnetic filaments are closely related to normal ferrofluids, the presence of the permanent links leads to specific characteristics that give to these systems a broad potential for many applications. For instance, they can be thought as improved substitutes of current ferrofluids, or as elements for magnetic data-storage devices, chemical and pressure nanosensors, nano-propellers and nano-pumps, watermark systems, non-permanent photonic crystals, or magnetoresponsive coatings, to just mention a few possible applications [1]. In this contribution we will present our recent results on the fundamental physics of magnetic filaments, obtained by means of extensive computer simulations and the application of advanced analytical theories. In particular, we will discuss the equilibrium structural behavior of single magnetic filaments in a quiescent carrier fluid, either in bulk and near attractive flat surfaces [2, 3]. We will also present the structural phase diagram for magnetic filaments whose magnetic colloids exhibit short-range LJ attractive interactions (supramolecular Stockmayer polymers) in the limit of strong dilution [4].

Acknowledgments

We thank Prof. C. Holm for his former collaboration on the subject. We acknowledge the financial support of the START project (Y 627-N27), founded by the FWF. We also thank the projects FISICOS (FIS2007-60327), GRID-CSIC, and the Vienna Scientific Cluster for the computational resources.

References

[1] H. Wang, Y. Yu, Y. Sun, O. Chen, *Nano* **6**, 1–17 (2011)

[2] P. A. Sánchez, J. J. Cerdà, T. Sintes and C. Holm, *J. Chem. Phys.* **139**, 044904 (2013).

[3] P. A. Sánchez, J. J. Cerdà, V. Ballenegger, T. Sintes, O. Piro and C. Holm, *Soft Matter* **7**, 1809–1818 (2011).

[4] J. J. Cerdà, P. A. Sánchez, T. Sintes, O. Piro and C. Holm, *Soft Matter* **9**, 7185–7195 (2013).

How frustrated can 8 dipoles be?

S. Förster[1], T. Friedrich[2], S. Mehdizadeh Taheri[1],
I. Rehberg[2], and S. Rosenfeldt[1]

[1] *Physikalische Chemie I, Universität Bayreuth, 95440 Bayreuth (Germany)*
[2] *Experimentalphysik V, Universität Bayreuth, 95440 Bayreuth (Germany)*

Motivation

The self-assembly of magnetic nanoparticles into a simple cubic lattice [1,2] triggers questions like:

- What is the overall magnetization of those clusters?
- How susceptible are they to external magnetic fields?
- What is the arrangement of the individual magnets within those clusters?

The minimal model to attack these problems consists of 8 dipoles arranged in the corners of a cube as shown below.

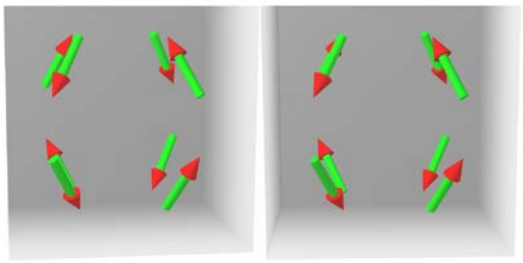

Figure 1: Stereoscopic image of one (out of many) minimal energy arrangement of 8 dipoles in simple cubic arrangement.

Method

We consider the dipole-dipole interaction of point dipoles with magnetic moments $\vec{m}_\mathrm{i} = m_0 \vec{e}_\mathrm{i}$ of equal strength m_0 oriented along the individual unit vector $\vec{e}_\mathrm{i}$. The interaction energy is then

$$U = U_0 \sum_{\mathrm{j}>\mathrm{k}} \frac{\vec{e}_\mathrm{j} \cdot \vec{e}_\mathrm{k} - 3\left(\vec{e}_\mathrm{j} \cdot \vec{e}_\mathrm{jk}\right)\left(\vec{e}_\mathrm{k} \cdot \vec{e}_\mathrm{jk}\right)}{(r_\mathrm{jk}/d)^3},$$

with $U_0 = \frac{\mu_0 m_0^2}{4\pi d^3}$, d being the edge length, r_jk is the distance between the two dipoles, and $\vec{e}_\mathrm{jk}$ is the unit vector along the line joining two point dipoles labelled with j and k [3].

The magnetic configuration is discussed in a 16-dimensional configuration space formed by the polar and azimuthal angles of the 8 dipole orientations. Using symmetry constraints, the dimensionality of the problem can further be reduced.

Results

Figure 2 shows the binding energy per particle as a function of the azimuthal and polar angles of one of the dipoles. The blue valley denotes the configuration of lowest energy, given by a binding energy per particle of

$$\frac{U}{8U_0} = -2 + \frac{\sqrt{2}}{16} + \frac{\sqrt{3}}{18}$$

Fig. 1 corresponds to one of these states within this valley.

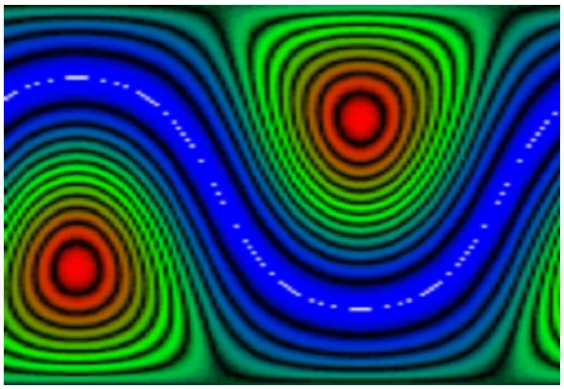

Figure 2: The field energy of 8 dipoles in a cubic arrangement is color coded as a function of the azimuthal (horizontal axis, 0° – 360°) and polar angle (vertical axis, 0°– 180°) of one of the dipoles. Blue corresponds to energy minima, red to maxima. The black and white lines are guides to the eye.

Does this valley consist of a finite number of local minima, or is it a continuous line of frustrated states?

Acknowledgments

It is a pleasure to thank Thomas Fischer and Reinhard Richter for stimulating discussions.

References

[1] A. Ahniyaz, Y. Sakamoto, and L. Bergström, PNAS **104**, 17570–17574 (2007).

[2] S. Disch, E. Wetterskog, R. P. Hermann, G. Salazar-Alvarez, P. Busch, T. Brückel, L. Bergström, and S. Kamali, Nano Letters **11**, 1651–1656 (2011).

[3] J. D. Jackson, *Classical Electrodynamics* (Wiley, New York, 2001).

First-order reversal curve (FORC-) analysis of magneto-active materials with mixed magnetic phases

J. Linke, D. Borin, S. Odenbach

Institute of Fluid Mechanics, Chair of Magnetofluiddynamics, Measuring and Automation Technology, 01062 Dresden, Germany

Introduction

Owing to advancements in measurement automation and data processing first-order reversal curve measurements (FORC) have become a feasible technique for the characterisation of magnetic materials. Standard hysteresis loops present bulk averages; by contrast, the FORC method is based on a set of minor partial hysteresis loops. They provide information of the switching field distribution and local interaction fields between particles or grains, which allows a more profound exploration of the magnetic interactions in complex hybrid materials.

Magneto-active Elastomers (MAEs)

MAEs consist of magnetic particles embedded in a non-magnetic elastomeric matrix. The samples were prepared from mixtures of spherical carbonyl iron (~5 µm size) and FeNdB-alloy particles (MQP-S, ~50 µm) in 18 mass% of silicon methyl-vinyl rubber with cross-linking agent SIEL [1]. The mixtures were degassed before curing at 70-80°C for 3 hours. The final samples were characterised in a Lakeshore 7400 vibrating sample magnetometer.

First-order reversal curve method

Prior to measuring each FORC the sample is saturated in a positive field, then the magnetisation is decreased to the reversal field H_r. Starting from this reversal field the FORC is recorded as the magnetisation M when the applied magnetic field H_a is increased back to saturation. The reversal field H_r is changed for each FORC, covering a field range from positive to negative saturation as illustrated in figure 1b. The FORCs are fitted with a second-order polynomial function using FORCinel [2] to derive the FORC distribution:

$$\mu(H_r,H_a) = -\frac{1}{2}\frac{\partial^2 M(H_r,H_a)}{\partial H_r \partial H_a} \qquad (I)$$

This distribution is plotted with an axis transformation so that the horizontal axis relates to the coercive field H_c and the vertical axis to the interaction field H_u:

$$H_c = \frac{H_r - H_a}{2},\ H_u = \frac{H_r + H_a}{2} \qquad (II)$$

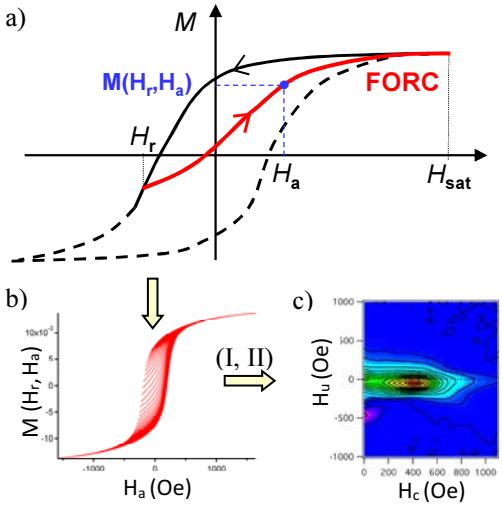

Fig. 1: a) FORC measurement protocol, b) Set of FORCs, c) FORC diagram

Results and Discussion

Samples which contain only FeNdB particles exhibit FORC distributions symmetrical to zero interaction field because they represent dipole-dipole interactions between particles of the same species. When the FeNdB particles are dispersed in a matrix, the inter-particle distance is larger compared to particles in a dense powder. The increase in the inter-particle distance reduces the dipole-dipole interactions and

the FORC distribution appears narrower because the high interaction field contributions are missing, as shown in figure 2. Hence the FORC distribution is a good monitoring tool for the quality of a sample. Sedimentation during the preparation process would reduce the inter-particle distance compared to a sample with a homogeneous particle distribution.

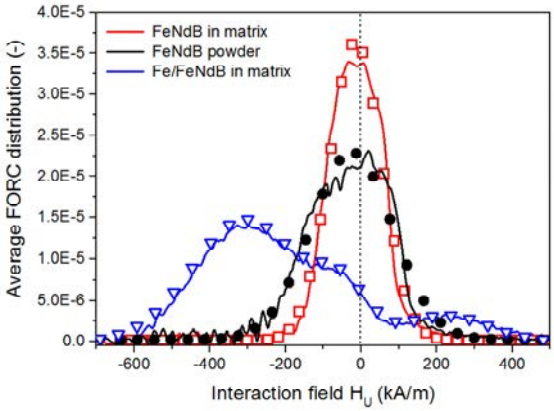

Fig. 2: Average FORC distribution (lines) with Gaussian fits vs. interaction field for dense FeNdB powder (circles), MAE with FeNdB (squares) and MAE with Fe:FeNdB 45:55 vol% (triangles)

When magnetically soft iron is introduced into the system, the FORC distribution becomes asymmetric to zero interaction field. For certain negative reversal and applied fields the magnetically hard NdFeB particles are still positively magnetised and their stray field pins the magnetically soft iron moments. This biasing effect displaces the FORC distribution of the soft phase

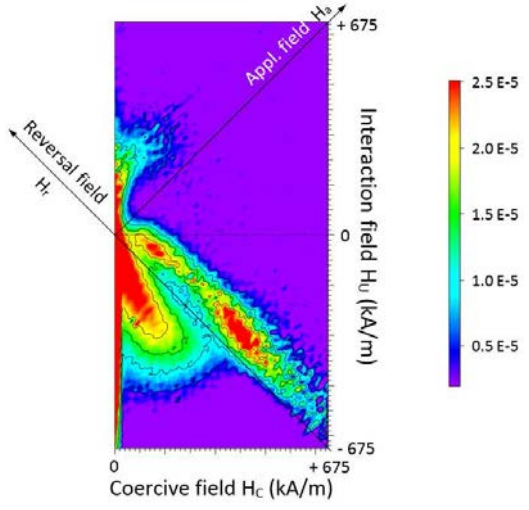

Fig. 3: FORC distribution diagram of a MAE with Fe:FeNdB 45:55 vol%

towards more negative interaction fields [3], as shown in figure 2.

For positive applied fields the FORC diagram presented in figure 3 reveals two different reversal mechanisms. The first reversal at $H_r \approx 740$ kA/m and $H_c \approx 400$ kA/m is due to the switching of FeNdB particles or clusters by domain wall motion [4]. The second reversal occurs at a lower reversal and coercive field, $H_r \approx 160$ kA/m, $H_c \approx 128$ kA/m, for those FeNdB particles which experience an additional positive magnetisation by vicinal Fe particles which have already reversed their magnetisation.

The existence of two reversal mechanisms can also be confirmed from the initial magnetisation curves and their derivatives dM_{ini}/dH_a for the unmagnetised MAEs presented in figure 4.

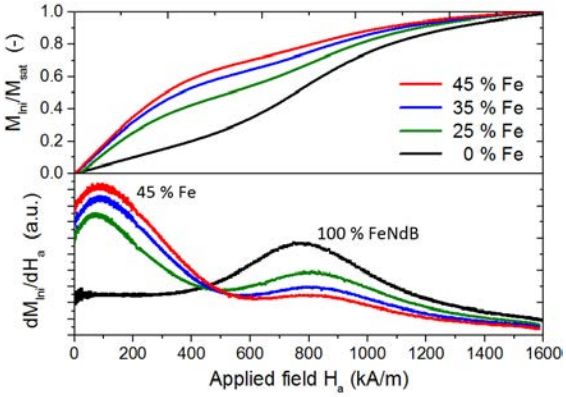

Fig. 4: Initial magnetisation curves and their derivatives by the applied magnetic field for MAEs with different Fe to FeNdB ratios

Our future work will focus on understanding the role of the elastomeric matrix during the magnetisation process in MAEs.

We gratefully acknowledge the funding by the DFG (Od18/18-3).

References

[1] D. Borin et al., J. Phys.: Conf. Ser. 412, 012040, 2013.
[2] R. J. Harrison et al., Geochem. Geophys. Geosys. 9 (5), Q05016, 2008.
[3] I. Panagiotopoulos: J. Mag. Mag. Mat. 323 (16), 2148-2153, 2011.
[4] Y. Zhang et al., J. Phys. D: Appl. Phys. 47, 015002, 2014.

Measurement of microviscosity in crosslinked polyacrylamide ferrohydrogels by Mössbauer spectroscopy

J. Landers[1], L. Roeder[2], A. Schmidt[2], H. Wende[1]

[1] *Faculty of Physics and Center for Nanointegration Duisburg-Essen (CENIDE), University of Duisburg-Essen*
[2] *Department Chemie, Institut für Physikalische Chemie, Universität zu Köln*

Introduction

While the rheology of polymer systems has been extensively studied in the past decades, the effect of direct constraint of particle movement by polymer networks in nanoparticle-hydrogel hybrids has not yet been completely understood. The use of magnetic nanoparticles as probes allows examining dynamic properties of liquid samples by ^{57}Fe-Mössbauer spectroscopy on an atomic scale. The motion of the iron ions contained in the nanoparticles is reflected in a considerable line broadening of the associated Mössbauer spectrum, so even slow translatory or rotational motion and very low relaxation times can be measured and quantified by this method.

Preparation

Several polyacrylamide (PAAm) hydrogels with different amounts of methylenebisacrylamide (MBA) as crosslinker were prepared, containing acicular hematite (α-Fe_2O_3) nanoparticles with an average length of 390 nm and an average diameter of 85 nm [1].
The hydrogel samples were mounted on a self-constructed sample holder with an integrated Peltier cooling-element. This setup allowed us to perform Mössbauer spectroscopy measurements in the 'liquid' as well as the 'solid' hydrogel state at tunable temperatures down to 245K. Mössbauer spectra were recorded up to velocities of about 200 mm/s by the combination of a laser interferometer used for calibration and a high-velocity Mössbauer driving-unit, which is essential to measure spectra with distinct line broadening.

Results

We observed static and sharp sextet spectra at temperatures up to 265K, corresponding to the frozen state without nanoparticular motion. A moderate increase of the linewidth Γ indicated beginning movement at about 270K before reaching the liquid state, while linewidths up to 30 mm/s were measured above the water melting point.
This reveals that, contrary to expectations, embedded nanoparticles are not completely immobilized even in strong crosslinked hydrogel networks. We can quantify those effects of Brownian motion by Mössbauer spectroscopy.

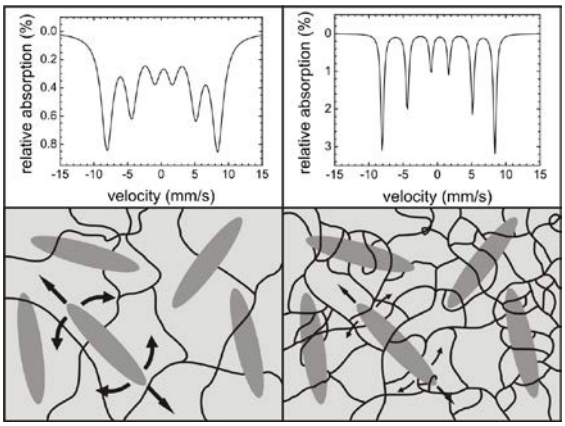

Figure 1: Hydrogel networks with different degrees of cross-linkage. Associated Mössbauer spectra (simulated, same temperature) illustrate the effect of reduced particle motion.

Theoretical calculations result in a temperature dependent effective microviscosity $\eta(T)$ estimated from $\Gamma(T)$ [2], which exceeds η_{H2O} by far and is correlated to the amount of MBA crosslinker.

Acknowledgments

This work was supported by DFG WE2623/7-1, SPP 1681. The authors are grateful to U. von Hörsten for his expert technical assistance.

References

[1] L. Roeder, P. Bender, A. Tschöpe, R. Birringer, A. M. Schmidt, *J. Polym. Sci. Part B: Polym. Phys.,* **50(24)**, 1772-1781 (2012).

[2] P. Fornal and J. Stanek, *Acta Phy*s. *Pol., A,* **114**, 1667-1673 (2008).

Magnetic Particle Nanorheology of Complex Fluids

E. Roeben, S. Teusch, M. Dörfer, M. Effertz, L. Kibkalo, A. M. Schmidt*

Department Chemie, Universität zu Köln, Luxemburger Str. 116, D-50939 Köln, D
**email: annette.schmidt@uni-koeln.de*

Motivation

Static and dynamic rheology is an established method for the investigation of the flow and deformation properties of complex fluids.
Recently, a variety of different particle-based passive and active microrheological approaches are followed, with the advantages of small sample volume and the possibility to extract local information, e. g. in microstructured systems and in biological environments.[1] In the context of nanostructured materials and composites, it opens the pathway to experience the interaction between the particles and the surrounding matrix. Special interest is paid to the relative size of the tracer particles and the structural length scale of the material under investigation.

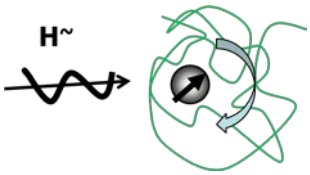

Fig. 1. Magnetic Particle Nanorheology

In this respect, different tracer particle-based microrheological methods are developed. An additional advantage is the small sample volume, enabling the exploration of the viscoelastic properties of soft matter which cannot be produced in bulk quantities like biological polymers or living cells.[1] A tracer-free method is based on dielectric spectroscopy, relating the dielectric function to the complex dynamic viscosity according to the DiMarzio-Bishop model.[2]

Method

In the present work, we introduce a novel approach to investigate the nanorheological properties of soft materials by analyzing the (complex) susceptibility of magnetic nanoprobes exposed to an oscillating magnetic field (AC susceptometry, Fig. 2).

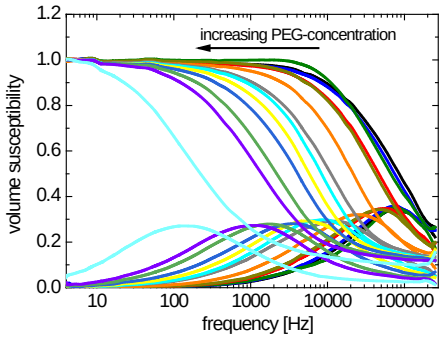

Fig. 2. AC susceptometry of aqueous PEG1000 mixtures

The resulting frequency-dependent complex susceptibility data is treated using different theoretical approaches. We demonstrate the feasibility of the approach as well as its limits on model systems based on aqueous polyethylene glycol (PEG) solutions, and ferromagnetic $CoFe_2O_4$ nanoparticles as tracer particles.

Results and Discussion

By adapting different methods including an extended Debye relaxation model, a model adapted to the DiMarzio-Bishop approach for the magnetic case, and on the Cole-Cole formalism and Havriliak-Negami equation, the experimental data can be fitted to deliver the frequency-dependent rheological properties including viscosity and loss moduli.
All applied methods are verified experimentally by using Newton fluids of various composition and viscosity based on ethylene glycol (EG) and triethylene glycol (TEG). The nanorheological results of these methods are in close correspondence with results from strain-sweep and oszillating rheology.

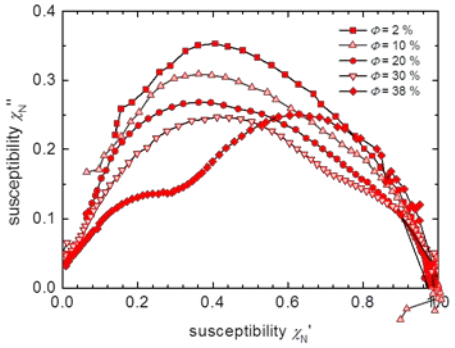

Fig. 3. Cole-Cole plots of aqueous PEG35000 mixtures

The findings are subsequently applied to aqueous PEG solutions with systematic variation of the concentration and the molecular weight of the polymer. By comparing the results with outcomes of conventional rheology, the validity and the limits of the nanorheological method are demonstrated.

Acknowledgments

We thank Stefan Roitsch for TEM. Financial support is acknowledged from DFG-SPP 1681 “Particle-Field-Interactions”.

References

[1] C. Wilhelm, J. Browaeys, A. Ponton, J.-C. Bacri, *Physical Review E* 67, 011504, **2003**

[2] E. A. DiMarzio, M. Bishop, *J. Chem. Phys.* 60, 3802-3811, **1974**

The effect of the addition of magnetic micro particles on the mechanical properties of soft polyurethane foams

M. Schümann and S. Odenbach

Chair of Magnetofluiddynamics, Measuring and Automation Technology, Technische Universität Dresden, Dresden 01062, Germany

Introduction

Magnetoelastic foams are a new kind of magnetic field-responsive smart materials developed in the last years. Due to their high elasticity, soft foams loaded with magnetic particles show a great potential for an usage as magnetorheological material [1].
An investigation on the mechanical properties is essential to gain a fundamental understanding of the complex behaviour of this new material.
In the frame of this work, compressive tests with polyurethane foam samples loaded with magnetic microparticles were performed. The results were compared with those of solid, bubble free elastomer samples and a theoretic model of the mechanical behaviour of particle loaded elastomer foams, based on the Gibson-Ashby model.

Materials and Methods

All investigated foam samples were prepared using components provided by the company Elantas Beck GmbH. BASF Carbonyl iron powder CIP CC (d50 = 3.8-5.3 µm) was used as magnetic particles in concentrations up to 50 wt%. Besides the foam samples bubble free elastomer samples were prepared with slightly altered components.
For all samples stress-strain curves were captured with a DYNA-MESS universal testing machine. For the initial linear part of the curve, Young's modulus was evaluated.

Pore Size Distribution

In an earlier investigation utilizing the same foam material and particles the effect of the particles on the foam structure was examined. It was shown, that the frequency distribution of pore sizes could be described with the Weibull function and that the Weibull distribution parameters are significantly affected by the particle concentration. For an increase of concentration, this is apparent as a general shift of the pore sizes towards smaller pores, but also as an increase of the amount of scarce, very large pores. At high particle concentration these large pores are visible to the eye.

Stress-strain curves and the Gibson-Ashby model

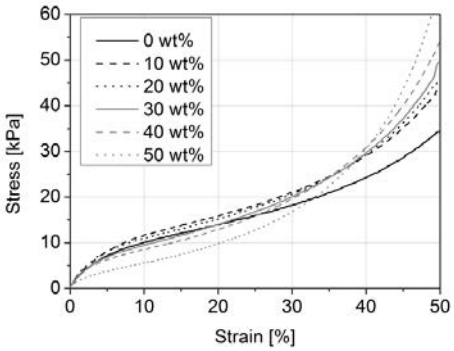

Figure 1: Stress-strain curves of the foam samples with up to 50 wt% particles.

Figure 1 shows the averaged stress-strain curves for the examined particle concentrations. The foam-typical shape of the curves, consisting of three regions is apparent. These stages of compression were explained by Gibson et al. [2]: The initial linear elastic behaviour is caused by the bending of the cell walls, the following plateau area is caused by the buckling of these, whereas high strains lead to a touching of the cell walls, which creates the final densification region.
Based on geometric considerations on a simplified foam structure model shown in Figure 2, the Gibson-Ashby model allows a prediction of Young's modulus of the foam.

Based on the works of Goods et al. [3] the Gibson-Ashby model was enhanced taking into account the effect of the particles on the matrix material.

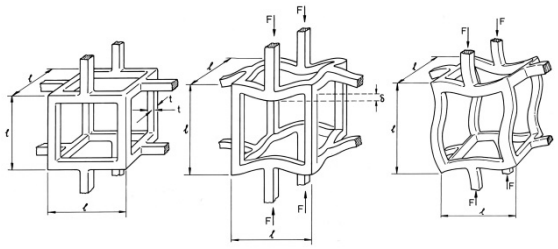

Figure 2: Monodisperse cubic cells used in the Gibson-Ashby model: no compressive load, linear elastic bending, buckling [2]

Results

As visible in Figure 3, Young's modulus of the foams decreases with increasing particle concentrations. With the results of the reference samples it can be concluded, that the behaviour of the matrix material alone shows an increase of Young's modulus with increasing particle concentrations. Thus it can be concluded, that the mechanical behaviour of the foams is dominated by the effect of the particles on the pore structure, which is, as sad, significant. The appearing larger pores lead to a weakening of the pore structure and thus of the compressive strength.

The calculation of theoretic Young's modulus with the enhanced Gibson-Ashby model by Goods et al. shows also a slight increase of Young's modulus as a result of reinforcement of the matrix by the particles.

The main reason for the large deviation of the calculated values is the simplification of the pore geometry of the Gibson-Ashby model. In contrast to the model, the analysed real foam shows pores that are rounded with sturdy non equal diameter beams. Their size follows the broad Weibull distribution.

Last but not least, the model does not regard the effect of the particles on the pore sizes, which has the most dominant effect on the mechanical properties of the foam.

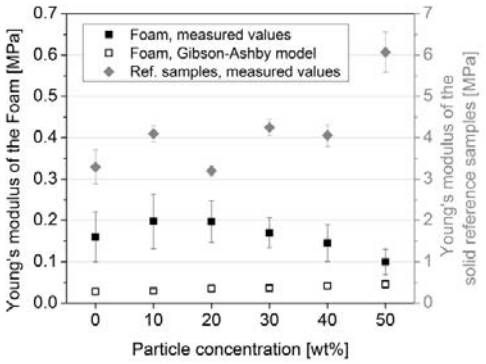

Figure 3: Comparison of the measured Young's modulus of the foam samples and those, calculated from the enhanced Gibson-Ashby model for various particle concentrations of the foam. Also pictured are Young's modulus for the bubble free reference samples.

Conclusion

Through the comparison of Young's modulus of the foams with theoretical calculations and measurements with solid reference samples it could be shown, that the addition of particles leads to a weakening of the compression properties. This is caused by a major effect of the particles on the foam structure. The expected mechanical enhancement of the foam by addition of particles could not be confirmed with the observed material, reason being the comparatively small effect of the particles on the stiffness of the matrix material.

Acknowledgements

We gratefully thank the company Elantas Beck GmbH for providing the components. Financial support by DFG (Grant. No. OD18/21) within SPP1681 is gratefully acknowledged.

References

[1] Gong Q, Wu J, Gong X, Fan Y, Xia H RSC Advances **3** 3241 (2013)

[2] Gibson L. J., Ashby M. F. Cellular solids: structure and properties. Cambridge university press (1997)

[3] Goods S. H., Neuschwanger C. L., Whinnery L. L., Nix W. D. J. Appl. Polym. Sci. **74** 2724 (1999)

Further Abstracts
(Posters)

Ground State Clusters of Magnetic Cubes.

Joe G. Donaldson[1], Sofia S. Kantorovich[1,2]

[1] *Faculty of Physics, University of Vienna, Boltzmanngasse 5, A-1090 Vienna, Austria*
[2] *Ural Federal University, Lenin av. 51, Ekaterinburg, 620000 Russia*

Traditionally ferrofluids are composed of spherical ferro (or ferri) -magnetic particles suspended in a carrier liquid. However, with the increasing sophistication of colloidal synthesis techniques, deviations from spherical particle geometry are now possible. Numerous examples of these magnetic particles exist such as spheroids and rods, as well as more unusual shapes [1]. We are particularly interested in the cube, or cube-like structures, which nowadays form an active area of experimental research. In contrast to spheres, these alternative geometries are anisotropic; their interactions with each other is characterised by directionality. Given the fact that magnetic interactions are inherently anisotropic as well, an interesting interplay between the two is expected. This scenario allows one to study the consequences of the internal and external anisotropy on cluster formation.

In order to describe the macroscopic properties of this system we first consider its behaviour on the microscopic scale at low temperatures. We have performed molecular dynamics computer simulations in order to determine ground state structures [2]. For simulation purposes our model consists of constituent spheres which form the cubic particle's surface. The magnetic behaviour is approximated as a point dipole positioned centrally within the cube. To date we have considered two different orientations for the dipole: one in which the direction is along the [100] crystallographic axis and the second, along the [111] axis. The particles are confided to quasi-two dimensions (Q2D) , whereby the particle centres are limited to two dimensions but the dipole is allowed to rotate in three dimensions [3].

Predictions of the more favourable configurations have been made by analytical calculations of the magnetic energy of idealised Q2D structures, such as chains, rings and combinations of each. It has been shown that for the [100] orientation, chain formation is dominant at low T and, depending on system confinement, antiparallel agglomeration of these chains occurs. For the [111] orientation the situation is more difficult to rationalise, however clusters tend to form planar structures, within which dipoles form rings typically consisting of four dipoles. Knowledge of cluster formation at these low temperatures will allow us to extrapolate and understand those appearing at higher temperatures. In time this will enable predictions to be made about the macroscopic regime, such as thermodynamic and magnetic properties.

Acknowledgments
Austrian Science Fund (FWF):
START-Project Y 627-N27.

References

[1] S. C. Glotzer *et. al*, Nat. Mater., 2007, **6**, 557-562

[2] B. S. John *et. al*, J. Chem. Phys., 2004, **120**, 9383-9389

[3] T. A. Prokopieva *et. al*, Phys. Rev. E, 2009, **80**, 031404

The influence of polymer-coated superparamagnetic nanoparticles on the survival-associated Akt signalling pathway in human blood-brain barrier-forming cells

Christine Gräfe[1], Franziska Bähring[1], Christian Bergemann[2], Florian Schlenk[3], Dagmar Fischer[3], Andreas Hochhaus[1], Joachim H. Clement[1]

[1]Abt. Hämatologie/Internistische Onkologie, Universitätsklinikum Jena, Erlanger Allee 101, 07747 Jena, Deutschland, christine.graefe@med.uni-jena.de
[2]chemicell GmbH, Eresburgstrasse 22-23, 12103 Berlin, Deutschland
[3]Institut für Pharmazie, Abt. Pharmazeutische Technologie, Friedrich-Schiller-Universität Jena, Otto-Schott-Straße 41, 07745 Jena, Deutschland

Introduction

Based on their unique and versatile features nanomaterials attract widespread interest in both research and industry. While several iron oxide-based nanoparticles (NP) are already clinically approved for human application as contrast agents their actual biological effect on the distinct tissues or individual cell is still unclear. As the human blood-brain barrier is a critical and sensitive interface necessarily exposed to systemically applied NP we investigated the NP-induced effect on the central Akt signalling pathway in human blood-brain barrier-forming cells.

Methods

Human brain microvascular endothelial cells (HBMEC) representing an important component of the blood-brain barrier, were cultured in RPMI1640 + 10% fetal calf serum. Long-term real-time cell viability analysis was performed with the xCELLigence system (Roche Applied Bioscience). Subconfluent cell layers were exposed to 25µg/cm^2 NPs comprising coatings of different polymers, i.e. carboxymethyldextran (anionic), starch (neutral), and polyethylenimine (PEI-750kDa, cationic).The Akt signalling pathway was studied via immunoblotting using phospho-Akt(Ser473) and pan-Akt antibodies. Transcription levels of Akt target genes *BIRC5* and *FOXO3* were analysed by quantitative PCR. Immunofluorescent staining using AF647-labeled anti-Foxo3 antibodies revealed subcellular distribution of Akt-target protein.

Results

Real time cell analysis via impedance measurements reveal that HBMEC tolerate both neutral and anionic NP at concentrations up to 100µg/cm^2, whereas cationic NP reduce cellular viability at concentrations exceeding 25µg/cm^2. Signaling cascade analyses reveal a two-fold increase of phospho-AKT after incubation with cationic particles potentially triggering survival cascades. PEI polymers alone show similar but less pronounced effects. Anionic NP formulations slightly but persistently increase Akt phosphorylation by 40%. Transcription levels of Akt-activated *BIRC5* are increased by all NP and free polymer formulations, whereby cationic ones show the most pronounced effects. The Akt target protein Foxo3 appears to be regulated in treated HBMEC, too. Thus, immunofluorescent staining show pronounced Foxo3 nuclear translocation upon exposure to cationic NP.

Conclusion

We show that neutral, anionic and cationic iron-oxide nanoparticles affect blood-brain barrier forming HBMECs in central cellular signalling. Especially cationic PEI-coated but also anionic CMX-coated NP increase the essential survival-associated pathways. Nevertheless the consequences for the individual cell and the integrity of the tissue remain to be investigated.

This work was supported in part by DFG high priority program 1681, CL202/3-1, and by the BMBF joint research project NanoMed, FKZ 03X0104D

Peristaltic Transport of a Magnetizable Fluid by a Periodically Travelling Magnetic Field

J. Popp[1], I. Zeidis[1], V.A. Naletova[2], T. Kaufhold[1], V. Böhm[1], R. Gärtner[1], K. Zimmermann[1]

[1]*Department of Technical Mechanics, Faculty of Mechanical Engineering, TU Ilmenau, PF 100 565, 98684 Ilmenau*
[2]*Department of Mechanics and Mathematics, Moscow State Lomonosov University, Moscow, 119992, Russia*

Peristaltic material transport of a magnetizable fluid can be affected by a periodically traveling, inhomogeneous magnetic field. [1] accounted on this effect due to experiments. The analytical problem was presented by [2] for a thin layer of a viscous, magnetizable fluid in an periodical, inhomogeneous magnetic fields, in search for a causative magnetic field, while the surface deformation was known.
The present paper describes the inverse problem, [3]. The evidence of the peristaltic transport of a magnetizable fluid caused by a inhomogeneous magnetic field is provided.

Setting of the Problem

Considered is a plane flow $\boldsymbol{v}^* = (u^*, 0, w^*)$ of a magnetizable fluid with the magnetic permeability μ, the kinematic viscosity ν, the density ϱ, and the coefficient of surface tension γ set on a horizontal, rigid and impermeable wall, within the influence of gravitation, see the configuration in figure (1). A periodically, alternating magnetic field H^{*2} is applied to the fluid, which is defined

$$H^{*2} = H_0^2 + A^{*2}(z^*)\sin(\zeta), \qquad (1)$$

with $\zeta = k^* x^* - \omega^* t^*$. Here, H_0 is the unperturbed magnetic field strength, A^{*2} the amplitude of the perturbation, x^* and z^* are coordinates, t^* the time, k^* the wave number, and ω^* the angular frequency,

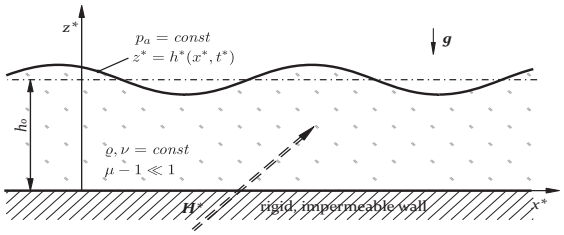

Figure 1: Sketch of the considered system

asterisks mark dimensions. Under the influence of the magnetic field the free surface is periodically deformed and assumes the shape $z^* = h^*(x^*, t^*)$.

Approach

Working non-dimensionalized, the occuring Reynolds number is assumed to be small. With this, the Stokes approximation, the two-dimentional continuity equation and the introduction of the stream function $\Psi(z, \zeta)$ are applied to create the harmonic differential equation

$$0 = \Delta\Delta\Psi(x, z, t). \qquad (2)$$

The kinematic boundary conditions are $\boldsymbol{v} = 0$ at the motionless wall ($z = 0$) and $0 = h_{\prime t} + h_{\prime z} u - w$ at $z = h(x, t)$. The undulating free surface provides a dynamic condition, which is subjected to the non-inductive approximation

$$[-p + \frac{\gamma}{h_0 P_c R} - \frac{(\mu - 1)}{8\pi}\frac{H_0^2}{P_c} \times \\ \times(1 + \varepsilon\sin(\zeta))]\mathbf{n} + \boldsymbol{\tau}_{ij} n_j e_i = \mathbf{0}. \qquad (3)$$

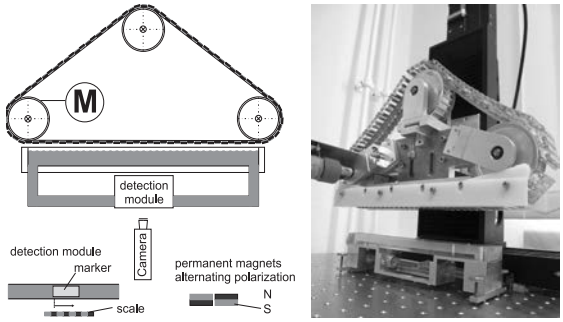

Figure 2: Experimental setup.

with p the fluid and P_c the characteristic pressure, R the radius of surface curvature, τ the viscous stress tensor. The structures of the magnetic field, which forms a power series with regard to the small parameter $\varepsilon = H_0^2/A^2(h_0) \ll 1$ and also a periodic character, are applied in the approach on the stream function Ψ and the perturbed surface contour $h(x,t)$.

$$\Psi(x,z,t) = \Psi_0 + \sum_{n=1}^{\infty} \varepsilon^n \Psi_n(z,\zeta), \qquad (4)$$

The averaged flow rate adopts the same structure of a power series with regard to ε, whereas for its first non-zero member must be solved

$$\bar{Q}_2 = \frac{k}{2\pi} \int_{kx-2\pi}^{kx} \Psi_1(1,\zeta)\Psi_{1'z}(1,\zeta)\,\mathrm{d}\zeta. \quad (5)$$

Solution

The redimensionalized average flow rate states the analytical non-zero solution of the peristaltic material transport.

$$\bar{Q}^* = \frac{A^4 \varkappa^2 k^{*2} h_0^2 \omega^* (\sinh(\lambda) - \lambda)}{\Lambda}, \quad (6)$$

where $\lambda = 2k^* h_0$ and

$$\Lambda = (\varrho g + \gamma k^{*2})^2 (\sinh(\lambda) - \lambda)^2 + \\ + 4k^{*^2} \varrho^2 \nu^2 \omega^{*2} (1 + \cosh(\lambda) - \lambda^2/2)^2.$$

The experimental validation, the setup in figure (2), confirmed the positive peristaltic material transport qualitatively, see

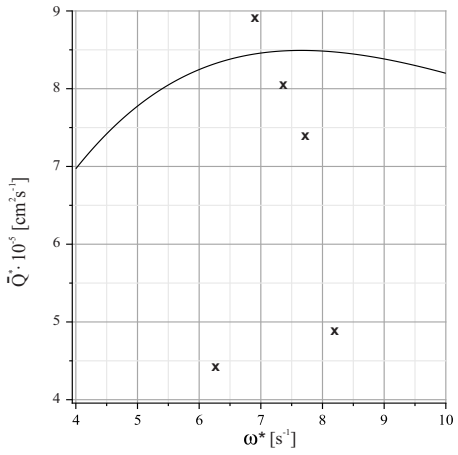

Figure 3: Experimental (diagonal cross) and analytical (solid line) results.

figure (3). A quantitative aberration is stated by exceeding experimental values owing to the compromises in favor to the feasibility of the monitoring a small effect.

Acknowledgments

This work is supported by DFG (project Zi 540–14/1), the RFBR (project 10–01–91333) and the free state of Thuringia, Germany (postgraduation scholarship).

References

[1] Friedrich, T., Rehberg, I. & Richter, R. 2010 Magnetic traveling-stripe forcing: Enhanced transport in the advent of the Rosensweig instability. *Phys. Rev. E* **82**, 3, 036304.

[2] Zimmermann, K. & Zeidis, I. & Naletova, V.A. & Turkov, V.A 2004 Travelling waves on a free surface of a magnetic fluid layer. *J. Magn. Mag. Mat.* **272**, 2343–2344

[3] Popp, J. 2012 Theoretical and Experimental Investigations of Ferrofluids Focusing on Locomotion Systems. *PhD thesis*, Technische Universität Ilmenau

Magnetically Actuated Compliant Locomotion System

T. Kaufhold[1], V. Böhm[1], I. Zeidis[1], K. Zimmermann[1]

[1] *Technische Universität Ilmenau, Department of Mechanical Engineering, Technical Mechanics Group, Ilmenau, D-98693, phone: +49-3677-69-2474, fax: +49-3677-69-1823, e-mail: tobias.kaufhold@tu-ilmenau.de, valter.boehm@tu-ilmenau.de, klaus.zimmermann@tu-ilmenau.de*

Introduction

A lot of conventional terrestrial locomotion systems have disadvantages like a restricted mobility and a complex assembly, because they are using conventional actuation principles [1]. The resulting problems are that they have a limited field of application and that they are difficult to miniaturize.
Therefore, a biologically inspired locomotion system was developed in [2]. This system uses a compliant elastomeric structure with embedded permanent magnets in combination with a magnetic actuation for locomotion. Inspired by [3], the system introduced in [2] was advanced and simplified by using magneto-sensitive elastomers. This paper describes the advanced locomotion system. In contrast to the known locomotion systems of this kind, the current system enables locomotion in the plane with only a single actuator.

Modelling aspects

The goal was the realization of a planar compliant locomotion system with a simple assembly. Therefore, a compliant magneto-sensitive elastomeric structure with a geometry based on an equilateral triangle was considered (Fig. 1).

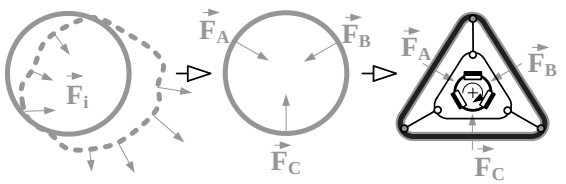

Fig. 1. Abstraction of the simulation model.

The idea for the realization of a simple actuation is based on permanent magnets which are attached to the shaft of a rotary drive, inside of the structure. Due to the rotation of the drive, a periodic deformation of the structure occurs because of the attractive forces between the magnets and the magneto-sensitive elastomeric structure, since the structure only passively reacts to a magnetic field and not actively operates as an actuator (Fig. 1).
To be able to move in the plane the system uses an asymmetric geometry of the compliant magneto-sensitive elastomeric structure.
Due to the mechanical compliance of the planned prototype and the used asymmetry the modes of vibration are complex and the locomotion performance of the system is highly dependent on the driving frequency. To analyze this specific behavior we focus on the description of the mechanical point of view. According to the specific task, geometric nonlinear transient structural finite element analyses were carried out. A detailed description of the fundamental method is given in [2].
For a first specification of the dynamic system performance, modal analyses, using the Block Lanczos solver, were performed and evaluated. Two characteristic types of eigenmodes were found: longitudinal oscillations along the symmetry axis and rotational oscillations around the vertical axis.
To describe the movement of the system dependent on the driving frequency, transient dynamic geometric nonlinear analyses, including all contact conditions and Coulomb-Friction between the elastomeric structure and ground, were carried out. Therefore, the magnetic field and the actuating forces were determined by magnetostatic simulations in dependence of the position of the permanent magnets (Fig. 2).
The numerical simulations prove the locomotion of the system. In accordance to the results of the modal analysis, the locomo-

tion direction and velocity can be changed by varying the driving frequency.

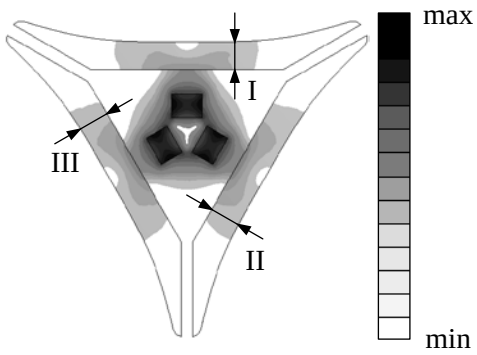

Fig. 2. Simulation of the magnetic flux density. (Initial position of the magnets, I=4.5 mm, II=III=5 mm).

Experimental evaluation

Based on the theoretical considerations a prototype was developed and built (Fig. 3; diameter: 67.5 mm, height: 23 mm, total mass: 21.6 g).

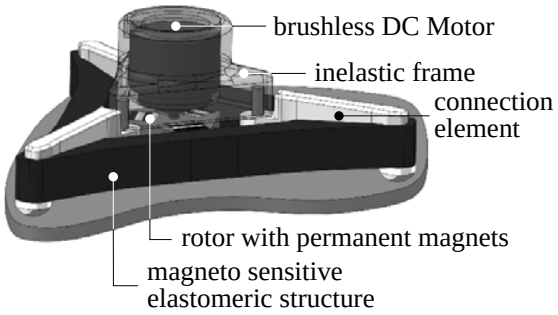

Fig. 3. Basic configuration of the locomotion system.

The periodic deformation is magnetically induced only by one central rotary drive (DC-Gear-motor). Attached to the shaft of the motor are six permanent magnets (material: NdFeB, dimensions: 5x5x2 mm³, residual induction 1.37 T) in pairs of two. The magneto-sensitive elastomer body has a mass of 12.7 g and is made of addition-curing silicone elastomer (shore hardness: A8). The mass ratio of the silicone elastomer and carbonyl iron particles (particle size 6 μm) is 3:1. The particles were added to the silicone elastomer during the manufacturing process and the composite was vulcanized in absence of a magnetic field.
The experiments have shown that the prototype is able to move in the plane and, in accordance to the theoretical analyses, the velocity as well as the locomotion direction of the system depends on the output speed of the motor (Fig. 4). A maximum average speed of 6.54 mm/s (at 150 rpm) was determined.

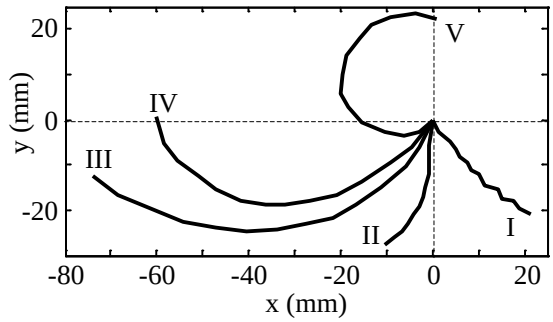

Fig. 4. Planar motion of the prototype at different output speeds of the motor. I: 100 rpm, II: 117 rpm, III: 133 rpm, IV: 150 rpm, V: 167 rpm. Time interval for all speeds: 13 s.

Future work is addressed to increase shape variability of the system, determine optimal control strategies, and investigations on the behavior of the robots at loose/compliant ground and in liquid media.

Acknowledgments

This work was supported by DFG as part of priority program 1681 grant ZI 540-17/1.

References

[1] K. Zimmermann, I. Zeidis, C. Behn, “Mechanics of Terrestrial Locomotion – With a Focus on Non-pedal Motion Systems”, Springer, Berlin, 2009.

[2] T. Kaufhold, V. Böhm, K. Zimmermann, “Design of a miniaturized locomotion system with variable mechanical compliance based on amoeboid movement” in Proc. of the 4th IEEE RAS & EMBS Int. Conf. on Biomedical Robotics and Biomechatronics, Roma, 2012, pp. 1060 – 1065.

[3] K. Zimmermann, V. Böhm, I. Zeidis, “Vibration-driven mobile robots based on magneto-sensitive elastomers,” in Proc. of the IEEE/ASME Int. Conf. on Intelligent Advanced Mechatronics, Budapest, 2011, pp. 730-735.

Concentration-Dependent Diffusivity in Binary Fluids

L. Sprenger[1], A. Lange[1], A. Yu. Zubarev[2] and S. Odenbach[1]

[1] *TU Dresden, Institute of Fluid Mechanics, Chair of Magnetofluiddynamics, Measuring and Automation Technology, 01062 Dresden, Germany*
[2] *Department of Mathematical Physics, Urals State University, 620083 Ekaterinburg, Russia*

Introduction

Since a lot of applications of ferrofluids on the one hand depend on the amount of magnetic nanoparticles dispersed and on the other of the temperature applied, transport processes driven by concentration or temperature gradients have to be investigated theoretically as well as experimentally. Molecular diffusion in ferrofluids is often regarded theoretically while thermal diffusion is mostly investigated experimentally. In the following an experimental approach to the molecular diffusion coefficient D is as well presented as a theoretical ansatz for the thermal diffusion coefficient D_T. Both values then lead to the Soret coefficient $S_T = D_T/D$ as characteristic of thermal diffusion.

Theoretical Thermal Diffusion

Diffusion due to a gradient in concentration (c) and temperature (T) is described by the phenomenological mass flux $\vec{j}$ [1]

$$\vec{j} = -\rho \left(D\vec{\nabla}c + D_T c(1-c)\vec{\nabla}T \right) \quad (1)$$

with the fluid's density ρ. A thermodynamic approach for the particle density flux

$$\vec{j}_{pd} = -D_{th}\vec{\nabla}n - D_{T_{th}}\vec{\nabla}T \quad (2)$$

leads to the mass flux ($\vec{j} = V_p \rho_p \vec{j}_{pd}$)

$$\vec{j} = -\rho \left(D_{th}\vec{\nabla}c + V_p \frac{\rho_p}{\rho} D_{T_{th}}\vec{\nabla}T \right) , \quad (3)$$

where D_{th} and $D_{T_{th}}$ denote the theoretical molecular and thermal diffusion coefficient. V_p and ρ_p stand for one particle's volume and density. Based on an ansatz of Batchelor [2] and Buyevich [3], the general mobility term β of the ferrofluid is

$$\beta = \frac{(1-\varphi_h)^{4.5}}{3\pi\eta_{CL}(d+2s)} \quad (4)$$

with η_{CL} being the carrier liquid's viscosity, and $(d+2s)$ the particles' hydrodynamic diameter. β enters the description of D_{th} [6]

$$D_{th} = \beta k_B T \left[1 + 2\varphi_h \frac{4-\varphi_h}{(1-\varphi_h)^4} \right] \quad (5)$$

as well as the one for the $D_{T_{th}}$ [6]

$$D_{T_{th}} = \beta k_B \frac{\varphi_h}{V_p} \left[\frac{1+\varphi_h+\varphi_h^2-\varphi_h^3}{(1-\varphi_h)^3} \right] \quad (6)$$

which will be used to determine the theoretical Soret coefficient by

$$S_{T_{th}} = \frac{D_{T_{th}} V_p \rho_p}{\rho c(1-c) D_{th}} \quad (7)$$

which can be directly compared with the phenomenological value of S_T.

Experimental Thermal Diffusion

For the experimental investigation 5 differently concentrated magnetic fluids composed of magnetite particles and a kerosene-based carrier liquid provided by Ferrotec Corp. are used. The magnetic concentration ranges from 2 vol.% to 10 vol.%. Two different experiments with the horizontal thermodiffusion cell [4,5] are carried out. The separa-

tion of the fluids due to a temperature gradient of 900 K/m is followed by a homogenisation process for which the temperature applied to the fluids is set back to the initial homogeneous temperature of 298 K. The Soret coefficient is derived from the experimental separation curves via a numerical investigation [5]. The theoretical diffusion coefficient is used for its determination, see Fig. 1 (●). It is compared with the theoretical coefficient (■) and the one being experimentally determined (×) using the experimental diffusion coefficient, which is presented in Fig. 2. The different approaches including

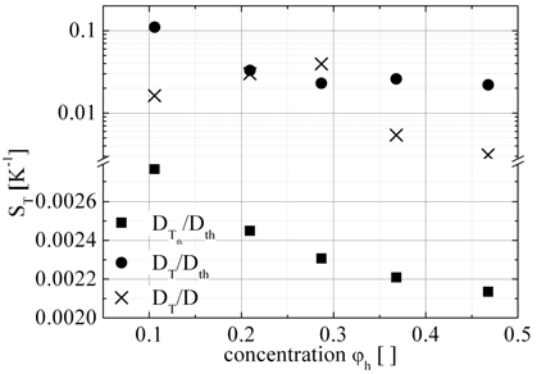

Figure 1: Comparison of experimental (●) and theoretical (■) Soret coefficient using D_{th}, both showing a weakening of the Soret effect for concentrated fluids. Experimental Soret coefficient (×) using experimental D.

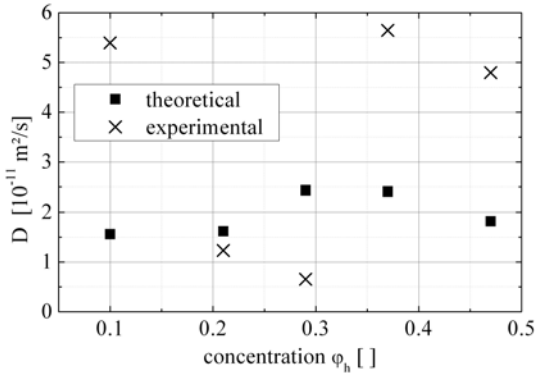

Figure 2: Comparison of D_{th} (■) and D (×).

a theoretical diffusion coefficient lead to an agreement on the general dependence of the Soret coefficient on the hydrodynamic concentration: the higher the concentration, the weaker is thermodiffusion. The order of magnitude of the theoretical and experimental Soret coefficient is quite different which can be drawn back to unknown influences on the thermally driven transport process due to the amount of particles in the fluid.

Conclusion

The experimental and theoretical investigations of 5 differently concentrated ferrofluids point out that thermodiffusion characterised by the Soret coefficient depends on the definition of the molecular diffusion coefficient. By the assumptions made here for the molecular and with the new theoretical model for the thermal diffusion coefficient the Soret effect is weaker in highly concentrated ferrofluids.

Acknowledgments

Financial support by DFG Grant No. LA 1182/3, Russian Fund of Fundamental Investigations in grants 12-01-00132, 13-02-91052, 13-01-96047, and 14-08-00283, Act 211 Government of the Russian Federation No. 02.A03.21.0006, program of Ministry of Education of Russian Federation 2.1267.2011 is gratefully acknowledged.

References

[1] S. de Groot et al., Non-Equilibrium Thermodynamics, Amsterdam (1962)

[2] G. K. Batchelor, J. Fluid Mech. **74**, 1-29 (1976)

[3] Y. A. Buyevich, A. O. Ivanov, Physica A **190**, 276-294 (1992)

[4] T. Völker, S. Odenbach, Phys. Fluids **17**, 037104 (2005)

[5] L. Sprenger, et al., Phys. Fluids **25**, 122002 (2013)

[6] L. Sprenger, et al., submitted to Phys. Fluids (2014)

Magnetic Field- and Temperature-Responsive Ferrogels: A Time-Resolved Small Angle Neutron Scattering Study

Sarah Metzke[1], Sylvain Prévost[1,2]

[1]*Technische Universität Berlin, Straße des 17. Juni 124, 14109 Berlin, Germany*
[2]*Hemholtz-Zentrum-Berlin, Hahn-Meitner-platz 1, 14109 Berlin, Germany*

Thermoreversible ferrohydrogels, where magnetic nanoparticles (NP) are incorporated in a self-assembled temperature-responsive network, are studied by time-resolved small angle neutron scattering (SANS), in order to elucidate the interplay between NP and the network and enable the control of the macroscopic rheology and magnetic response.

Background

Usually, ferrogels are obtained by adding large amounts of polymer to a ferrofluid. [2] The high amount of gelator required results in a dilution of the magnetic properties of the material, and the gel obtained is a polymer matrix encompassing blobs of the original ferrofluid without synergism. In this project, low molecular weight hydrogelators are used that self-organize into crystalline fibers and have a gelation temperature near ambient. NP are functionalized, offering nucleation sites. We employ single-domain spherical ferro/ferrimagnetic NP coated with silica, offering protection against oxidation, biocompatibility, pH-tunable charge, as well as a large palette of surface chemistry for functionalization.

Nanoparticles synthesis

Spherical particles with uniform size distribution, with different diameter (from 12 to 20 nm) are produced by thermal decomposition. [3] Fe_3O_4 (with variable γ-Fe_2O_3 content), $CoFe_2O_4$ and Fe_3C [4] have been synthesized. The silica shell, which must have a uniform thickness and low porosity, is formed in a reverse microemulsion. [5] The original TEOS reducing agent is ammonia, and others are being tested, in particular L-Lysine and L-Arginate.

Matrix

In general for such a network/nodes coupled system, parameters to be systematically varied are the stiffness of the fibrils; the adhesion strength at junctions; the mesh size, density of nodes and number of junctions. We are currently investigating surfactants forming wormlike micelles than can rigidified into nanofibrils [6] when lowering the temperature to form a stiff gel.

Particles dynamics

Different results are expected based on the strength and number of junctions relative to the field type (AC, DC, AC+DC), strength and frequency, with rotation and locomotion of individual particles [8] and collective dynamics [9] being allowed, hindered or fully inhibited. [7]

Memory effect and material recycling

Under zero field, temperature cycles should allow the full recovery of the initial properties. Oppositely, gelation under field should prevent a relaxation into the original state, leading to reversible memory features.

Investigation techniques

The main investigative tool of the final system will be small angle neutron scattering

(SANS), with AC and/or DC magnetic field. SANS is unique for such complex composite materials in that it probes the nanoscale (fibrils, core/shell NP, locus of particles), also dynamically up to several 10 kHz (transient structures, Néel and Brownian relaxations), can extract individual components by selective nuclear contrast matching, and distinguishes nuclear and magnetic domains using polarized neutrons. [10–12]

Acknowledgments

This work is supported by DFG PR1473/1 within the Priority Program SPP1681.

References

[1] G. Lattermann and M. Krekhova *Macromolecular Rapid Communications* vol. 27, no. 22, p. 1968, Nov. 2006.

[2] M. Krekhova and G. Lattermann *Journal of Materials Chemistry* vol. 18, no. 24, pp. 2842-2848, 2008.

[3] J. Park, K. An, Y. Hwang, J.G. Park, H.J. Noh, J.Y. Kim, J.H. Park, N.M. Hwang, and T. Hyeon *Nature Materials* vol. 3, no. 12, pp. 891-895, Nov. 2004.

[4] C. Schliehe, J. Yuan, S. Glatzel, K. Siemensmeyer, K. Kiefer, and C. Giordano *Chemistry of Materials* vol. 24, no. 14, pp. 2716-2721, Jul. 2012.

[5] H. L. Ding, Y. X. Zhang, S. Wang, J. M. Xu, S. C. Xu, and G. H. Li *Chemistry of Materials* vol. 24, no. 23, pp. 4572-4580, Dec. 2012.

[6] S. R. Raghavan and J. F. Douglas *Soft Matter* vol. 8, no. 33, p. 8539, 2012.

[7] A. Y. Zubarev *Soft Matter* vol. 8, no. 11, pp. 3174-3179, Feb. 2012.

[8] P. Ilg *Soft Matter* vol. 9, no. 13, p. 3465, 2013.

[9] J. Dobnikar, A. Snezhko, and A. Yethiraj *Soft Matter* vol. 9, no. 14, p. 3693, 2013.

[10] A. Wiedenmann, R. Gähler, R. P. May, U. Keiderling, K. Habicht, S. Prévost, M. Klokkenburg, B. Erné, and J. Kohlbrecher in *Studying Kinetics with Neutrons* vol. 161, G. Eckold, H. Schober, and S. E. Nagler, Eds. Berlin, Heidelberg: Springer Berlin Heidelberg, 2009, pp. 241-263.

[11] A. Wiedenmann, R. Gähler, C. D. Dewhurst, U. Keiderling, S. Prévost, and J. Kohlbrecher *Physical Review B* vol. 84, no. 21, Dec. 2011.

[12] D. Honecker and A. Michels *Physical Review B* vol. 87, no. 22, Jun. 2013.

Molecular organization in binary mixtures of liquid crystalline rod-like and spherical ferro- particles: A simulation study

S. D. Peroukidis and S. H. L. Klapp

Institut für Theoretische Physik, PN 7-1, Technische Universität Berlin, Hardenbergstrasse 36, D-10623 Berlin, Germany

Soft magnetic materials that consist of magnetic particles in liquid crystalline matrices [1] are promising candidates e.g. as stimuli-responsive materials.
Herein, we attempt to elucidate the basic aspects that dictate the molecular self organization both in ordered and disordered phases in this class of systems. To this end, we have performed monte carlo simulations to study the phase behavior of binary mixtures that consist of liquid crystalline rod-like Gay-Berne particles and soft repulsive spherical ferro- particles with an embedded permanent dipole. The interactions between unlike particles are modeled via the potential introduced in ref. [2]. A rich variety of phase structures is obtained, including fully miscible isotropic, nematic and smectic phases, as a function of temperature and concentration ratio at zero or low dipolar coupling of the spherical particles (see Fig. 1a). By increasing the dipolar coupling ordered chains of spherical particles (wires or threads) are formed within the nematic phase (see Fig. 1b). Interestingly, the system becomes antiferromagnetic in the absence of external magnetic field. Hence, this intriguing fluid possesses two main orientational order parameters. The dependence on thermodynamic conditions of the size of the chains of spherical particles is also examined. An enhancement of the orientational order of these chains occurs at lower temperature nematic and smectic phases.

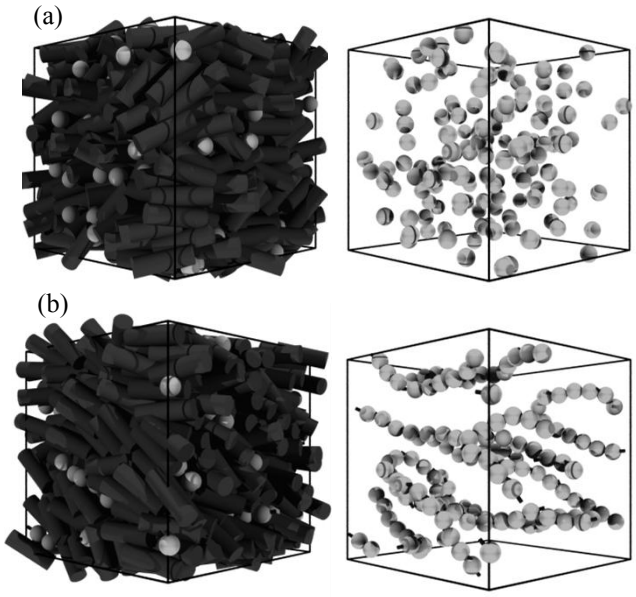

Fig. 1. Representative snapshots of: a) a fully miscible nematic phase with zero dipolar coupling of the spherical particles and b) a nematic in which dipolar coupling of spheres enhances the formation of ordered chains (threads) of spherical particles. Right: the rod component is removed.

Acknowledgments

This research has been financed by DFG-Priority Programme 1681 'field controlled particle matrix interactions: synthesis multiscale modeling and application of magnetic hybrid materials'.

References

[1] A. Mertelj, D. Lisjak, M. Drofenik and M. Copic, *Nature*, **504**, 237 (2013).
[2] D. J. Cleaver, C. M. Care, M. P. Allen, and M. P. Neal, *Phys. Rev.* E, **54**, 559 (1996).

Magnetic Nanoparticle Targeting Flow Phantom with real-time Quantification using Magnetic Particle Spectroscopy

P. Radon[1], M. Liebl[1], N. Löwa[1], N. Pömpner[2], M. Stapf[2], F. Wiekhorst[1], K. Gitter[3], I. Hilger[2], S. Odenbach[3], L. Trahms[1]

[1] *Physikalisch-Technische Bundesanstalt, Berlin*
[2] *Experimentelle Radiologie, Universitätsklinikum Jena*
[3] *Institut für Strömungsmechanik, Technische Universität Dresden*

Introduction

Magnetic Nanoparticles (MNP) are used in biomedical applications, such as magnetic drug targeting (MDT) or magnetic hyperthermia dedicated for cancer treatment [1]. For MDT the MNP are injected into the blood system and shall be accumulated by an external magnetic field (gradient) at the region of interest. To assess the choice of suitable MNP for a preclinical combined MDT and hyperthermia study in a tumor mouse model we established a simple flow phantom. With this flow phantom the magnetic targeting (MT) efficiency of different MNP types can be quantified. Furthermore, physical parameters of the experimental set-up like magnetic field gradient strength/distance and physiological parameters like flow rate can be adjusted in a controlled way.
For the quantification of the MNP concentration we employed Magnetic Particle Spectroscopy (MPS) [2]. MPS is a sensitive and specific method to quantify MNP amounts that is based on the detection of the non-linear part of the magnetic AC-susceptibility.
Furthermore, a variation of the harmonic ratio A5/A3 in the Fourier transform of the MPS signal indicates changes in the magnetic behavior of the MNP [3].
So far our targeting procedure was stopped after time interval t_M, then the setup was disassembled to harvest sample aliquots of the MNP suspension which finally were quantified by MPS.

Here we present as proof-of-principle an elaborated refinement of our set-up integrating the MPS into the existing flow system for continuous nearly real-time quantification of the MNP retention during magnetic targeting.
We tested our system with MNP diluted in BSA and MNP diluted in blood.

Materials and Methods

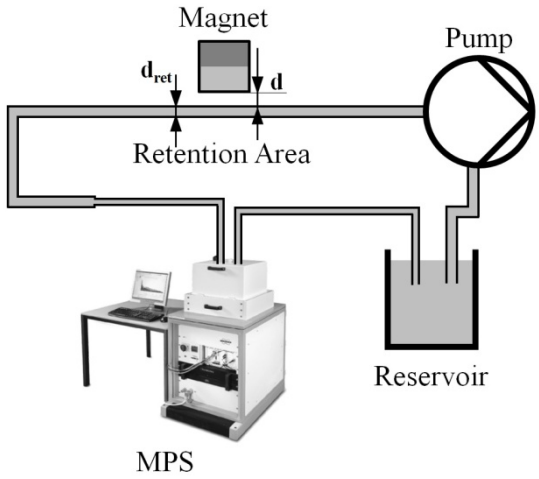

Fig. 1: Set-up of the MT flow system with integrated Magnetic Particle Spectrometer for real-time MNP quantification.

As shown in Fig. 1, the MT flow phantom incorporates a reservoir to be filled with up to 2 ml MNP suspension, and a peristaltic pump (Ismatec IPC 4), which pumps the suspension at a fixed flow rate of 350 µl/min through a tube of 1.4 mm diameter, first passing the retention area of a strong cube-shaped neodymium magnet (edge length 9 mm, remnant magnetization

1.2 T) and then through the detection coil system of the MPS. By winding the tube on a spool the effective volume inside the detection coil of the MPS was enlarged to about 7 µl.

We used hydroxyethyl starch coated MNP (chemicell, Berlin) of mean hydrodynamic diameter d_{hydr} = 200 nm. We investigated the targeting of these MNP diluted in distilled water (containing 0.1 % bovine serum albumin) down to an iron concentration of 7.5 mmol/l (corresponding to 300 µmol/kg body weight dosage typically used in preclinical drug targeting experiments). Additionally, the targeting of the MNP diluted in EDTA stabilized human blood (same concentration) was analyzed.

First the suspension was pumped through the system without magnetic field for a few minutes and every 10 s repetitive MPS measurements at a drive field B_{drive} = 25 mT were performed. Then the magnet was moved into the retention area (distance to tube of d = 1.2 mm) defining the start point of the MT.

From the MPS spectra (Fourier transform of the magnetization response of the MNP exposed to the oscillatory 25 kHz drive field) we used the third harmonic moment A_3 to monitor changes of the MNP concentration due to MT. By relating A_3(t) to the moment prior to MT the retention was determined as the ratio $(1\text{-}A_3(t)/A_3(0))\cdot 100\%$.

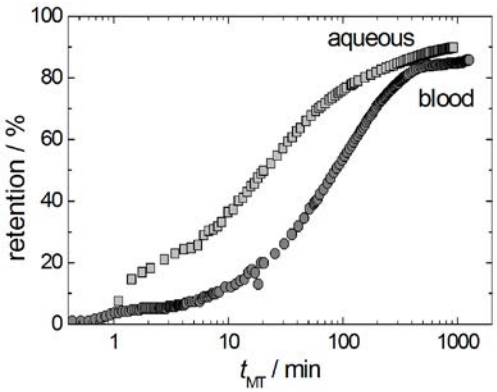

Fig 2: MNP retention as a function of magnetic targeting time for MNP suspended in distilled water (squares) and in blood (circles).

Results

Already after 1 min of targeting a decrease of MPS moment A_3 was detectable. The retention behavior of MNP in water and in blood as a function of targeting time is shown in Fig. 2. After about 10 min the retention of MNP in water was higher (35 %) than for MNP suspended in blood (10 %) most probably due to the higher viscosity of blood. After about 500 min the retention shows saturation behavior with MNP accumulation of about 90 % for water and 85 % for blood.

Accompanied with the increase of retention a change in the MPS spectra shape was observed. This can be interpreted as a size selective targeting by the magnet which attracts larger particles more efficiently.

Conclusions

The integration of MPS into our existing flow phantom permits a continuous nearly real-time quantification of the MNP retention during MT. Due to the high sensitivity of MPS our set-up allows the analysis of targeting behavior of MNP at clinical relevant concentrations. After this proof-of-principle, this setup will be used to assess the targeting behavior of a dedicated targeting magnet developed for tumor studies in a mouse tumor model. While our simplified MT model may not reflect the complicated physiologic situation, it enables the observation of the targeting behavior of MNP under defined physical conditions.

Acknowledgments

This work was financially supported by the DFG research program “Magnetische Nanopartikel für die Krebstherapie” TR408/4-3, OD18/13-3 and HI698/7-4.

References

[1] Q A Pankhurst et al. *J Phys D* 36:167-181(2003).

[2] S R Snyder et al. http://www.bruker-biospin.com/mps-apps.html (2012).

[3] J B Weaver et al. Med Phys 39:2765 (2012)

Coarsening dynamics of ferromagnetic networks

Robin Maretzki[1] and Reinhard Richter[1]

[1] *Experimentalphysik 5, Universität Bayreuth, 95440 Bayreuth Germany*

Introduction

Permanent magnetic dipoles may self-assemble to linear chains and rings, even without an externally applied magnetic field. This has been investigated for nano-sized particles in ferrofluids; see e.g. [1,2]. However, in this system the emerging structures and their dynamics are difficult to observe. Similar aggregates have also been observed in a mixture of glass beads and magnetized steel spheres, which are shaken in a vessel [3]. In our contribution we focus on the formation of transient networks in this system, when quenching the amplitude of the vibrations.

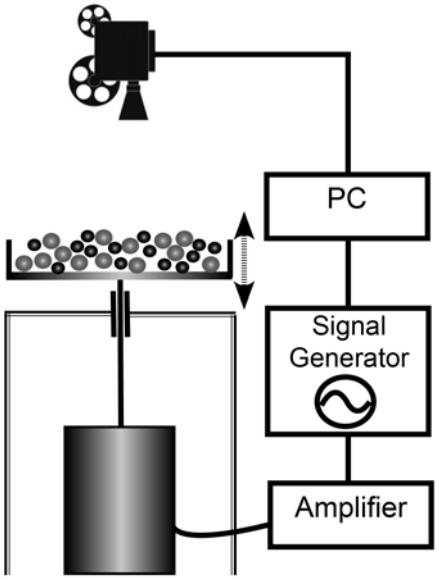

Figure1: Sketch of the experimental setup.

Experimental setup

Steel spheres with a diameter of 3mm are permanently magnetized in a homogeneous field of 1.15T. Consecutively they are filled together with glass spheres (diameter of 4mm) in a rectangular vessel which is vibrated by an electromagnetic shaker. As sketched in Fig.1, a long rod takes care that the alternating magnetic field generated in the shaker has no significant influence on the steel spheres. A personal computer controls the sinusoidal output of a signal generator, connected via an amplifier to the shaker. The beads are illuminated from below utilizing an electroluminescent display, as sketched in Fig.2. The dynamics of the beads is recorded from above using a charge coupled device camera connected to the computer.

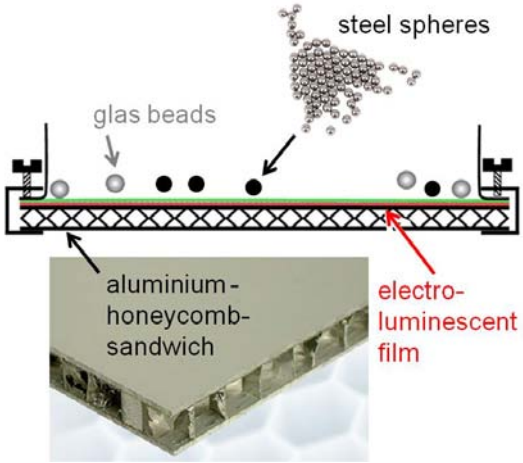

Figure2: The vessel and its illumination.

Experimental observations

For large shaker amplitudes we observe a gas-like state of single steel and glass spheres, as shown in Fig.3. After a quench of the shaker amplitude to a lower value

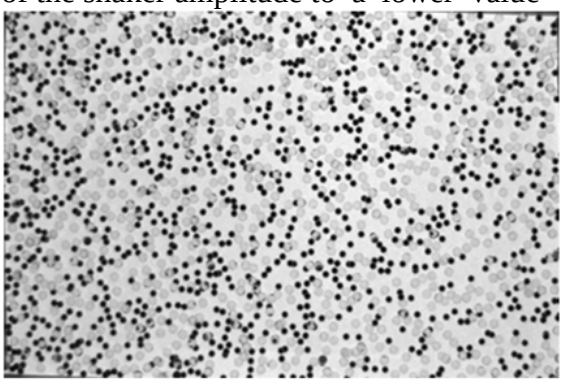

Figure3: Gas-like state of shaken **s**teel spheres (black) and glas spheres (grey).

Figure 4: Formation of transient networks.

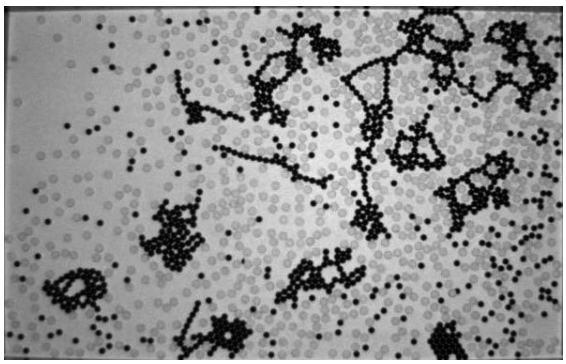

Figure 5: Coarsening of the network results in more compact aggregates.

we record the assembly of steel spheres to chains, networks, see Fig. 4. Eventually compact clusters emerge, as shown in Fig. 5. A movie of this transition can be accessed at [4].

We are investigating the evolution of order parameters like chain length, or Euler characteristics during the transitions.

Moreover we discuss our observations in the context of a recently proposed model of *viscoelastic phase separation* [5]. In this model the dynamic asymmetry between the glass spheres and the magnetized steel spheres, with their enhanced shear viscosity, leads to phase separation and the formation of transient networks.

Acknowledgments

The authors would like to thank K. Oetter for construction work with the setup, and I. Rehberg for discussion.

References

[1] P.G. De Gennes and A. Pincus, *Pair Correlations in a Ferromagnetic Colloid*, Phys. Kondens. Mater. **1**, 189 (1970).

[2] T. A. Prokopieva, V. A. Danilov, S. S. Kantorovich, Ch. Holm, *Ground state structures in ferrofluid monolayers*, Phys. Rev. E **80**, 031404 (2009).

[3] D. L. Blair, A. Kudrolli, *Clustering transitions in vibrofluidized magnetized granular materials*, Phys. Rev. E **67**, 021302 (2003).

[4] A movie can be accessed at http://www.youtube.com/watch?v=Tt82K6osdzM

[5] H. Tanaka, *Viscoelastic phase separation*, J. Phys.: Condens. Matter. **12**, R207 (2000). H. Tanaka, Y. Nishikawa and T. Koyama, *Network-forming phase separation of colloidal suspensions*, J. Phys.: Condens. Matter. **17**, L143 (2005).

Image-based XFEM modeling and multiscale simulation of magnetosensitive materials

M. Kästner, C. Spieler, F. Kresinsky, V. Ulbricht

Institute of Solid Mechanics, Technische Universität Dresden, 01062 Dresden, Germany

Introduction

Magnetosensitive materials are novel composites with interesting and adjustable properties. These materials are in great demand from science, medicine and technology with a special interest on the macroscopic material behavior. Since this effective material behavior is essentially determined by the constitutive properties of the individual components and their geometrical arrangement in the composite, this contribution will apply multi-scale modeling strategies to magnetosensitive materials, exemplarily focusing on magnetorheological elastomers. Starting from the properties of the magnetizable particles and the polymeric matrix, numerical homogenization techniques are used to predict the effective mechanical, magnetic and magneto-mechanical behavior. In this context, the availability of micro- and mesoscopic numerical models is a crucial requirement for the application of the proposed computational homogenization methods. Therefore, efficient procedures which automatically convert micro- and mesostructural images into a numerical model of the local material structure are to be developed. By combining image segmentation algorithms with the extended finite element method (XFEM), advantageous features of voxel-based approaches such as the non-conforming, structured mesh are joint by a smooth representation of material interfaces which results in an improved accuracy of the local field quantities compared to a voxel discretization. In order to provide acceptable computational costs, we benefit from a parallelization of image segmentation, computation of the element matrices as well as the solution procedures. To this end, graphics processing unit (GPU) computing is applied.

Image-based XFEM modeling

The XFEM (see [1] for a detailed review) uses a structured, non-conforming mesh which is essentially independent of, e.g., material interfaces. The location of interfaces is represented implicitly by a level-set based computed as the signed distance to the interface. Using the level-set information, the physical behavior at such an interface is modeled by an enrichment of the finite element approximation. The level-set function therefore provides a direct link of the image information obtained from, e.g., computed tomography (CT) scan (Fig. 1 (a)) to a numerical XFEM model:
(i) In the first approach which has recently been proposed by Legrain et al. [2, 3], level-set-based algorithms for image segmentation are applied to obtain a level-set representation of different material phases and the corresponding interfaces which directly serves as input for XFEM.
(ii) Here, a new method based on marching square (2D) or marching cube (3D) algorithms for the reconstruction of surfaces is used for the computation of nodal level-set values which implicitly represent the interface. In this approach, several pixels are combined into a quadrilateral domain, the marching square. Based on the grey scale values of the pixels forming such a square

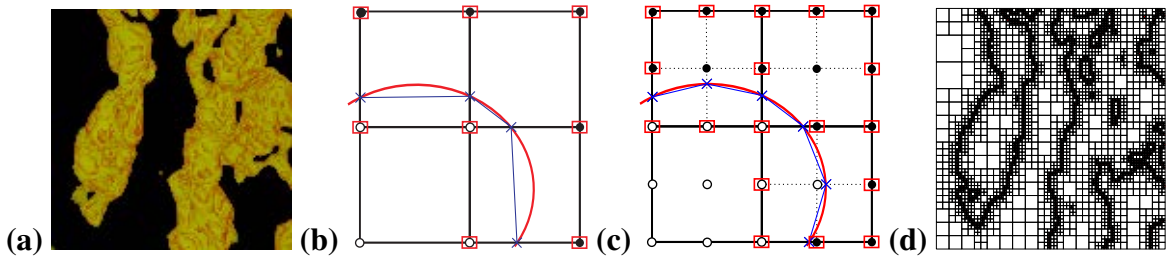

Figure 1: 2D image-based modeling: **(a)** Image [4], **(b)** Marching cube algorithm to compute the nodal level-set values, **(c)** Improved interface representation using higher-order approximations and geometric subgrids, **(d)** Structured, non-conforming XFEM mesh with adaptive quadtree refinement.

and a threshold value, it can be detected if a material interface intersects the square and the points of intersection with the edges of the square and the corresponding level-set values can be computed (Fig. 1 (b)). It is expected that marching cube segmentation will improve the robustness and efficiency of the approach compared to level-set-based image segmentation.
It is then straightforward to convert each square or cube into an element domain of the subsequent FE discretization which will, however, result in very fine meshes and a high computational effort comparable to a simple voxel discretization. In order to exploit the potential of the XFEM formulation, coarse analysis meshes are used in combination with higher-order approximations and a refined geometric discretization (Fig. 1 (c)). Both linear and higher-order elements can be applied in conjunction with an adaptive quadtree refinement in the vicinity of a material interphase to further improve the numerical efficiency of the approach (Fig. 1 (d)).

Formulation and solution of the problem

Eventually the image-based microstructural models are used to predict the effective magneto-mechanical behavior of magnetosensitive materials using the approaches developed in [5–7]. Based on continuum theories all considered length scales are modeled in a phenomenological way and homogenization techniques are applied to predict the effective macroscopic material behavior. It is anticipated that the application of the developed multiscale modeling techniques and the comparison to analytical and experimental results will promote the understanding of structure-property relationships for magnetosensitive materials in the future.

Acknowledgements

The present study is funded by the German Research Foundation (DFG), Priority Program (SPP) 1681, grant KA 3309/2-1.

References

[1] T. P. Fries and T. Belytschko, Int. J. Numer. Meth. Engng. 84, 2010.

[2] G. Legrain et al., Int. J. Numer. Meth. Engng. 86, 2011.

[3] W. Lian et al., Comput. Mech. 51, 2013.

[4] D. Günther et al., Smart Mater. Struct. 21, 2012.

[5] C. Spieler et al., Tech. Mech., accepted manuscript.

[6] M. Kästner et al., Int. J. Numer. Meth. Engng. 93, 2013.

[7] C. Spieler et al., Acta Mech. 224, 2013.

The effects of superparamagnetic iron oxide nanoparticles on three-dimensional cell culture systems

Anja Theumer[1], Christine Gräfe[1], Franziska Bähring[1], Christian Bergemann[2], Andreas Hochhaus[1], Joachim H. Clement[1]

[1]*Abt. Hämatologie/Internistische Onkologie, Universitätsklinikum Jena, Erlanger Allee 101, 07745 Jena, Deutschland, Anja.Theumer@med.uni-jena.de*
[2]*chemicell GmbH, Eresburgstraße 22-23, 12103 Berlin, Deutschland*

Introduction
Due to their versatility iron oxide magnetic nanoparticles have been used in many medical applications as drug delivery systems or contrast agents in magnetic resonance imaging (MRT) as well as in hyperthermal anti-cancer therapy successfully. The effect of such nanoparticles on biological systems is affected by different parameters including particle size, shape, surface coating and interactions with biological borders. Particularly the blood-brain barrier is a critical and sensitive interface. Three-dimensional cell culture systems consisting of barrier-forming cells represent a suitable model to reflect the particles´ actions in the body, e.g. toxic effects, as they exhibit features of real tissues.

Methods
Human brain microvascular endothelial cells (HBMEC), a representative of the human blood brain barrier, were cultured in RPMI1640 + 10% fetal calf serum. Viability assays were performed on HBMECs with the CellTiter-Glo® Luminescent Cell Viability Assay (Promega, Mannheim) after incubation with various concentrations of nanoparticles or the corresponding shell-building substances for three hours. Nanoparticles with different types of shells (starch, anionic carboxymethyldextran (CMD) and cationic polyethylenimine (PEI)) were provided by chemicell GmbH. HBMEC spheroids were created by the hanging-drop method. Formation and growth properties of spheroids were analysed with light microscopy repeatedly for several days after initiation. Spheroids were incubated with nanoparticles to evaluate their viability with the LIVE/DEAD® Viability/Cytotoxicity Kit (life technologies, Karlsruhe) and confocal laser scanning microscopy. Both the intracellular Akt- and GSK-3β- signalling pathways and MAP kinase activity were analysed after incubation with various nanoparticles in different concentrations using immunoblotting.

Results
Viability assays demonstrated that PEI-coated nanoparticles or PEI alone exhibit concentration-dependant cytotoxic effects on HBMECs starting at a concentration of 25 µg/ cm². Spheroid staining confirmed these results by indicating an increased amount of dead cells when incubating spheroids with PEI-particles. Starch and CMD-covered particles did not affect the viability of cells at any concentration tested. By analysing the growth properties differences in spheroidal shape could be observed over time. Immunoblotting focussing on the phosphorylation status of several proteins could show that especially PEI-particles influence intracellular signalling pathways, e.g. by strengthening pro-proliferative signalling via MAPK p44/42.

Conclusion
We show that neutral, anionic and cationic iron oxide nanoparticles interact with HBMECs which are capable of forming multicellular spheroids. Three-dimensional cultures offer more highly predictive data for designing nanoparticle-based therapeutics for *in vivo* applications as they provide a better insight into the situation of real tissues compared to two-dimensional systems.

Can turbulence occur at low Reynolds numbers?

Sebastian Altmeyer[1,⋆], Younghae Do[2], Ying-Cheng Lai[3]

[1] *Institute of Science and Technology Austria (IST Austria), 3400 Klosterneuburg, Austria*
[2] *Department of Mathematics, Kyungpook National University, Daegu 702-701, Korea*
[3] *School of Electrical, Computer and Energy Engineering, Arizona State University, Tempe, Arizona 85202, USA*

It is commonly known that, in classical fluids, turbulence [1] typically occurs at high Reynolds numbers. But can turbulence occur at low Reynolds numbers? Here we show that in ferrofluids [2], manufactured fluids with magnetized nanoparticles embedded in liquid carriers, in the presence of a magnetic field, turbulence can occur at Reynolds numbers that are at least one order of magnitude smaller than those required in classical fluids [3]. This is established by extensive

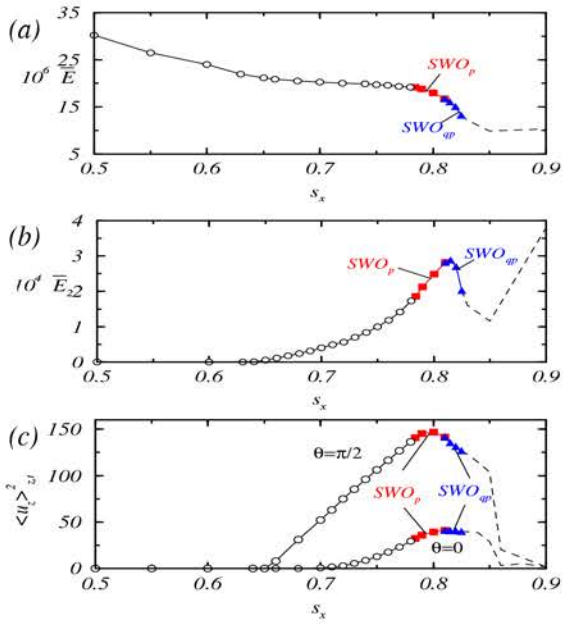

Figure 1: Bifurcations with Niklas parameter s_x [6]: (a) time-averaged modal kinetic energy $\overline{E}$, (b) its $m = 2$ contribution, and (c) spatiotemporally averaged axial flow field at mid-gap for $\theta = 0$ and $\theta = \pi/2$. Open and filled symbols are for steady-state and time-dependent solutions, respectively.

computational ferrohydrodynamics through a detailed bifurcation analysis and characterization of various physical quantities such as the energy, the wave number, and the angular momentum. A striking finding is that, as the magnetic field is increased, the onset of turbulence can be determined accurately and reliably. Our results imply that experimental investigation of turbulence can be greatly facilitated by using ferrofluids, and this opens up a new avenue to probe into the fundamentals of turbulence.

Our extensive computations of the governing equation [4, 7, 5, 6]

$$(\partial_t + \mathbf{u}\cdot\nabla)\mathbf{u} - \nabla^2\mathbf{u} + \nabla p_M = s_x^2\{\nabla^2\mathbf{u} - 4[\nabla\cdot(\mathbb{S}\mathbf{H})] - \mathbf{H}\times[\nabla\times((\nabla\times\mathbf{u})\times\mathbf{H}) - \mathbf{H}\times\nabla^2\mathbf{u}) + 2\nabla\times(\mathbb{S}\mathbf{H})]\}$$

reveals a sequence of bifurcations (Fig. 1) leading to time-dependent flow solutions such as standing waves with periodic or quasiperiodic oscillations, and turbulence (see Figs. 2 and 3). Surprisingly, we find that turbulence can occur for Reynolds numbers at least one order of magnitude smaller than those required for turbulence to arise in classical fluids. The occurrence of turbulence is ascertained by a bifurcation analysis and by examining characteristics of physical quantities such as the energy, the wave number, and the angular momentum. We also find that the onset of turbulence can be determined accurately, in contrast to classical fluid turbulence where such a determination is typically qualitative and involves a high degree of uncertainty [1]. Our findings have the following implications:

(1) ferrofluids under magnetic field is a new paradigm for investigating turbulence, especially experimentally where the study can be greatly facilitated due to the dramatic relaxation in the Reynolds-number requirement,

(2) the critical magnetic-field strength for the onset of turbulence can be pinned down precisely, possibly leading to deeper insights into the physical and dynamical origins of the transition, and

(3) turbulence can be controlled externally, e.g., by an external magnetic field.

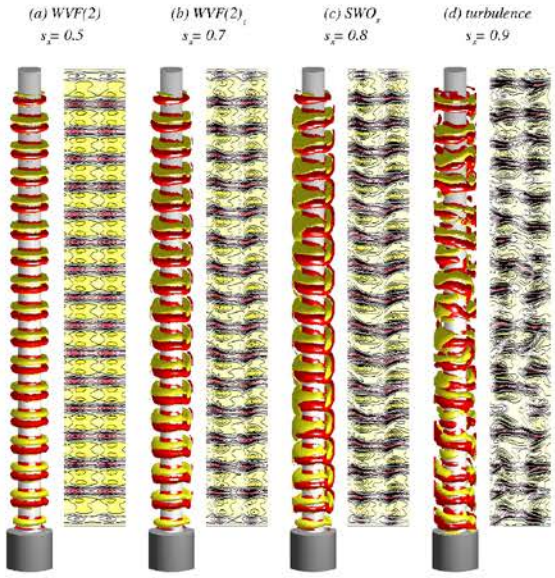

Figure 2: (a-d) For four values of s_x corresponding to WVF_2, WVF_t, SWO_p, and turbulence regimes, respectively, isosurfaces of η and contours of the radial velocity $u(\theta, z)$ on an unrolled cylindrical surface in the annulus at mid-gap. Red (dark gray) and yellow (light gray) denote $\eta = \pm 100$ for isosurfaces, and inflow and outflow for contour plots, respectively. The patterns in (c,d) are snapshots due to time dependence of the corresponding flow.

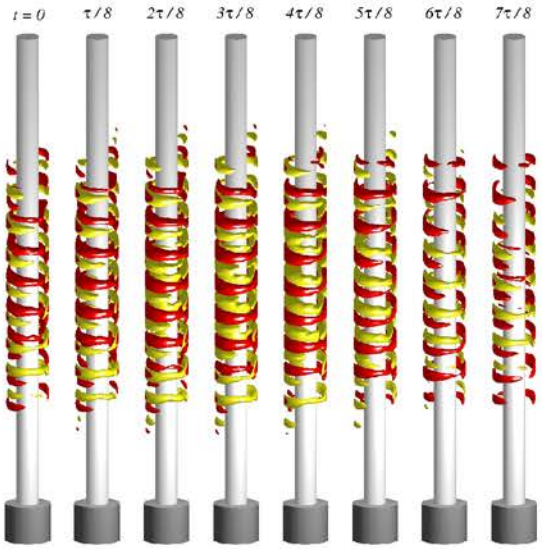

Figure 3: For $s_x = 0.8$ (periodic regime, SWO_p, cf. Fig. 1), isosurfaces of the relative angular momentum $ru_\theta - \int_0^\tau ru_\theta dt$ at eight time instants in one period of oscillation, where $\tau \approx 0.058$ and the isolevels are $ru_\theta = \pm 5$.

References

[1] U. Frisch, *Turbulence*, (Cambridge Univ. Press, Cambridge, UK, 1995).

[2] R. E. Rosensweig, *Ferrohydrodynamics*, (Cambridge University Press, Cambridge, UK, 1985).

[3] S. Altmeyer, Y. Do, and Ying-Cheng Lai, *Can turbulence occur at low Reynolds numbers?*, *Paper submitted.*

[4] H. W. Müller and M. Liu, *Structure of ferrofluid dynamics*, *Phys. Rev. E*, **64**, 061405 (2001).

[5] S. Altmeyer, Y. Do, and J. M. Lopez, *Effect of elongational flow on ferrofluids under a magnetic field*, *Phys. Rev. E*, **88**, 013003 (2013).

[6] M. Niklas, *Influence of magnetic fields on Taylor vortex formation in magnetic fluids*, *Z. Phys. B* **68**, 493 (1987).

[7] S. Altmeyer, Ch. Hoffmann, A. Leschhorn, and M. Lücke, *Influence of homogeneous magnetic fields on the flow of a ferrofluid in the Taylor-Couette system*, *Phys. Rev. E*, **82**, 016321 (2010).

⋆ **sebastian.altmeyer@ist.ac.at**

Spatial-sensitivity based optimization of inhomogeneous excitation fields for magnetorelaxometry imaging of magnetic nanoparticles

D. Baumgarten[1], J. Haueisen[1]

[1]*Institute for Biomedical Engineering and Informatics, Technische Universitt Ilmenau, Germany*

Introduction

Magnetic nanoparticles (MNP) offer promising novel applications in biomedicine. These applications require the quantitative knowledge of the in-vivo particle distribution. Magnetorelaxometry (MRX) non-invasively obtains the characteristic relaxation behaviour of the MNP after being exposed to sudden changes of an external excitation field. From multichannel MRX measurements, the MNP distribution can be quantitatively determined by minimum norm estimation techniques [1]. It could be shown that sequential activation of inhomogeneous excitation fields considerably enhances the imaging quality compared to homogeneous activation of the particles [2,3]. In first studies, single coils were consecutively activated. We aim at further advancing this imaging technology by finding suitable activation patterns involving multiple excitation coils. Here, approaches for defining these patterns based on the spatial sensitivity in the source space are presented and compared in simulation studies.

Methods

Dividing the source space into K voxels, the forward problem explaining the magnetic flux density in one sensor resulting from the relaxation of the particles is formulated as:

$$B_k = \frac{\mu_0}{4\pi}\left[\frac{3\vec{n}^T(\vec{r}_k\vec{r}_k^T)}{|\vec{r}_k|^5} - \frac{\vec{n}^T}{|\vec{r}_k|^3}\cdot\vec{H}_k\chi\right]c_k \tag{1}$$

Here, $\vec{n}$ is the normal vector of the sensor, $\vec{r_k}$ is the position of the k-th voxel containing an amount of c_k particles with the magnetic susceptibility χ. $\vec{H}$ is the magnetization field in this voxel. Combining these equations for all voxels and sensors leads to

$$\vec{B} = \mathbf{L}\cdot\vec{\mathbf{c}} \tag{2}$$

with the relaxation amplitude vector $\vec{B}$, the concentration vector $\vec{c}$ and the system matrix $\mathbf{L}$. The amount of particles in the voxels can be estimated by minimizing the difference between this forward model and the measured relaxation amplitudes $\vec{B}_{meas}$:

$$\vec{c}_{est} = \min\|\mathbf{L}\cdot\vec{c} - \vec{B}_{meas}\| \tag{3}$$

This problem can be solved using the Moore-Penrose pseudoinverse and Truncated Singular Value Decomposition. The system matrix $\mathbf{L}$ is influenced by the positions of voxels and sensors and by the excitation field. Whereas the first are fixed in the given setup, the latter can be controlled by the currents I_c in the excitation coils. The impact of the k-th voxel on the sensor system is given by the spatial sensitivity S_k [3]:

$$S_k = \sum_{j=1}^{N_s}\|L_{jk}\| \tag{4}$$

The relation between the sensitivities $\vec{S}$ and the currents can be described by an interaction matrix $\vec{A}$. By defining a sensitivity distribution S^* and solving an inverse problem using the algorithms mentioned above, the respective currents can be determined:

$$\vec{I_c}^* = A^+\cdot\vec{S}^* \tag{5}$$

In this paper, different paradigms for the provided spatial sensitivity are investigated. The

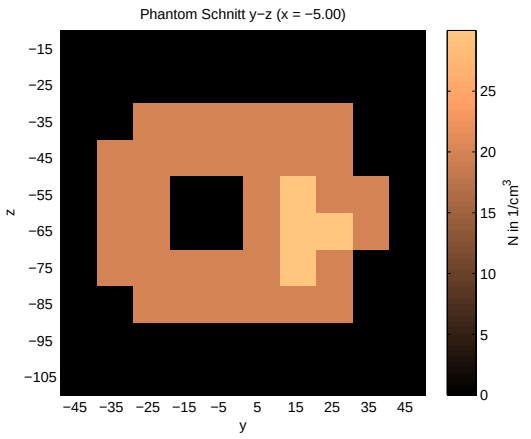

Figure 1: Vertical slice of simulated MNP distribution emulating a Shepp-Logan phantom.

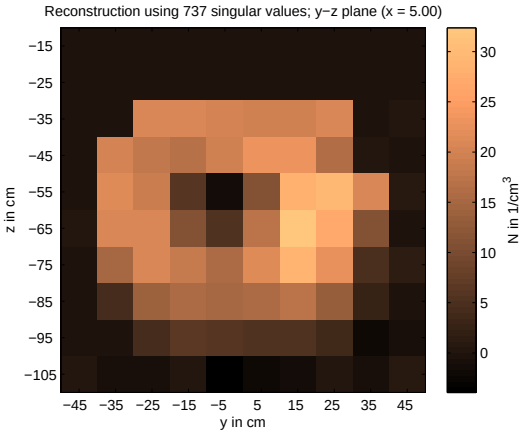

Figure 2: Vertical slice of reconstructed distribution employing the third paradigm.

first approach consecutively moves a plane of voxels with sensitivity $S_k^* = 1$ through the source space. Secondly, an inverse paradigm is employed where all voxels except for one plane are sensitive. In the third paradigm, one sample seeking homogeneous sensitivity is appended. The approaches are investigated in simulation studies involving surrogate sensor and coil setups and particle distribution phantoms (cf. figure 1).

Results

Two-dimensional and three-dimensional particle distributions could be reconstructed using all approaches (cf. figure 2). Visual inspection yields similar imaging results for all three paradigms. Correlation coefficients between simulated source and reconstructions reveal values above 0.95. However, the condition number that has crucial importance for the stability of the inverse solution is considerably lower for the combined approach.

Conclusions

Our results demonstrate the principal applicability of our approaches for defining inhomogeneous activation patterns for magnetorelaxometry imaging of magnetic nanoparticles. The obtained activation patterns allow for a better imaging quality using a lower number of activation sequences compared to the conventional single coil activation.

Acknowledgments

This work was supported by the German Research Foundation (DFG; grant BA4858/1-1) and the German Federal Ministry of Education and Research (BMBF) as part of the Innoprofile Transfer project MAMUD (grant 3IPT605X).

References

[1] D. Baumgarten et al. Magnetic nanoparticle imaging by means of minimum norm estimates from remanence measurements. *Med Biol Eng Comp*, 46(12):1177–1185, 2008.

[2] U. Steinhoff et al. Imaging of magnetic nanoparticles based on magnetorelaxometry with sequential activation of inhomogeneous magnetization fields. *Biomed Tech*, 55:22–25, 2010.

[3] G. Crevecoeur et al. Advancements in magnetic nanoparticle reconstruction using sequential activation of excitation coil arrays using magnetorelaxometry. *IEEE Trans Magn*, 48(4):1313–1316, 2012.

High frequency relaxation dynamics of Ni nanorod colloids studied by Small Angle Neutron Scattering

P. Bender[1], A. Tschöpe[1], A. Günther[2], D. Honecker[2], A. Wiedenmann[3], R. Birringer[1]

[1]*Experimentalphysik, Universität des Saarlandes*
[2]*Laboratory for the Physics of Advanced Materials, University of Luxembourg*
[3]*Institut Laue Langevin, Grenoble*

With diameters below 42 nm, Ni nanorods are ferromagnetic single-domain particles magnetized along the long rod axis [1]. Dispersed in viscoelastic matrices the orientation distribution of such rod ensembles can be manipulated by applying either static or time-modulated external magnetic fields. Any physical quantity which reflects the mechanical response could then be used to infer the viscoelastic properties, such as the static shear modulus G [1–3] or viscosity η [4].
Subjected to an oscillating field of magnitude $\mu_0 H_0$ the relaxation frequency ω_c of a rod with magnetic moment m is

$$\omega_c = \frac{m\mu_0 H_0}{K_v \eta}\,(1 + K_v G) \qquad (1)$$

with

$$K_v = \frac{\pi l^3}{3\,(ln(l/d) + k(l/d))}. \qquad (2)$$

Here, $k(l/d)$ is a correction term for a cylinder with length l and diameter d [5]. Analysis of the relaxation dynamics of the rods in oscillating magnetic fields thus enables the characterization of the viscoelastic properties of a wide range of complex fluids on the nanoscale. However, the response of the rods has to be detected in the microsecond range. Regarding for example a rod with $l \approx 170$ nm and $d \approx 24$ nm dispersed in water (as for the rods in this study) the relaxation frequency in a field with $\mu_0 H_0 = 6$ mT amounts to $\omega_c \approx 50000$ 1/s.
To study the relaxation dynamics of magnetic particles stroboscopic Small Angle Neutron Scattering (SANS) can be applied, which gives both a nuclear as well as magnetic scattering intensity. The time-resolution in conventional stroboscopic SANS experiments however is restricted to ~ 200 Hz due to the wavelength distribution of the neutron beam. To increase the maximal detectable sample oscillation to $\omega \sim 60000$ Hz the so-called TISANE-mode has to be applied [6]. This technique was recently implemented at the instrument D 22 at the ILL in Grenoble.
In the present study the relaxation dynamics of a water-based colloidal dispersion of Ni nanorods ($l = 170$ nm, $d = 24$ nm) subjected to oscillating fields with $\mu_0 H_0 = 6$ mT was monitored at the D 22 applying the TISANE mode. Due to the shape anisotropy of the rods their field and time-dependent orientation could be extracted from the corresponding scattering patterns (Figure1) enabling the detection of their field-driven os-

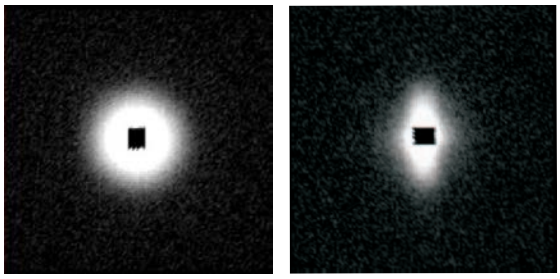

(a) parallel (b) perpendicular

Figure 1: Scattering pattern of an ensemble of Ni nanorods aligned parallel and perpendicular to the neutron beam.

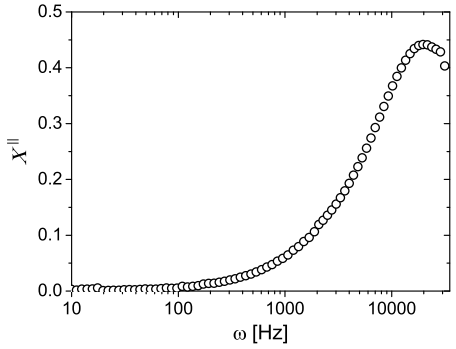

Figure 2: Imaginary part of the response function of the rods determined from optical transmission measurements.

cillation as a function of frequency. To test the validity of the results corresponding optical transmission-(OT)-measurements were performed with identical field parameters.

Results

By analyzing the OT-measurements the imaginary part $X^{||}$ of the response function of the rods – orientation of the rods with respect to the field vector – could be determined from the oscillating light intensity (Fig.2, $X^{||} = A\sin\Phi$), where A is the amplitude and Φ the phase shift with respect to the field vector. Assuming a Log-Normal distribution of the relaxation frequency the mean value of ω_c according to the OT-measurements is $\omega_{c,0} = 18500\,\mathrm{Hz}$, which is by a factor of ~ 2.7 below the theoretical value. This discrepancy can be attributed to the surfactant and/or counter ion layer surrounding the rods [4].

To determine the response function from SANS at first the intensity in the vertical sector of the time-dependent scattering patterns was integrated. As shown in Figure 3, at $\omega = 157\,\mathrm{Hz}$ the oscillation of the rods is basically in phase whereas with increasing frequency a phase shift and damping of the oscillation is detected. Both observations are in good agreement with OT and in this presentation it will be shown that by evaluating the scattering data the response function of the rods can be calculated equivalently to OT.

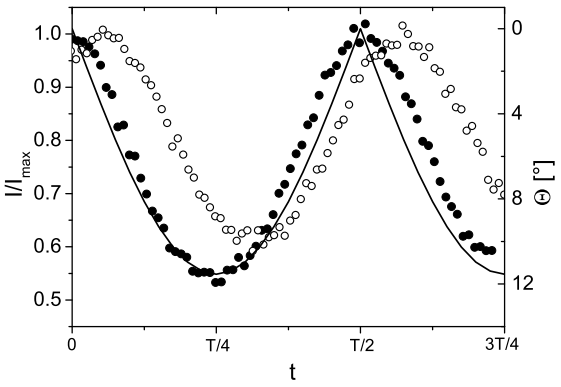

Figure 3: Integrated intensity in the vertical sector of the scattering patterns for $\omega = 157$ (black) and $6283\,\mathrm{Hz}$ (white) as function of time. The straight line indicates the angle Θ between the field vector and the neutron beam.

Acknowledgments

The authors would like to thank the ILL for the provision of neutron beamtime at D 22 and the BMBF for financial support.

References

[1] P. Bender, A. Günther, A. Tschöpe, R. Birringer, *JMMM*, 2055-2063 (2011)

[2] P. Bender, A. Tschöpe, R. Birringer, *JMMM*, 2055-2063 (2011)

[3] L. Roeder, P. Bender, A. Tschöpe, R. Birringer, A. M. Schmidt, *J. Polym. Sci. Pol. Phys.*, 1772-1781 (2012)

[4] A. Günther, P. Bender, A. Tschöpe, R. Birringer, *J. Phys.: Cond. Mat.*, 325103 (2011)

[5] M. Tirado, J. de la Torre, *J. Chem. Phys*, 1986 (1980)

[6] A. Wiedenmann, U. Keiderling, K. Habicht, M. Russina, R. Gähler, *Phys. Rev. Lett.*, 057202 (2006)

Magnetic targeting of superparamagnetic iron oxide nanoparticles (SPIONs) in the flow model of arterial bifurcations

J Matuszak, J Zaloga, C Alexiou and I Cicha

Section of Experimental Oncology und Nanomedicine (SEON), ENT-Department, University Hospital Erlangen, Glückstr. 10a, 91054 Erlangen

Background

Development of novel diagnostic and therapeutic nanoparticles is one of the most urgent tasks in cardiovascular medicine. Magnetic targeting is considered a promising method to accumulate the nanoparticles at the sites of atherosclerotic lesions. However, little is known about the biological effects of magnetic nanoparticles on the vascular wall. The aim of this study was to analyse the endothelial accumulation of circulating SPIONs (superparamagnetic iron oxide nanoparticles) in an in vitro model of arterial bifurcations, without and with external magnetic force. Moreover, the effects of SPION uptake on cell morphology, activation by TNF-α, and resistance to physiologic levels of shear stress were investigated.

Methods

Human umbilical vein endothelial cells (ECs) were grown in the bifurcating flow-through slides (Ibidi, Munich) until 90% confluence. Subsequently, the cells were perfused at 10 dyne/cm^2 for 18 h with medium containing SPIONs at a concentration of 30 µg/mL (without magnet), or 3 µg/mL (with magnet). The iron content of ECs was estimated using Prussian blue stain. In some experiments, the effects of SPION uptake on monocytic cell recruitment in response to TNF-α were analysed. EC morphology and resistance to physiologic levels of shear stress were investigated by extending the exposure to shear stress in the absence of SPIONs for up to 96 h, following the initial 18 h perfusion with SPION-containing media.

Results

Our results showed a uniform distribution of endothelial SPION uptake independent of channel geometry or hemodynamic conditions: In the absence of magnetic force, no increase in accumulation of SPIONs at non-uniform shear stress region at the outer walls of bifurcation was observed. Application of external magnet allowed enhanced accumulation of SPIONs at the regions of non-uniform shear stress even at 10-fold decreased nanoparticle concentrations, accompanied by a reduced endothelial uptake in laminar shear stress regions. Increased uptake of SPIONs at non-uniform shear stress region was well tolerated by ECs and did not affect endothelial cell viability or resistance to prolonged shear stress exposure. At the tested concentrations, SPIONs were metabolized within 3 days post-application. Importantly, no significant increase in TNF-α-induced monocytic cell recruitment was detected upon SPION treatment.

Conclusions

Magnetic targeting allows localized accumulation of increased amounts of SPION at the region of interest under physiologic-like flow conditions, thus enabling a substantial reduction of the applied dose. These findings indicate that magnetic targeting can constitute a suitable technique for the delivery of imaging and therapeutic nanoparticles to atherosclerotic lesions. Further preclinical studies *ex vivo* and in animal models will be necessary to standardize the magnetic field and nanoparticle parameters for cardiovascular applications.

Acknowledgments

This work was supported by the DFG grant CI162/2-1 and the EU project FP7-NMP-2012-LARGE-6-309820.

Magneto-optical properties of colloidal mixtures of anisometric non-magnetic pigment particles and ferrofluids

A. Eremin[1], K. May[1], R. Stannarius[1], P. K. Challa[2], J. Gleeson[2], A. Jákli[2], S. Klein[3]

[1] *Otto-von-Guericke Universität, FNW/IEP/ANP, 39106 Magdeburg, Germany*
[2] *Liquid Crystal Institute, Kent State University, Kent, OH 44242-0001, USA*
[3] *HP Laboratories, Long Down Avenue, Stoke Gifford, Bristol BS34 8QZ, UK*

Colloidal suspensions of anisometric particles have become attractive materials for their ability to form structured phases (such as nematics and smectics) and their complex behaviour in electric fields. Such responsive anisotropic colloids have a great potential for the development of smart functional materials.

In our research, we study rod-shaped anisometric colloidal pigment particles dispersed in dodecane. The sub-micrometre size particles have a slenderness ratio of approx. 4:1 (Fig. 1). These dispersions belong to nonpolar colloids and they are distinguished by a formation of orientationally ordered states at a volume fractions as low as 0.17 (Fig. 2). At lower volume fractions, the dispersions behave optically isotropic, but show a strong shear-induced and electric field-induced birefringence as well as non-linear rheological behaviour.

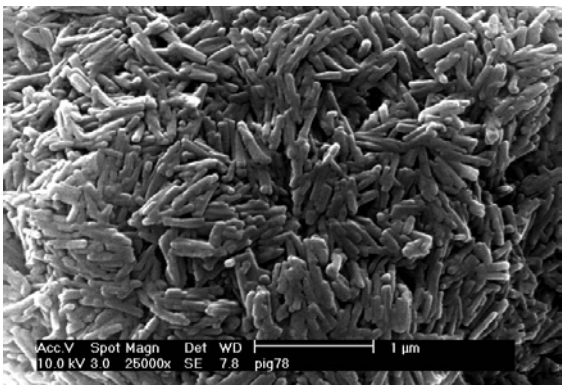

Figure 1. SEM image of the investigated pigment particles.

The pure dispersions of the pigment particles are diamagnetic. They show a very weak magneto-optical response, which was observed in very strong magnetic field up to 25T.

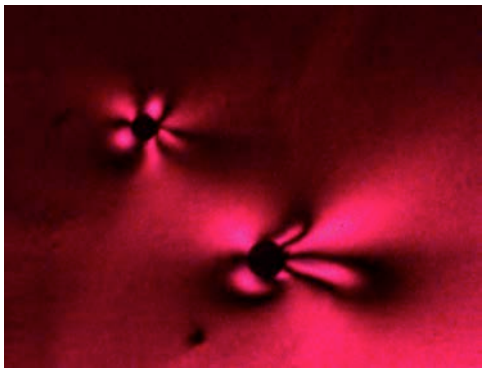

Figure 2. Schlieren texture around two trapped air bubbles (35 wt/% suspension between crossed polarisers, image width 1.4 mm). The dark brushes show the directions where the local optical axis is aligned parallel to one of the polarisers (here, vertical and horizontal)

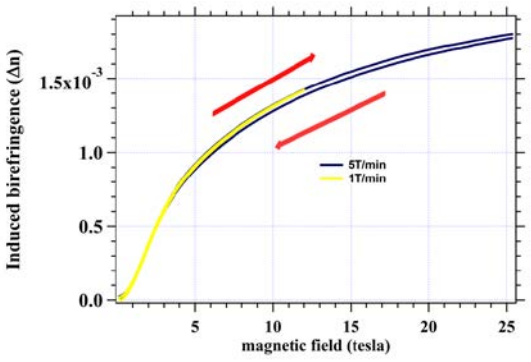

Figure 3. Birefringence vs. magnetic field strength of a 15wt% sample in 30 µm thick sandwich cell.

Yet in contrast to the experiments in an electric field, anisotropic dispersions with high volume fractions exhibited magneto-optical switching.

In 1984, Lekkerkerker et al developed a theory which showed that two-component hard rod dispersions with one magnetic and one non-magnetic component exhibit a stabilised anisotropic phase even at a small concentration of the magnetic particles. Such materials demonstrated in Refs. [3, 4], have an enhanced magneto-optical response. In this presentation, we show an enhancement of the magneto-optical response in the colloidal pigment suspensions mixed with commercially available ferrofluid APG935. The mixture shows good stability and a field-induced birefringence already in fields as low as few hundred Tesla (Fig. 3).

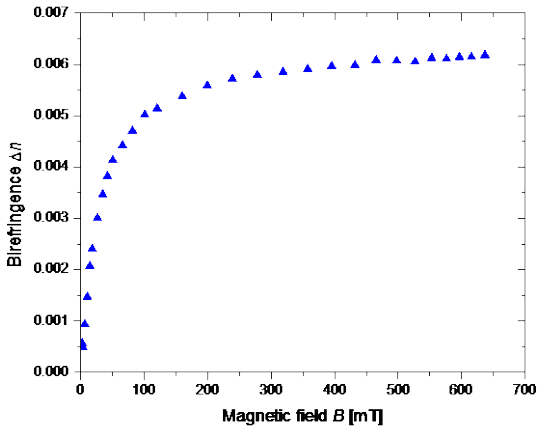

Figure 3. Magnetic-field induced birefringence in a mixture of 6.6 vol% of pigment particles and 0.96 vol% of APG935

Field-induced birefringence has been studied in mixtures of various concentrations of ferrofluid dopant and volume fractions of pigment particles. The results are compared with the predictions of the Onsager-Lekkerkerker theory. This opens door for a development of dichroic electro- and magneto-optic devices based on anisometric pigment particles.

Acknowledgments

This research was supported by Deutsche forschungsgemeinschaft (Project STA 425/28), European COST Action (IC1208), DAAD Grant 56038231. The authors acknowledge the support by NSF for experiments in the National High Magnetic Field Laboratory, Tallahassee.

References

[1] A. Eremin et al, *Adv. Funct. Mater.*, **21**, 402, (2011).
[2] H.N.W. Lekkerkerker et al, *J. Chem. Phys.* **80**, 3427 (1984)
[3] K. Slyusarenko et al, *Phil. Trans. R. Soc. Lond. A*, **371**, 1988, 20120250, (2013).
[4] S. Kredentser et al, *Soft Matter*, **9**, 20, 5061, (2003)

The relation between microstructure and mechanical properties of anisotropic magnetoactive composites

T. Gundermann[1], S. Odenbach[1]

[1] *TU Dresden, Chair of Magnetofluiddynamics, Measuring and Automation Technology, 01062 Dresden*

Introduction

The combination of soft materials like elastomers or foams and magnetically influenceable particles with a size from a few nanometers up to several micrometers leads to the development of a new kind of hybrid materials. Due to the magnetic response of the particles, the mechanical, chemical and electrical properties of such materials can be changed active and reversible by applying a magnetic field. An essential reason for these property changes are internal magnetodipolar forces. This leads to applications e.g. as dampers, actuators, and sensors in measurement technology. The production process of these materials enables various arrangements of the particles. By applying a magnetic field during the polymerization process, the particles align in chain like structures parallel to the magnetic field (fig.1) Due to the restoring force of the polymer network, these chains remain in their position after the polymerization.

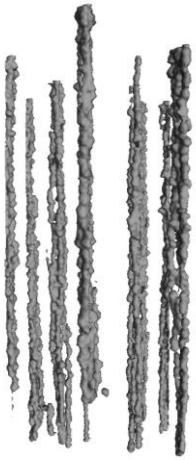

Fig.1: structure formation of particles inside a magnetoactive composite during the polymerization under a magnetic field

Setup

In previous studies it was found that the formation of different structures depends on the particle content [1]. Samples with a particle content of 10 – 30 wt.% were tested and the formation of chain- to cylindrical- up to canyon structures could be observed [1].
The results of [1] have been taken as a basis for investigations with a magnetic field depending stress/strain test (fig.2). Also different materials have been used.

Fig.2: magnetic field dependent stress test

Cylindrical stress test samples based on carbonyl iron particles with a mean size of $d \approx 5$ µm have been investigated. The particles have been dispersed in a soft polymeric matrix supplied by Wacker Corp. Germany. The basic matrix components were mixed with a softener to adjust the elastic modules of the samples. The particle content was varied from 10, 15, 20, 25 to 30 wt.%

Microstructural investigations

By using micro-computed tomography (µ-CT) it could be shown, that the morphology of samples represents the same behavior like in [1]. Fig.3 shows cross sections of the samples. With increasing the particle concentration, the chains change into cylinders (fig.3b) up to canyon structures (fig.3d). With further increasing of the content these structures disappear again to chain like structures (fig.3e).

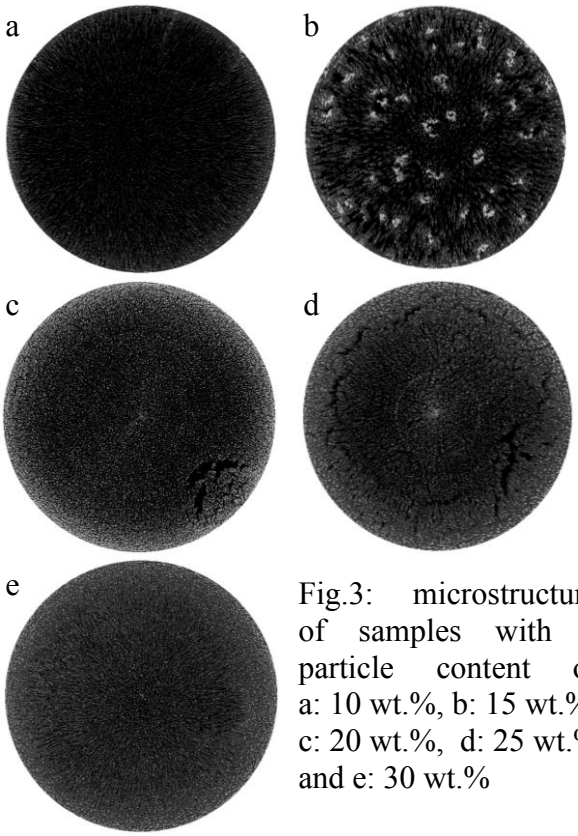

Fig.3: microstructure of samples with a particle content of a: 10 wt.%, b: 15 wt.%, c: 20 wt.%, d: 25 wt.% and e: 30 wt.%

Mechanical investigations

The stress-strain tests for each sample where performed without the influence of a magnetic field and also within a magnetic flux density of B = 150 mT. This allows a comparison of the measured stress within the magnetic field with respect to the stress without magnetic influence. Fig.4 shows the relative change of the stress for the different mass fractions. Obviously, the stress increases by applying a magnetic field. Also due to the increasing particle mass content, therefore more chains are formed and the resistance to an applied stress increases. Independent of the particle concentration the stress increases up to a strain of about 7%. For higher elongations the stress remains in a constant level regardless to the strain. As well it can be seen, that there is barley no difference between the sample with $\Phi = 20$ wt.% and $\Phi = 25$ wt.%. The only slight increase can be explained by the change of microstructure. By using the results of the tomography measurements it could be seen, that starting at approximately $\Phi > 20$ wt.% particle free canyons occur. This leads to a separation of areas and a decreasing influence of the magnetic forces. This can result in a decreasing resistance to an external stress.

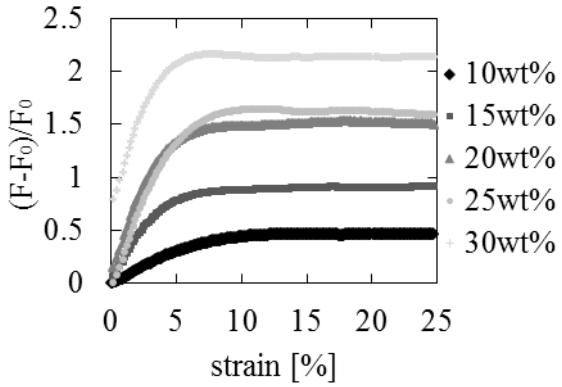

Fig.4: relative change of stress relating strain for magnetoactive elastomers with different mass fractions

Acknowledgments

This project is funded by the European Union and the Free State of Saxony

References

[1] D. Günther, D. Yu Borin, S. Günther, and S. Odenbach, Smart Mater. Struct. 21 015005 (2012).

3D, real-time investigation of magneto-mechanical properties of magnetic hybrid materials

Shilin Huang, Günter K. Auernhammer*

Max Planck Institute for Polymer Research, Ackermannweg 10, 55128 Mainz, Germany

The mechanical properties of a magnetic hybrid material can be controlled by using a magnetic field. It is widely accepted that this magneto-mechanical behavior is related to the magnetic dipolar interactions, which is sensitive to the microscopic structure, e.g., spatial arrangement of the magnetic particles in the hybrid material. However, the microscopic structure is still not easy to be detected especially in a 3D real-time form. This fact leads to the limited understanding of the magneto-mechanical property at a microscopic level.

In this project, we aim at studying the influence of 3D microstructure on the magneto-mechanical properties of magnetic hybrid materials. The local deformation of the magnetic hybrid materials under magnetic field and mechanical load will also be investigated.

Laser scanning confocal microscope (LSCM) is used to image the 3D microstructure of the magnetic hybrid materials. As LSCM can be combined with mechanical testing devices such as nanoindenter and piezorheometer, the microstructure and mechanical property can be detected at the same time [1]. A combination of two Halbach magnetic arrays is used to generate a tunable homogeneous magnetic field. In our study the magnetic particles are fluorescent-labeled in order to be visible under LSCM. The cross-linked polydimethylsiloxane (PDMS) is used as the matrix material. Some fluorescent-labeled tracer particles (non-magnetic, small size) are also used to track the deformation of the matrix material. Image analysis of the 3D confocal images allows us to determine the positions and trajectories of the magnetic particles and the tracers. From these data the internal deformation of the sample shall be deduced.

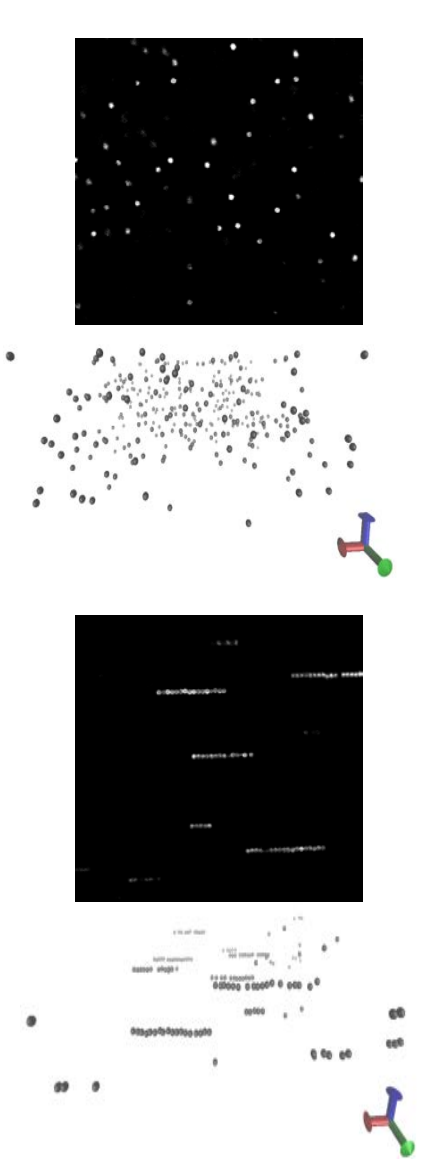

Figure 1: LSCM images (100*100 µm^2) and the 3D reconstructions of two samples with isolated magnetic particles (a) and particle chains (b).

(a)

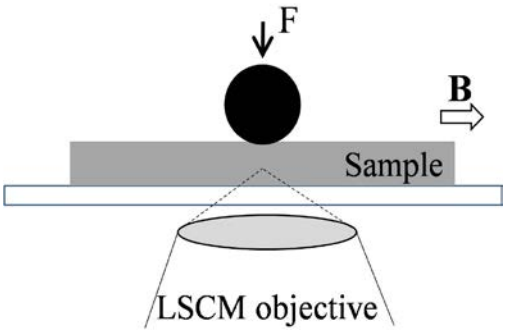

(b)

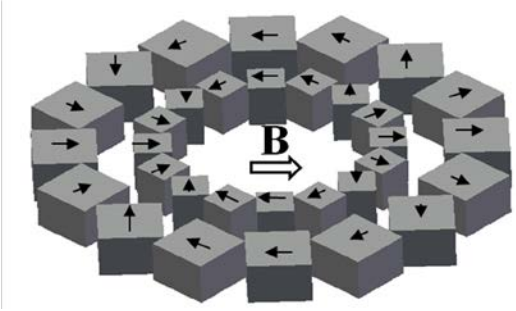

Figure 2: Experimental setup. Nanoindentation is used to apply a mechanical load and measure the elastic modulus of the sample, whose internal structure can be observed at the same time through LSCM. A combination of two Halbach magnetic arrays is used to provide a tunable, homogeneous magnetic field [2].

Acknowledgments

We thank Peter Blümler for inspiring discussions and acknowledge funding by the DFG through the SPP 1681.

References

[1] M. Roth, C. Schilde, P. Lellig, A. Kwade, and G. K. Auernhammer; Eur. Phys. J. E 35 (2012), 9801.

[2] C. Bauer, H. Raich, G. Jeschke 1, P. Blümler; J. Magn. Reson. 198 (2009), 222.

Silica-Encapsulated Ni Nanorods as Model Particles for Stroboscopic Small Angle X-Ray Scattering (S-SAXS)

F. Krämer[1], P. Bender[1], S. Disch[2], M. Kundt[2], D. Honecker[3], A. Tschöpe[1], R. Birringer[1]

[1]*Experimentalphysik, Universität des Saarlandes, Saarbrücken, Germany*
[2]*Department Chemie, Universität zu Köln, Germany*
[3]*Laboratory for the Physics of Advanced Materials, University of Luxembourg, Luxembourg*

Ni nanorods are ferromagnetic single domain particles with distinct anisotropy. Using a polyvinylpyrrolidone (PVP) surface layer, added to prevent agglomeration, the nanorods can be dispersed in water [1]. Alignment of the rods in external magnetic fields can be detected by magnetization and optical transmission measurements [2]. Analysis of the rotation dynamics allows to extract information regarding viscoelastic properties of the surrounding matrix and hydrodynamic parameters of the nanorods [2]. As a new approach, we encapsulated the Ni nanorods with an inorganic silica shell to benefit from

- well defined particle-matrix-interface,
- increased stability in colloidal suspensions.

Due to these properties, silica-coated Ni nanorods serve as model particles for novel S-SAXS experiments. During the measurements, the rods are exposed to a rotating magnetic field. In the S-SAXS modus, a series of SAXS patterns, each with a recording time of 2 ms, was collected. These snapshots can be associated with different rod orientations. To obtain appropriate parameters for the field settings, the rotation friction coefficient of the rods was estimated by independent AC magnetization measurements.

The rods were synthesized by current-pulsed electrochemical deposition of Ni into porous alumina templates [3, 4]. During the dissolution of the alumina matrix, PVP adsorbed

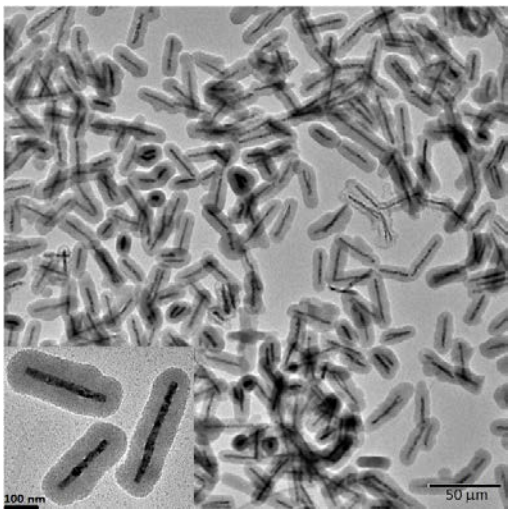

Figure 1: TEM micrograph of silica coated nanorods. The inset shows rods in higher magnification.

at the rod surfaces and served as steric stabilizer in the resulting colloidal dispersion. The Stöber process was used to encapsulate the rods with silica [5].
Fig.1 shows a transmission electron microscopy (TEM) image of the silica encapsulated Ni nanorods. Analysis of several micrographs revealed an average core-diameter of $22\,\mathrm{nm}$, a core-length of $243\,\mathrm{nm}$ and a thickness of the silica shell of $49\,\mathrm{nm}$.
The relaxation behavior of the rods in aqueous dispersions was characterized by AC-magnetization measurements (Fig. 2). The solid line shows a regression of the frequency dependent imaginary part of the magnetic moment $\mathrm{m}''(\omega)$ with a superposition of a Debye and a Cole-Cole relaxation, representing the dynamics of individual nanorods and

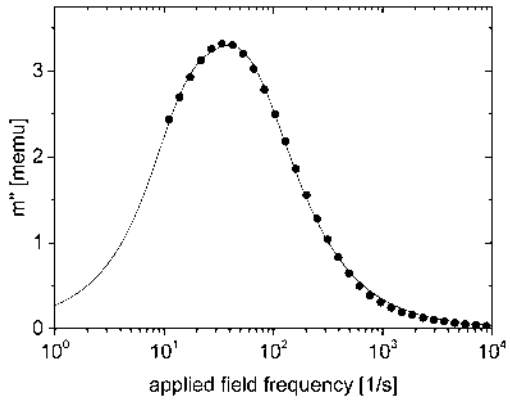

Figure 2: AC-magnetization measurements (field amplitude $1.42\,\mathrm{mT}$) of an aqueous colloidal dispersion of silica-encapsulated nanorods.

agglomerates, respectively. The Brownian relaxation frequency of the rods could be extracted to $\omega_B = 55.5\,\mathrm{rad/s}$, which corresponds to a rotational friction coefficient of $\xi = 1.5 \cdot 10^{-22}\,\mathrm{Js}$.
Considering this result, we chose a field amplitude of $\mu_0 H = 10\,\mathrm{mT}$ (Langevin parameter $\zeta = 148$) and a frequency of $25\,\mathrm{Hz}$ for the applied rotating field to ensure a sufficiently small phase lag of $2.2°$ during the S-SAXS measurements. The left column of Fig.3 shows two scattering patterns obtained in S-SAXS mode. While the top pattern was recorded, the external field rotated from $0°$ to $18°$ relative to the incident X-ray beam. This pattern exhibits rotational symmetry.
The bottom patterns shows uniaxial symmetry and was grabbed while the external field rotated from $90°$ to $108°$. The right column in Fig.3 represents SAXS pattern simulations using a cylindrical core-shell model in SASView. The simulation was based on the given geometric parameters obtained by TEM analysis. For rods parallel to the incident X-rays (top) a rotational symmetric pattern was found while for the perpendicular case (bottom) uniaxial symmetry was obtained in agreement with the experimental observation.
The distinct differences between the snapshots recorded in the S-SAXS mode and their correlation to the calculated diffraction patterns for different rod orientations, show the viability of the S-SAXS method to capture the orientation of silica encapsulated Ni nanorods in a continously rotating magnetic field.

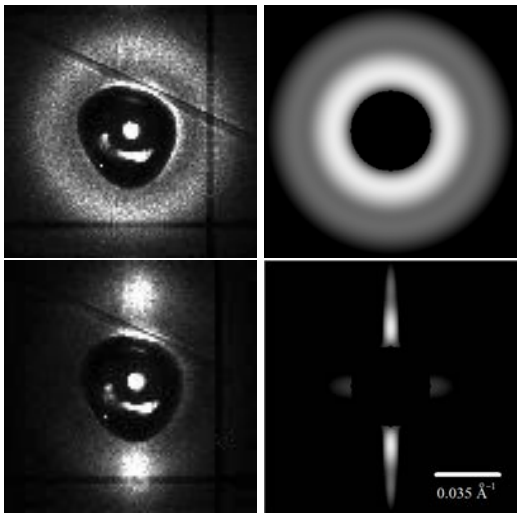

Figure 3: Measured S-SAXS (left) and simulated SAXS (right) patterns for rods parallel (top) and perpendicular (bottom) to the incident X-rays.

Acknowledgments
We acknowledge the European Synchrotron Radiation Facility, Grenoble, France, for providing the synchrotron radiation facilities at beamline ID13. Particularly, Dr. M. Szucki and Dr. M. Burghammer are acknowledged for their support in data acquisition.

References

[1] T. Klein et al, 2009, J. Appl. Phys. 106 114301.

[2] A. Günther et al, 2011, J. Phys.: Condens. Matter 23 325103.

[3] H. Masuda, Jpn. J. Appl. Phys. **35** (1996), L126-L129.

[4] K. Nielsch et al, Adv. Mat. 2000; 12 No.8; 582.

[5] V. V. Hardikar et al, J. Colloid Interface Sci. 221, 133-136 (2000).

Porous composites of elastic matrix and particles with magnetostructural transition

S. Kolay[1], M. Krautz[1], S. Kauffmann-Weiss[2], A. Funk[1], B. Weise[1], O. Gutfleisch[3], J. Eckert[1], A. Waske[1]

[1]*IFW Dresden, Institute for Complex Materials, P.O. Box 270116, D-01171 Dresden, Germany*
[2]*IFW Dresden, Institute for Metallic Materials, P.O. Box 270116, D-01171 Dresden, Germany*
[3]*Materials Science, TU Darmstadt, Alarich-Weiss-Str. 16, 64287, Germany*

Magnetically active hybrid materials of anisotropic magnetic particles in an elastic matrix are of high scientific and technological interest. Within the framework of SPP 1681, we extend this approach by inserting porous structures, such as channels, as a third component. For the intended flow control, the channels' geometry can be changed by a tilt of the shape anisotropic particles when an external field is applied under different angles. The interaction between the different components is a key issue and their mechanical and magnetic properties have to be adjusted carefully. As a model system we chose Ni_2MnGa fibres prepared by melt-extraction [1] and a two-component polymer matrix. Kauffmann-Weiss et al. already showed on a combination of polycrystalline, martensitic Ni_2MnGa fibres and a polymer matrix that a remanent strain of $\approx 10\%$ can be induced by a moderate magnetic field of 1T [2]. In our study Ni_2MnGa fibres and the polymer were mixed with a ratio of 0.7g : 2.0g. After precuring, space holders were infused into the mixture. During curing under ambient conditions a magnetic field of about $\mu_0 H = 0.5$ T was applied to align the fibres along the field direction. After completion the polymerisation the space holders were extracted. In Fig. 1 the subvolume of such a porous composite with austentic Ni_2MnGa fibres is shown. The field was applied perpendicular to the space holders. For simplicity the polymer matrix is kept transparent and only fibres (grey) and channels (black) are shown.

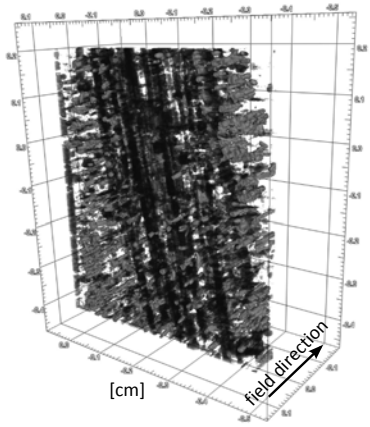

Figure 1: X-ray tomograph of a porous composite with Ni_2MnGa fibres (grey) in a polymer matrix (tranparent). The channels (black) are perpendicular to the fibre chains.

The fibres are well aligned along the field direction and form chains with regular widths. We will present preliminary results of different materials combinations as well as different techniques to insert the channels.

Acknowledgments

The authors greatfully acknowledge SPP 1681.

References

[1] Jian Liu et al., Adv. Eng. Mater. (2012) 14, 653–667.

[2] Kauffmann-Weiss et al., Adv. Eng. Mater. (2012) 14, 20–27.

Investigation of the influence of Kelvin forces on aqueous solutions with paramagnetic ions

G. Lucero, U. Shadewald, B. Halbedel

Technische Universität Ilmenau, Institute of Materials Engineering - Department Group of Inorganic-Nonmetallic Materials, Ilmenau/Germany

Important physical properties of fluids, such as aqueous solutions or glass melts, depend on the distribution of their ionic components. This ion distribution can be influenced by the action of magnetic gradient (Kelvin-) forces [1,2,3]. These forces generated in an inhomogeneous magnetic field - unlike other forces are used to modify the distribution of the components - offer the advantage of acting on fluids without being in direct contact with them.

In these experiments the effect of Kelvin forces on the mass transport of paramagnetic ions in homogeneous aqueous solutions of Dy^{+3} is evaluated. The paramagnetic species used are Dy^{+3} ions due to their high magnetic susceptibility ($\chi_{Sol} = 1.1886 \cdot 10^{-4}$ for a 0.1 molar aqueous solution).
In the experiments a cell with two compartments divided by a PVDF membrane is used. Both compartments contain Dy^{+3} solutions and/or water and one of the compartments additionally contains platinum electrodes for the measurement of the conductivity. The required magnetic field is provided by a cryogen - free high magnetic system. The variables to be considered in these experiments are the direction and magnitude of the Kelvin force and the concentration of the paramagnetic ions. The influence of the magnetic forces on the ions transport is researched through in situ conductometric measurements in one of the compartments. Due to the experimental setup the influence of thermal convection and Lorentz forces on the mass transport will be negligible. The mass transport will be determined in dependence of the concentration difference of the Dy^{+3} ions in both compartments without a magnetic field and then removed from the measurement results with magnetic field.

References

[1] Yang X., Tschulik K., Uhlemann, M., Odenbach S. and Eckert K. (2012) Enrichment of Paramagnetic Ions from Homogeneous solutions in Inhomogeneous Magnetic Fields. *J. Phys. Chem. Lett.,*3, 3559−3564

[2] Chie K., Fujiwara M., Fujiwara Y. and Tanimoto Y. (2003) Magnetic Separation of Metal ions. *J. Phys. Chem. B., 107, 14374 – 14377*

[3] Schadewald, U.; Halbedel, B.(2012) Einfluss magnetischer Gradientenkräfte auf Fluide mit paramagnetischen Ionen. Proceedings Workshop Elektroprozesstechnik, Heyda.

Influence of the viscosity on the MPS performance of magnetic nanoparticles

F. Ludwig, C. Kuhlmann, H. Remmer and T. Wawrzik

Institut für Elektrische Messtechnik und Grundlagen der Elektrotechnik, TU Braunschweig, Hans-Sommer-Str. 66, 38106 Braunschweig

Introduction

An elegant method for the determination of the local viscosity of magnetic nanoparticle (MNP) suspensions is to study their dynamics. Proposed that the magnetic moments are blocked, they follow a time-varying magnetic field via the Brownian mechanism with a time constant given by

$$\tau_B = \frac{\pi \eta d_h^3}{2 k_B T}.$$

Here η is the viscosity, k_B the Boltzmann constant, T the temperature and d_h the hydrodynamic diameter.

Generally, MNP dynamics are investigated applying ac susceptibility (ACS) and magnetorelaxometry (MRX). For example, Fig. 1 depicts relaxation curves measured with a fluxgate MRX setup on FeraSpin^{TM} R MNP in different water-glycerol mixtures.

Similarly, ACS measurements show a monotonous shift of the maximum in the imaginary part χ'' with increasing viscosity towards lower frequencies.

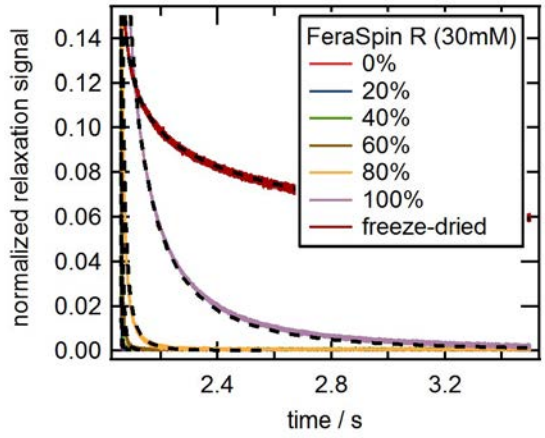

Fig. 1: *MRX curves of FeraSpin R MNP in water-glycerol mixtures. For comparison, MRX curve measured on freeze-dried reference sample is also shown.*

The relaxation curves were fitted with the cluster moment superposition model (CMSM) [1,2]. To restrict the number of free parameters, the core parameters were determined by fitting the MRX curve measured on the immobilized reference sample. The parameters of the hydrodynamic size distribution were determined from the MRX curve measured on the pure aqueous sample with known viscosity. Fitting the remaining MRX curves, the viscosity was left as only free parameter. The obtained viscosities are depicted in Fig. 2. The line shows the nominal viscosities calculated using the formula by Cheng [3]. As can be seen, the viscosities determined from MRX measurements agree excellently with the expected values. For comparison, the viscosities estimated from rheometric (plate-plate rheometer) and ACS measurements (from maximum in χ'') are also shown.

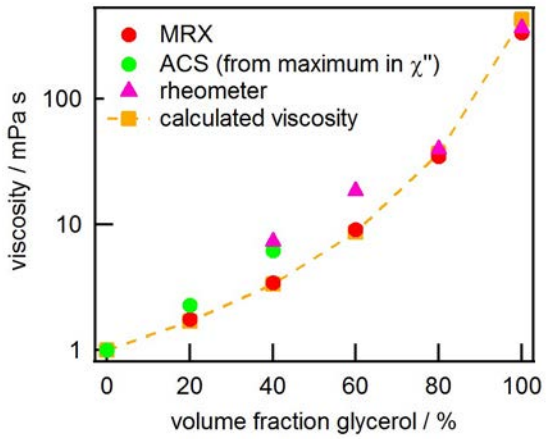

Fig. 2: *Viscosities of FeraSpin R MNP in different water-glycerol mixtures.*

Influence of the viscosity on the MPS spectrum

Magnetic Particle Spectroscopy (MPS) has turned out to be a powerful technique for

testing the Magnetic Particle Imaging (MPI) performance of MNP. The MNP sample is exposed to a sinusoidal excitation field with amplitude of typically 25 mT. Since the amplitude exceeds the linear range of the Langevin function, the signal induced in the gradiometric detection coil also contains higher harmonics. This harmonic spectrum directly reflects the distribution of magnetic moments in the sample and – if performed at various excitation frequencies – the MNP dynamics.

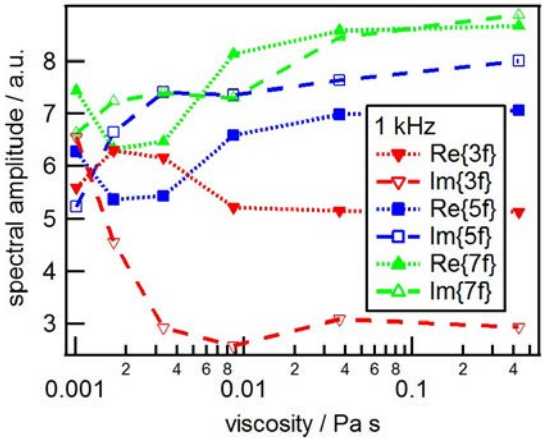

Fig. 3: *Measured spectral amplitude of real and imaginary part of 3rd, 5th and 7th harmonics as a function of viscosity.*

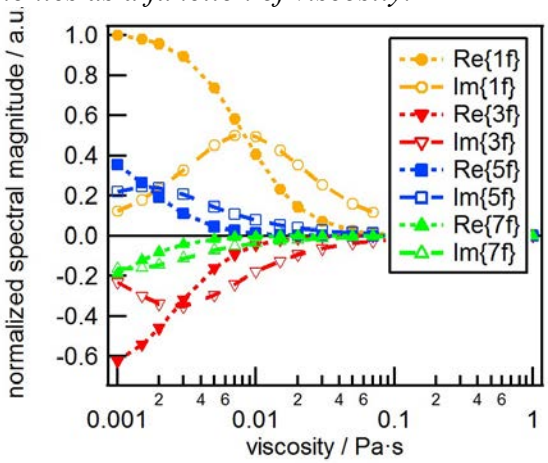

Fig. 4: *Simulated viscosity dependence of spectral amplitudes of real and imaginary parts of harmonics.*

Performing MPS measurements on the water-glycerol mixture series of FeraSpin R MNP, we found, however, a non-monotonic variation of the harmonic spectrum when increasing the viscosity. Naively, one would expect a gradual change of the spectrum between that of the aqueous suspension and the immobilized reference sample when increasing the viscosity. In Fig. 3, the spectral amplitudes of real and imaginary parts of the 3rd, 5th and 7th harmonics are shown. Clearly, real and imaginary parts of the various odd harmonics depend very differently on viscosity.

To explain this very complex response, we developed a refined Debye-based magnetization model [4] which – at least qualitatively – explains the experimentally observed behavior. Fig. 4 depicts the calculated normalized spectral amplitudes of real and imaginary parts for the 3rd, 5th and 7th harmonics. The differences between the measured (Fig. 3) and simulated results (Fig. 4) can be attributed to the fact that the model accounts either for the Brownian or the Néel process whereas in the FeraSpin R sample both relaxation mechanisms are present [5].

Acknowledgments

Financial support by the DFG via SPP 1681 (grant no. LU 800/4-1) and by the BMWi under grant no. KF3061201UW2 are acknowledged.

References

[1] D. Eberbeck, F. Wiekhorst, U. Steinhoff, and L. Trahms, J. Phys. D: Appl. Phys. 18, S2829 (2006)

[2] F. Ludwig, E. Heim, M. Schilling, and K. Enpuku, J. Appl. Phys. 103, 07A314 (2008)

[3] N.-S. Cheng, Industrial & Engineering Chemistry Research 47, 3285 (2008).

[4] T. Wawrzik, T. Yoshida, M. Schilling, and F. Ludwig, IEEE Trans. Magn. (submitted)

[5] F. Ludwig, T. Wawrzik, T. Yoshida, N. Gehrke, A. Briel, D. Eberbeck, and M. Schilling, IEEE Trans. Magn. 48, 3780 (2012)

A size-selective Synthesis of Cobalt Nanoparticles with Thin Shell of Silica

N. Matoussevitch[1*], E. A. Prasetyanto[2], N. Licciardello[1,2], L. De Cola[1,2]

1:Karlsruhe Institut fuer Technologie (KIT), Karlsruhe, Germany
2: ISIS, Univeristy of Strasbourg, France

Cobalt nanoparticles are well known for their performance in the magnetic fluidic and other magnetic related applications. However the utilization of this type of nano materials in biomedical related applications has not been widely studied; mostly due to the toxicity of the cobalt particles. One strategy to overcome this limitation is by building a completely non-toxic layer on the outer surface of cobalt nanoparticles. And since size of the particles is very important for this application, herein we report the synthesis route to produce well-controlled different size of cobalt nanoparticles covered by thin layer of silica shell.
A size selective preparation route of cobalt nanoparticles is done via the thermal decomposition of $Co_2(CO)_8$ in the presence of aluminum alkyls [1]. This technique leads to air stable colloidal cobalt nanoparticles. By varying the Al-alkyl chain length and the Co : Al ratio, we could adjust the particles size between 3 and 10 nm. The particle size distribution of particles was examined by TEM technique.

AlR_3	Co : Al	d [nm]
$Al(CH_3)_3$	10 : 1	3-4.5
$Al(C_2H_5)_3$	10 : 1	6.5 – 8.5
$Al(C_8H_{17})_3$	5 : 1	8.5 –10.5
$Al(C_8H_{17})_3$	1 : 2	5±1.1

Table 1. Correlation of the Co-particles size with AlR_3 - chain length and the molar Co: AlR_3

The silica shell was created through ligand-like interaction of sililated mercapto functional group and followed by condensation of silica in basic media.
In other cases, the cobalt nanoparticles also can be dried in vacuo giving a long term air stable magnetic Co-powder which can be handled under ambient conditions and remain they magnetic properties a long time. The isolated from suspension the Cobalt particles also may be peptized in different carrier liquid with the suitable surfactants which combine the strong adsorption properties on the particle surface, good protecting abilities to prevent the particles from oxidation and a good solubility in carrier-liquids to give remarkably stable magnetic fluids applicable for a many practical purposes [2].

References:

1. H. Bönnemann, W. Brijoux, R. Brinkmann, N. Matoussevitch, N. Waldöfner, DE10227779.6 (WO 2004/001776; PCT/EP 2003/003814)
2. N. Matousevitch, A. Gorschinski, W.Habicht, et.al."Surface modification of metallic Co nanoparticles", J. Magnetism and Magnetic Materials, 308, (2007)

The influence of hydrodynamic diameter and core composition on the magnetoviscous effect of biocompatible ferrofluids.

J.Nowak[1], F. Wiekhorst[2], L. Trahms[2], S. Odenbach[1]

[1] *Chair of Magnetofluiddynamics, Measuring and Automation Technology, Technische Universität Dresden, Dresden 01062, Germany*
[2]*Physikalisch-Technische Bundesanstalt, Abbestr. 2-12, 10587 Berlin*

Regarding the biomedical application ferrofluids receive a growing importance as they show the potential to e.g. aid in the treatment of cancer by targeting of the employed chemotherapeutics or by a destruction of the cancerous tissue using magnetic heating treatment.
To enable an effective and safe application of the fluids a detailed knowledge of the flow behaviour is essential. As strong magnetic fields are required for most of the applications especially the rheological behaviour, if a magnetic field is applied, has to be investigated as a rise of viscosity is well known from ferrofluids used in the engineering context [1].
This behaviour is denoted as the magnetoviscous effect (MVE) *R* and can be calculated using the viscosity without the influence of a magnetic field $\eta_{(H=0)}$ as well as the viscosity if a magnetic field of certain strength is applied $\eta_{(H)}$ [1] :

$$R = \frac{\eta_{(H)} - \eta_{(H=0)}}{\eta_{(H=0)}}. \qquad (1)$$

It has been shown in previous work that a strong MVE can be measured for biocompatible ferrofluids [2]. To gain a more detailed understanding of the parameters influencing this effect for ferrofluids used in the biomedical context this experimental study compares three different fluids obtained from the Chemicell GmbH (Berlin). Detailed parameters are given in table 1. All fluids use starch as surfactant, feature a concentration of suspended material of 25 mg/ml and are denoted as fluidMAG-D.

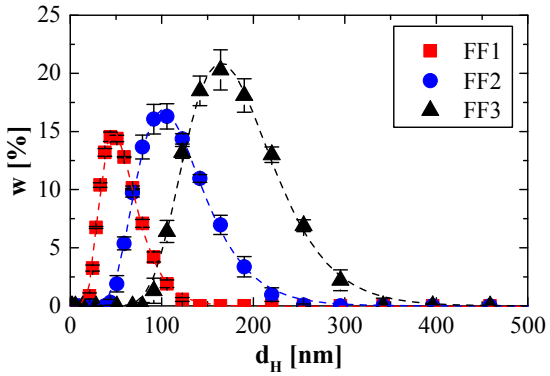

Figure 1: Particle size distribution obtained by DLS including the respective log-normal fits.

The microscopic structure of the magnetic nanoparticles used in the suspensions is investigated using dynamic light scattering (DLS), magnetorelaxometry (MRX) and transmission electron microscopy (TEM). Figure 1 shows the results measured with DLS while table 2 compares the results of log-normal fits used to describe the particle size distribution obtained from DLS and MRX.
The results show slight deviations and closely confirm the mean sizes of the hydrodynamic diameter given by the manufacturer. The differing cores regarding single- and multicore composition were proved using the aforementioned TEM images.

Ferrofluid	core composition	d_H [nm]	M_S [kA/m]
FF1	singlecore	50	0,771
FF2	multicore	100	0,978
FF3	multicore	200	1,319

Table 1: Parameters of the ferrofluids under investigation. The parameter d_H refers to the hydrodynamic diameter given by the manufacturer and M_S to the saturation magnetization measured with a vibrating sample magnetometer.

Ferrofluid	$d_{H,DLS}$ [nm]	$\sigma_{H,DLS}$ [nm]	$d_{H,MRX}$ [nm]	$\sigma_{H,MRX}$ [nm]
FF1	55,6	0,39	55	0,36
FF2	114,1	0,35	80	0,45
FF3	178	0,29	181	0,49

Table 2: Parameters obtained from log-normal fits to the particle size distributions measured with dynamic light scattering ($d_{H,DLS}$ and σ_{DLS}) as well as Magnetorelaxometry ($d_{H,MRX}$ and σ_{MRX}).

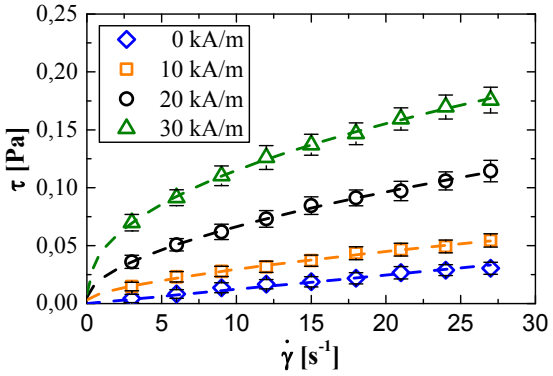

Figure 2: Flow curves of the ferrofluid FF3 for several magnetic field strengths.

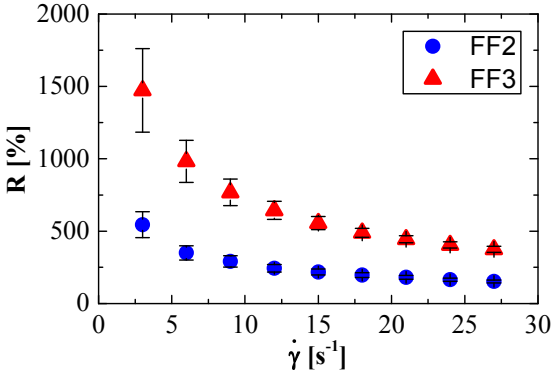

Figure 3: The MVE of the multicore ferrofluids for a magnetic field strength of 35 kA/m.

The measurements regarding the rheological characteristics were realised using a specially designed rheometer [3].

For the ferrofluid FF1 no MVE could be detected. This is connected to a very small modified interaction parameter [4] $\lambda^*<<1$. An interaction of the particles and therefore a change in viscosity can only be expected for $\lambda^* >1$.

In contrast the results show a strong influence of the magnetic field on the flow curves for the ferrofluids having a multicore composition (e.g. for FF3 in figure 2). For the mathematical description of the flow curves the Herschel-Bulkley model can be used. The MVE calculated with equation (1) is shown in figure 3. Therefore the higher hydrodynamic diameter of FF3 has a major influence on the MVE of the ferrofluid, as this fluid has an effect being approximately three times greater.

Regarding the interaction parameter for those multicore ferrofluids the abovementioned modified interaction parameter can not be used due to the multiple magnetic moments in the cores. Previous studies showed good results using a modified interaction parameter originally introduced for magnetorheological fluids [5]:

$$\lambda_{MC} = \frac{\pi \mu_0 \mu_F \beta^2 (d/2)^3 H_0^2}{2 k_B T} \left(\frac{d}{d+2s}\right)^3. \qquad (2)$$

The calculation of this parameter results in values significantly greater than one for both multicore ferrofluids.

Therefore the hydrodynamic diameter as well as the interaction parameter calculated for the respective fluids are appropriate parameters for an estimation of the magnetoviscous effect which has to be expected from the respective fluid. This leads to the possibility to adapt manufacturing as well as application of the fluids to the expected changes in viscosity under the influence of an external magnetic field.

Acknowledgments

We thank the research group Mechanical Process Engineering (TU Dresden) for the DLS measurements. Financial support by the Deutsche Forschungsgemeinschaft under grant no. OD18/13-3 and TR408/4-3 is gratefully acknowledged.

References

[1] S. Odenbach; (2002) The Magneto-viscous Effect in Ferrofluids; Berlin: Springer

[2] J. Nowak, D. Wolf, S. Odenbach; (2014) A rheological and microscopical characterization of biocompatible ferrofluids; J. Magn. Magn. Mater. 354: 98–104

[3] S. Odenbach, T. Rylewicz, M. Heyen; (1999) A rheometer dedicated for the investigation of viscoelastic effects in commercial magnetic fluids; J. Magn. Magn. Mater. 201: 155-158

[4] S. Thurm, S. Odenbach; (2002) Magnetic Separation of ferrofluids; J. Magn. Magn. Mater. 252: 247-249

[5] G. Bossis, O. Volkova, S. Lacis, A. Meunier; (2002) Magnetorheology: Fluids, Structures and Rheology; Berlin: Springer

The magnetic snail

Stefan Hartung[1], Ingo Rehberg[1], Reinhard Richter[1]

[1] *Experimentalphysik 5, Universität Bayreuth, 95440 Bayreuth, Germany*

Positioning a drop of ferrofluid next to a small permanent magnet can be used to demonstrate the superparamagnetic nature of ferrofluid on the slide of an overhead projector: Drop and magnet are instantly attracted by each other and eventually the magnet floats on a thin layer of ferrofluid. Similarly a ferrofluidic film is carrying load in magnetic bearings [1] and positioning systems [2]. Here we report for the first time how a magnet autonomously travels on a ferrofluidic film. The photo in Fig. 1 displays a trace (the text “Ep5”) together with the magnet. The latter moves on this trace, up to the end, like an inverse snail absorbing its own slime. In this way it is an autonomous mobile robot [2].

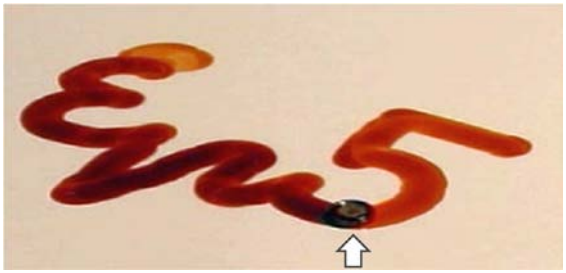

Figure 1 The magnetic snail (see arrow) is traveling on a trace forming the text “Ep5”.

For a quantitative investigation we use the setup sketched in Fig.2. An inclined plane made from perspex® is positioned in-between an electro luminescent film and a camera. The angle of inclination α is measured by means of an electronic goniometer connected to a computer. On top of the ramp a magnet with a mass of 2g and a diameter of 8 mm is positioned on a volume of 32 ± 3 µl ferrofluid and kept in place by a trigger. Activating the trigger, the magnet slides down the plane with the constant velocity v_1 leaving a straight trace of ferrofluid. Reaching the end of the plane

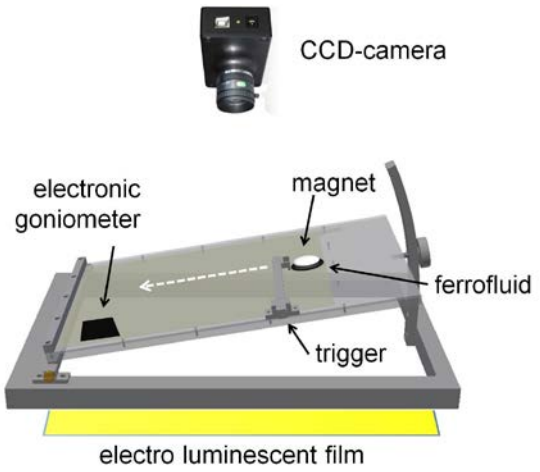

Figure 2 Scheme of the experimental set-up.

the inclination is switched to 0°. Now the magnet is traveling back on its own trace, as displayed in Fig. 3a. Figure 3b indicates that the ferrofluidic film ahead of the magnet is thicker than the one behind it. Apparently this asymmetry results in an effective Kelvin force, which is driving the magnet. The thickness of the film in Fig.3b is measured by means of light absorption. For calibration we use a ferrofluidic ramp as shown in Fig. 4. The solid line stems from the multi-exponential fit of Eq.(1), which is taking into account the polychro-

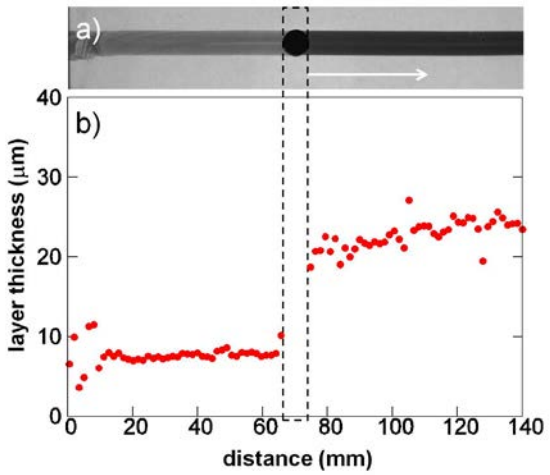

Figure 3 The trace of the snail (a) and its measured thickness (b).

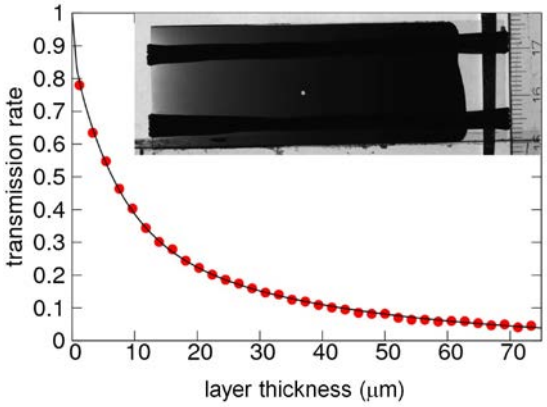

Figure 4 Absorption curve for a ferrofluidic ramp, enclosed by two microscope slides (see inset) with a distance of 0μm at the l.h.s and a distance of 100μm at the r.h.s.

matic nature of the radiation emitted by the light source [4]

$$\frac{I}{I_0}(x) = f_1 \exp(\beta_1 x) + f_2 \exp(\beta_2 x) + (1 - f_1 - f_2)\exp(\beta_3 x) \quad (1),$$

where β is the extinction coefficient. In our contribution we investigate the motion of the inverse snail in dependence of the inclination α of the plane it was sliding down before. Our preliminary results, as shown in Fig. 5, indicate an accelerated motion in the plane, following

$$x(t) = x_0 + v_0(\alpha)\cdot t + \frac{1}{2}a(\alpha)\cdot t^2 \quad (2).$$

In Fig. 5 we find that films generated at larger α result in a larger acceleration *a* of the inverse snail.

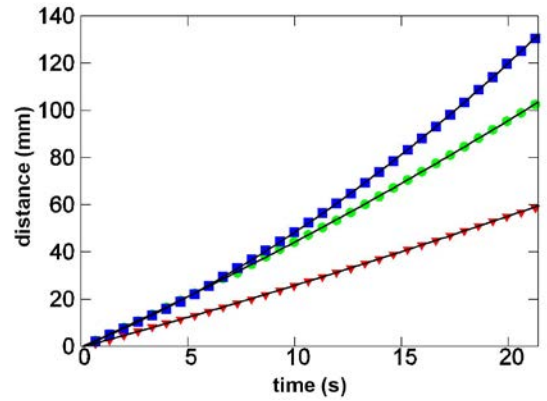

Figure 5 Propagation of the inverse snail on traces generated with an inclination of α =5° (triangles), 10° (circles) and 20° (squares).

Moreover the difference in film thickness ahead and behind the snail and its impact on *a* will be studied.

To conclude, a permanent magnet is sliding on a previously well prepared homogeneous film of ferrofluid. Its apparently autonomous motion is guided by the trace and driven by a reduction of the over-all magnetic field energy: the ferrofluid is collected at the magnet. Our magnetic snail may be used to transport small cargo, like drugs, on complex path ways. It can easily be miniaturized and may also be useful for microfluidic applications.

Acknowledgments

The authors thank Thomas Friedrich and Vidar Frette for valuable discussions, Klaus Oetter for constructing the setup and Stephan Messlinger for creating an USB-driver for the commercial goniometer-chip.

References

[1] B. Berkovski, V. Bashtovoi (Edts.) *Magnetic Fluids and application handbook*, Begell house, inc, New York, Wallingford (UK) (1996).

[2] N. Bayat, A. Nethe, J.M. Gulbak-ke, J. Hesselbach, V.A. Naletova, H.-D. Stahlmann, E. Uhlmann, K. Zimmermann, *Technical applications* p.359-427 *in* S. Odenbach (Edt.) *Colloidal magnetic fluids: Basics, Development and Application of Ferrofluids*, Lect. Notes Phys. 763, Springer, Berlin, Heidelberg, New York (2009).

[3] V. Bashtovoi, E. Blums, and S. Kamiyama, *Fluid mechanical phenomena*, chapter 3 in [1].

[4] Ch. Gollwitzer, R. Richter, I. Rehberg, G. Mathies and L. Tobiska, *The Surface Topography of the Rosensweig Instability — a Quantitative Comparison between Experiment and Numerical Simulation*, J. Fluid Mech. 571, 455-474 (2007).

Modelling the field dependence of the effective relaxation time in Magnetic Particle Spectroscopy

D. Schmidt[1], F. Palmetshofer[1], D. Heinke[2], U. Steinhoff[1], F. Ludwig[3]

[1] *1Physikalisch-Technische Bundesanstalt, 10587 Berlin, Germany*
[2] *nanoPET Pharma GmbH, 10115 Berlin, Germany*
[3] *Institute of Electrical Measurement and Fundamental Electrical Engineering, TU Braunschweig, 38678 Braunschweig*

Introduction

In the last years, Magnetic Particle Spectroscopy (MPS) has become one of the most powerful tools to characterize magnetic nanoparticles (MNP) for Magnetic Particle Imaging (MPI). For a detailed understanding of MNP dynamics a consistent simulation of the MPS signal is of considerable interest.
Traditionally, the Gilbert-Landau-Lifschitz equation is solved for distributions of anisotropy constant and effective magnetic diameter. The results are integrated in order to represent a realistic MNP ensemble, e.g. in [1]. However, realistic distribution parameters are not easy to obtain. Here, we investigate a simple phenomenological model for the whole MNP ensemble that incorporates the quasistatic magnetization curve and a field dependent time lag of the MNP in dynamic excitation fields.

Simulation method

We describe the total magnetic moment of an ensemble of MNP via a first order linear differential equation, which is based on the work of Shliomis [2], using only physical quantities directly accessible by measurements. This leads to the differential equation

$$m(t) = \chi V H - \tau \frac{dm(t)}{dt} \qquad (1)$$

based on the magnetic moment m, the susceptibility χ, the sample volume V, the magnetic field strength H, the time t and relaxation time τ. From the literature it is known [3] that the relaxation time is field dependent and that $\tau(H)$ decreases with increasing field strength H. However, there exists no generally accepted formula for the calculation of $\tau(H)$. Here, we parameterize $\tau(H)$ as a simple decreasing function

$$\tau(H) = \frac{\tau(H=0)}{1 + aH^b}, \qquad (2)$$

employing the zero field relaxation time $\tau(H=0)$, the magnetic field strength H and two unknown parameters a and b.
It has to be noted that our parameterization might lead to inconsistencies regarding the units, but as it is the first approach to show that this method is applicable it should be taken as a purely empirical relation.
With a time-varying MPI drive field $H(t)$, eq. (1) is now modified yielding the coupled differential equation

$$m(t) = \chi(t) V H(t) - \tau(H(t)) \frac{dm(t)}{dt}. \qquad (3)$$

Eq. (3) can be solved using small time intervals Δt where $\tau(H)$, H and χ are assumed to be constant. The solution for small steps in H is given by

$$m_n = m_{n-1} + (m_{n,eq}(H_n) - m_{n-1}) \left(1 - \exp\left(-\frac{\Delta t}{\tau_n(H_n)}\right)\right) \qquad (4)$$

with $m_{n,eq}$ as the equilibrium moment derived from the $M(H)$ measurement. Note that (4) is solely based on the magnetic moment m and the relaxation time $\tau(H)$. In order to prove the existence of a consistent solution for this model, we estimated a and

b by fitting the model output to measured MPS data and minimizing the difference by a correlation analysis.

Materials and measurements

Different MNP systems (FeraSpin^{TM} R and two experimental formulations, synthesized by nanoPET Pharma GmbH), exhibiting good MPS performance, were investigated. For these particle systems $M(H)$, magnetorelaxometry (MRX) and MPS measurements were performed.

The magnetic moment in equilibrium state was obtained from the $M(H)$ measurements. MRX was used to measure an effective relaxation time at $H = 0$, while MPS was necessary for the correlation analysis. Using the measured $M(H)$ and $\tau(H=0)$ in (4), we calculated MPS spectra for a large number of possible combinations of a and b. For each combination $[a,b]$, a time series $m^*(t)$ was reconstructed by an inverse Fourier transform using only A_3 and higher harmonics. The time series $m^*(t)$ was compared to the reconstructed time series $m_m^*(t)$ of the measured data and the coefficient of determination R^2 was used as a measure of similarity. This procedure was performed for $H = 10\ \mathrm{mT}/\mu_0$ and $H = 25\ \mathrm{mT}/\mu_0$. The parameter combination of a and b that yielded the maximum averaged R^2 for both field strengths was chosen as the result.

Results and discussion

Fig. 1 shows the calculated spectrum according to (4) of one of the particle systems compared to its measured spectrum for $H = 25\ \mathrm{mT}/\mu_0$. The absolute values of simulation and measurement coincide well up to the 15th harmonic and stay very close until the 31th harmonic. The phase of the simulated harmonics were close to the ones of the measured spectrum (deviation < 5°) up to the 13th harmonic and the deviation was always less than 30°. This comparison resulted in a coefficient of determination R^2=0.997. The same $[a,b]$ combination applied for $H = 10\ \mathrm{mT}/\mu_0$ yielded a coefficient of determination R^2=0.993 with coinciding harmonics up to the 9th harmonic.

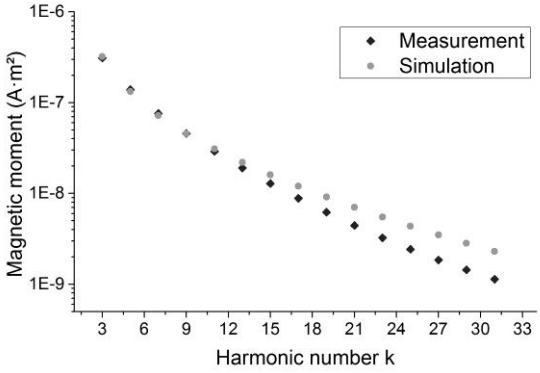

Fig. 1. Comparison of measured and simulated MPS spectrum for H=25 mT/μ_0.

For all three MNP formulations and all drive fields the coefficient of determination was R^2>0.99 (Fig. 1). Note that for each MNP formulation only one pair $[a,b]$ was used to simulate the spectra for $H = 10\ \mathrm{mT}/\mu_0$ and $H = 25\ \mathrm{mT}/\mu_0$.
We have proven that a phenomenological model based on $M(H)$ and MRX data with only two free parameters of $\tau(H)$ is able to predict the dynamic behavior of MNP suspensions in drive fields up to 25 mT.

Acknowledgment

This work was supported by the German Federal Ministry of Economics and Technology grant No. KF2303711UW2, KF3061201UW2 and KF2725002UW2.

References

[1] F. Ludwig et al., "Characterization of magnetic nanoparticle systems with respect to their magnetic particle imaging performance," *Biomedical Engineering*, pp. 1-11, 2013.

[2] M. Shliomis, "Magnetic fluids," *Soviet Physics Uspekhi*, vol. 17, pp. 153-167, 1974.

[3] R. J. Deissler, Y. Wu and M. A. Martens, „Dependence of Brownian and Néel relaxation times on magnetic field strength," *Medical physics*, vol. 41, pp. 012301, 2014.

Nanoscale rheometry of viscoelastic media using oscillating nanorods

A. Tschöpe, K. Birster, B. Trapp, P. Bender, R. Birringer

Universität des Saarlandes, Experimentalphysik, Gebäude D2 2, 66041 Saarbrücken

Nickel nanorods of sufficiently small diameter ($< 40\,nm$) are uniaxial ferromagnetic single-domain particles and exhibit optical anistropy and colloidal stability. Such particles have been employed as local probes for active microrheology using different types of magnetic stimulation. Magneto-optical transmission (MOT) measurements in rotating magnetic fields allowed to monitor changes in the viscosity of Newtonian fluids [1] as well as of the hydrodynamic size of the nanorods upon adsorption of proteins [2]. By contrast, transveral dc magnetic fields were applied to pre-oriented nanorods in soft elastic hydrogels to estimated their shear modulus. Obviously, both approaches are restricted to measurements of either viscous or elastic matrices, respectively. The present study is aiming at a magneto-optical method that enables microrheological characterization of general viscoelastic media. The magnetic nanorods in disperion are stimulated by a magnetic field of constant magnitude and oscillating orientation.

The viscoelastic sample with dispersed nickel nanorods is centered between two crossed Helmholtz coilsets. A constant field H_0 is superimposed with a perpendicular ac field $H_p = H_p^0 \sin(\omega t)$ with $H_p^0 \ll H_h$ resulting in a total field of nearly constant amplitude and direction oscillating within an angular range of $\pm\beta_0 = \arcsin(H_p^0/H_0)$. The magnetic field $H(t)$ generates a time-dependent magnetic torque

$$T(t) = m\,\mu_0 H_0 \sin[\beta(t) - \theta(t)] \qquad (1)$$

on the magnetic moment m of the particle and results in an oscillation of the nanorods $\theta(t)$ which is detected by measuring the transmission of laser light linearly polarized at 45° with respect to the dc field direction.
Mechanical interaction between the nanorods and the matrix is described by $T_\eta(\omega) = K_s \eta \omega$ associated with the viscosity η of the matrix and $T_G(\theta) = K_s G \theta$ determined by the elastic shear modulus G. The geometry factor K_s is a function of the size and aspect ratio of the nanorods [3].
Assuming sufficiently high magnetic fields ($\chi = m\mu_0 H_0/k_B T \gg 1$) the equations of motion for a viscoelastic matrix represented by either the Voigt-Kelvin or Maxwell model, can be solved analytically. For the former, the magneto-optical response function is

$$\hat{X}_{VK}(\omega) = \frac{\hat{\theta}(\omega)}{\beta_0} = \frac{\gamma}{1 + \imath\omega\tau_{VK}\gamma}, \qquad (2)$$

with $\gamma = 1/(1 + KG)$, $K = K_s/m\mu_0 H_0$ and $\tau_{VK} = K\eta$. For vanishing elastic modulus, $G \to 0$, the factor γ approaches unity, which provides the solution for a pure Newtonian fluid as matrix.
This model was applied to analyze oscillating-field magneto-optical transmission (OF-MOT) measurements of the sol-gel transistion of a $2\,wt.\%$ gelatin solution at $21.6^\circ C$, Fig.1. The most striking result is a large delay of the elasticity increase observed by nanoscale rheometry as compared to the macroscopic measurement. Apparently, the nanorod probe particles do not detect elasticity until the mesh size of the elastically active polymer network $\xi \approx (k_B T/G)^{1/3}$ falls below $\approx 70nm$. With continuing network formation, the difference between the

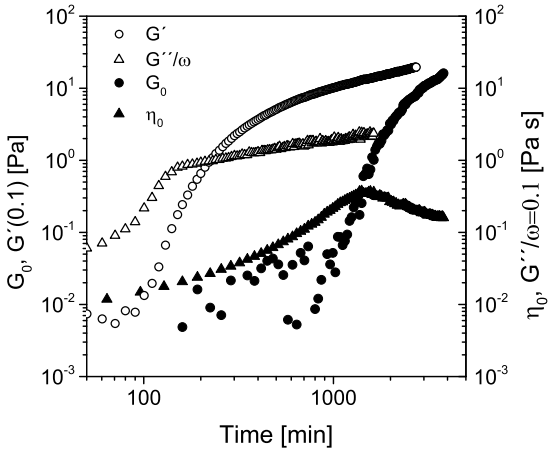

Figure 1: Temporal evolution of the shear modulus and viscosity during sol-gel transition of $2\,wt.\%$ gelatin solution at $21.6°C$ as measured by macroscopic (SAOS, open symbols) and nanoscale rheometry (OF-MOT, closed symbols).

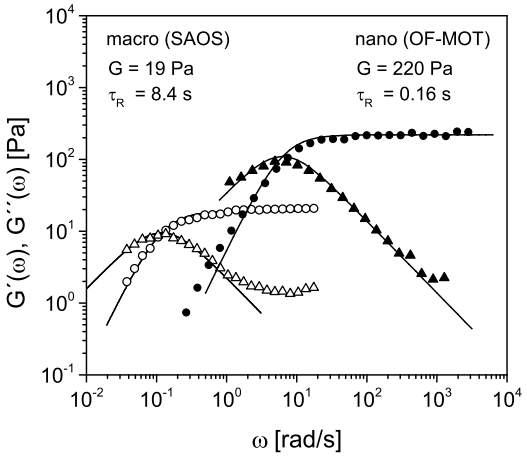

Figure 2: Complex shear modulus of 100mM CTAC / 120mM NaSal wormlike micellar solution at $40°C$ as determined by macroscopic (SAOS, open symbols) and nanoscale rheometry (OF-MOT, closed symbols) as function of angular frequency.

nano- and macroscale elasticity decreases.

The solution for the OF-MOT response function in a viscoelastic matrix, that can be represented by the Maxwell model, is

$$\hat{X}_{M}(\omega) = \frac{1 + i\omega\tau_{M}}{1 + i\omega\tau_{M}/\gamma}, \qquad (3)$$

with relaxation time $\tau_{M} = \eta/G$ and γ as defined above. The results of the OF-MOT measurements can be translated into the more familiar coordinates of frequency-dependent complex shear modulus allowing direct comparison, Fig.2. We found Maxwell-type relaxation in CTAC/NaSal wormlike micellar solution in the macroscopic rheometry as well as on the nanoscale. However, the latter provided a much higher plateau value of the elastic modulus and a much shorter terminal relaxation time.
The two examples demonstrate that magneto-optical measurements of nanorod rotation dynamics in an oscillating field reveal the signatures expected for Voigt-Kelvin or Maxwell-type viscoelastic response. However, bearing in mind that the size of the nanorods is comparable to characteristic length scales (correlation length, Debye length...), the particle-matrix interaction is determined by local mechanical response including steric obstruction, hydrodynamic interaction and local stress relaxation.

Acknowledgments

We greatfully acknowledge funding by the DFG (SPP 1681) and appreciate the support by Andreas Schneider and Christian Wagner (Universität Saarbrücken) with SAOS rheometry measurements.

References

[1] A. Günther, P. Bender, A. Tschöpe and R. Birringer, J. Phys. Cond. Matter **23** (2011) 325103.

[2] S. Schrittwieser, F. Ludwig, J. Dieckhoff, A. Tschöpe, A. Günther, M. Richter, A. Hütten, H. Brueckl, J. Schotter, Small **10** (2014) 407.

[3] M.M. Tirado and J.G. de la Torre, J. Chem. Phys. **73** (1980) 1986.

Computer simulations on the deformation of ferrogels

R. Weeber[1], S. Kantorovich[2], C. Holm[1]

[1] *Institute for Computational Physics, University of Stuttgart, Allmandring 3, 70569 Stuttgart, Germany*
[2] *University of Vienna, Sensengasse 8, 1090 Vienna, Austria*

Ferrogels, i.e., hydrogels that additionally contain magnetic single-domain particles, are interesting materials, because their properties arise from an interplay of magnetic and elastic forces. As they can be controlled by tayloring the polymer network forming the gel and by using external magnetic fields to change the interaction of magnetic particles, magnetic gels are considered for applications, e.g., as artificial muscles and drug delivery systems.

A magnetic gel can deform in a magnetic field for several reasons. In a field gradient, the magnetic particles tend to move to regions with a higher field. When one fixes one end of the gel in a plane perpendicular to the gradient, the material will shrink or expand, as the magnetic nanopartticles strain the polymer matrix. Gels can also deform in a homogeneous magnetic field, which can happen in two ways. First, in the case of highly concentrated and strongly interacting magnetic particles, a deformation can occur, because the magnetic field changes the average interaction between the magnetic particles. When no field is applied, the magnetic moments in the gel are randomly oriented. As a result, there is on average no interaction between them. This changes, once a field is applied and the dipole moments are aligned parallel to it. Then, net forces occur on the magnetic nanopartticles, which in turn strain the polymer matrix. For this mechanism, no coupling is required between the rotational degree of freedom of the magnetic particles and the polymer matrix.

The second way, by which a ferrogel placed into a homogeneous field can deform, depends on just such a coupling between the orientation of the magnetic particles and the polymers. This can be achieved by chemically binding the polymers to specific spots on the surface of the magnetic nanopartticles. When the external magnetic field turns the magnetic particles, the polymers are rolled up around them. This causes a stress on the polymers, which in turn deforms the gel. For this mechanism to work, magnetically hard particles have to be used, i.e., a rotation of the magnetic moment has to imply a rotation of the entire particle. A strong interaction between different magnetic moments in the system, on the other hand, is not required.

In order to better understand these two deformation mechanisms for gels in homogeneous magnetic fields, two simulation models have been introduced and studied, focusing

on each of the mechanisms, respectively. The first model deals with a gel which deforms through the change in interaction between the magnetic nanopartticles in the system. It consists of a two-dimensional network of polymers represented as a bead-spring model. Some of the beads in the chains are assigned a magnetic moment. Each magnetic moment interacts with other magnetic moments in the system, but its orientation is not coupled to the polymer chain. When the gel is placed into a magnetic field, we observe the bending of the polymer chains into the field direction due to the embedded magnetic particles. As a result, the network elongates in field direction and shrinks in the perpendicular direction. Overall, the area occupied by the gel is found to decrease in a magnetic field.

The second model magnetic gel is concerned with a gel's deformation due to the coupling between the orientation of the magnetic moments and the polymer matrix. To this end, magnetic particles are placed at the nodes of the network. These nodes are then connected by attaching polymers, again represented as a bead-spring model, onto specific spots on their surface. The model has been studied in both, two and three dimensions. In the two- dimensional case, an isotropic shrinking of the gel in a magnetic field was observed: all magnetic particles rotate around an axis perpendicular to the model plane, in order to align their moments to the magnetic field. This creates an equal amount of stress on all polymer chains attached to their surface. In the three-dimensional case, the deformation is non-isotropic. The magnetic particles can rotate around three axes to align to the external field. Once the magnetic moments are aligned, however, a further rotation around the axis parallel to the external field is possible without paying an energy penalty for rotating the dipole moment out of the magnetic field. Hence, stresses attached on the chains perpendicular to the field can be reduced to some degree without deforming the network. As a result, the gel contracts more in the direction parallel to the field than in the perpendicular direction. Two different network geometries, one with four chains attached to a node and a diamond cubic unit cell, and one with six chains attached to the node and a simple cubic unit cell, have been considered. The network geometry influences the shape and total amount of the deformation in a magnetic field as well as the elastic properties of the system.

References

R. Weeber, S. Kantorovich, C. Holm: Deformation mechanisms in 2D magnetic gels studied by computer simulations, Soft Matter **8**, 9923, 2012

Acknowledgments

RW and CH thank the DFG for funding through the SRC SimTech and SPP 1681. The computations have been done at the HLRS, Stuttgart. SK was supported by Austrian Science Fund (FWF): START-Project Y 627-N27, RFBR grants mol-a 1202-31-374 and mol-a-ved 12-02-33106, and the Grant of Ministry of Science and Education of RF 2.609.2011.

Magnetic drug targeting model: *In vivo* experiments in pigs

I. Slabu[1,2], A. Roeth[3], T. Schmitz-Rode[2], M. Baumann[2], **F. Wiekhorst[1]**, L. Trahms[1]

[1] *Physikalisch-Technische Bundesanstalt, Berlin, Germany*
[2] *Applied Medical Engineering, Medical Faculty, Helmholtz Institute, RWTH Aachen University, Germany*
[3] *Department of General, Visceral and Transplantation Surgery, University Hospital Aachen, Germany*

Introduction

SPIO (superparamagnetic iron oxides) can be used for therapeutic applications in magnetic drug targeting. Magnetic drug targeting describes the selective targeting of therapeutics in a tissue or a region in the body, e. g. in a tumor, by an external magnetic field in order to allow a controlled drug release.

A new concept of placing an array of permanent magnets (magnetic implant) inside hollow organs of the body was tested *in vivo* in pig experiments. The target site was the bile duct were Klatskin tumors can occur. These are endoluminal tumors which allow the minimally invasive endoscopic insertion of permanent magnets and coils very close to the target site (Figure 1). Hence, a stronger magnetic field and a higher magnetic field gradient in the tumor are achieved.

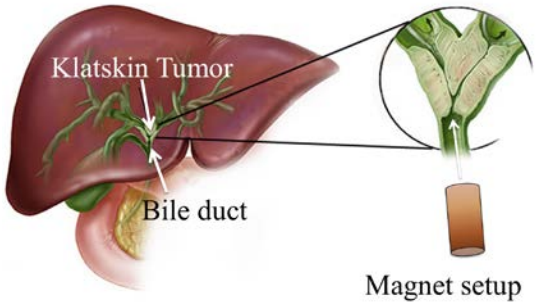

Figure 1: Targeting model of the Klatskin tumor in the bile duct [modified picture from www.hopkins-gi.org].

SPIO were injected into two pigs: a reference pig without the application of the magnet setup and a pig with a magnet setup placed in the bile duct (cf. Figure 1). In order to estimate the influence of the magnetic field on the distribution of the SPIO at the target site, magnetization measurements of different kind of tissues from both pigs were performed and the results were compared.

Materials and methods

An amount of 45 ml of SPIO with an iron concentration of 28 mg/ml was injected intravenously into a pig. Further physico-chemical characteristics of the injected SPIO are listed in Table 1.

Table 1: Physico-chemical characteristics of the SPIO used for magnetic targeting experiments in pigs.

Crystalline structure	Fe_3O_4
Crystal diameter	(8.6 ± 1.8) nm
Hydrodynamic radius	(22 ± 1) nm
Saturation magnetization	(84.0 ± 0.5) emu/g
Susceptibility	(0.124 ± 0.002) emu/(g · Oe)
Coating	Lauric acid

One self-assembled array of permanent magnets with magnetic field strength 0.1 T at their surface and magnetic field gradient of 9 T/m (for simulation results see Figure 2) was inserted in the bile duct. After a SPIO circulation time of 60 minutes, the pig was euthanized and the array was removed. In this way, further particle transport due to blood circulation or magnetic field attraction could be avoided in order not to falsify the results of the subsequent investigations. Tissue samples were extracted and cryopreserved for the recording of the magnetization curve *M(H)* using a SQUID. The experiments with the reference pig were performed in the same way only without the application of the magnets.

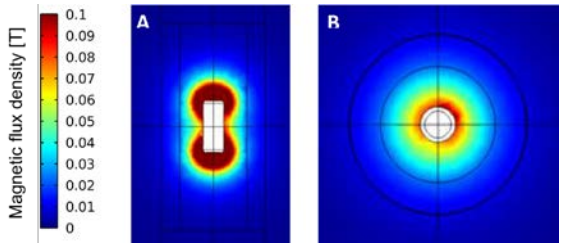

Figure 2: Simulation of the permanent magnet with the software COMSOL Multiphysics® (frontal view (A) and transversal view (B)) used for Klatskin tumor targeting.

As an alternative way to quantify the accumulated amount of SPIO at the target site, Magnetic Particle Spectroscopy (MPS), which is a sensitive quantification method for the specific detection of SPIO in biological systems, was used. MPS is based on the nonlinear part of the magnetic susceptibility response of magnetic nanoparticles induced by an oscillating magnetic field. MPS enables the quantification of the magnetic nanoparticle iron content without being affected by tissue or non-particular body iron. The MPS signal behavior of the SPIO was examined by means of a dilution series of the SPIO in distilled water.

Results and discussion

SQUID measurements confirmed the accumulation of SPIO at the target site, where only the tissues in close vicinity to the magnets changed their magnetic behavior from diamagnetic to paramagnetic (Figure 3). A superparamagnetic behavior was also identified for the liver where the SPIO were filtered out of the circulatory system. This is indication that the used SPIO agglomerated, as liver clearance occurs only for particles bigger than 200 nm. However, a quantification of the accumulated SPIO amount with *M(H)* measurements was not possible.

The MPS measurements revealed a linear dependency of the MPS signal amplitude with iron content and estimate an MPS detection limit of the used SPIO type of a few nanograms (Figure 4). These results evidence MPS as appropriate method to characterize the SPIO amount in tissues for therapeutic applications in magnetic drug targeting.

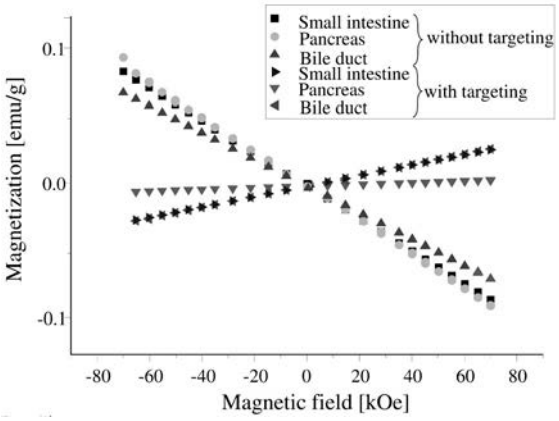

Figure 3: Magnetization measurements on tissues with and without previous targeting. The diamagnetic behavior (negative slope) of the sample changes to a paramagnetic behavior (positive slope) after targeting procedures.

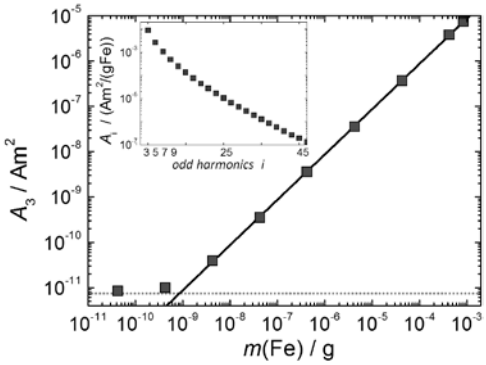

Figure 4: MPS calibration curve obtained from a dilution series of the SPIO in distilled water. The inset shows the MPS spectrum (odd harmonics) for the original suspension normalized to iron amount.

Conclusions

The study demonstrates the efficacy of the magnetic implant supported magnetic drug targeting. To this end, two magnetic measurement techniques were utilized: while *M*(*H*) reflects all kinds of magnetism (dia-, para, and superparamagnetism), MPS is sensitive to superparamagnetism of the SPIO alone.

Rheological properties of composites consisting of anisotropic magnetic particles in a hydrogel matrix

Annemarie Nack, Joachim Wagner

Institut für Chemie, Universität Rostock, Dr.-Lorenz-Weg 1, 18051 Rostock

Composites of spindle shaped hematite particles embedded in a hydrogel network are prepared with different volume fractions and aspect ratios of the colloidal particles. Due to a coil to globuli transition of the thermosensitve poly-N-isopropylacrylamid (pNIPAM) [1] close to ambient temperature the free volume available for the hematite particles can be tuned by the temperature as an external parameter. The orientational distribution function of the elongated hematite particles with an aspect ratio up to $\nu = 5$ can be influenced via external magnetic fields. The mobility of the hematite spindles is governed both, by the free volume available for the particles and their rotational degrees of freedom, which depend on the flux density of an external field. The nonergodic dynamic behavior of the nearly transparent matrix in dependence on the temperature is characterized by means of photon correlation spectroscopy using visible light. The viscosity as well as the complex shear moduli of these composites are investigated in dependence on both, temperature and magnetic flux density. First results show that the restricted rotational mobility of hematite spindles results in a rising viscosity of the composites with increasing flux density of the external field applied parallel to the shear gradient. Nonlinear viscoelastic properties of these materials investigated by means of Large Amplitude Oscillatory Shear experiments [2] are at moderate volume fractions of hematite particles not significantly influenced by external fields.

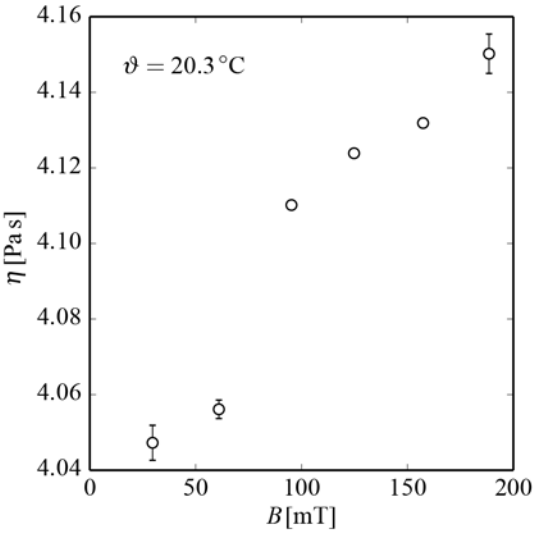

References

[1] D. S. Simmons, I. C. Sanchez , *A Model for a Thermally Induced Polymer Coil–to–Globule Transition*, Macromolecules, **41**, 5885–5889 (2008)

[2] M. Wilhelm, D. Maring, H.W. Spiess, *Fourier-transform rheology*, Rheologica Acta **37**, 399–405 (1998)

Measurement of microviscosity in crosslinked polyacrylamide ferrohydrogels by Mössbauer spectroscopy

J. Landers[1], L. Roeder[2], A. Schmidt[2], H. Wende[1]

[1] *Faculty of Physics and Center for Nanointegration Duisburg-Essen (CENIDE), University of Duisburg-Essen*
[2] *Department Chemie, Institut für Physikalische Chemie, Universität zu Köln*

Introduction

While the rheology of polymer systems has been extensively studied in the past decades, the effect of direct constraint of particle movement by polymer networks in nanoparticle-hydrogel hybrids has not yet been completely understood. The use of magnetic nanoparticles as probes allows examining dynamic properties of liquid samples by ^{57}Fe-Mössbauer spectroscopy on an atomic scale. The motion of the iron ions contained in the nanoparticles is reflected in a considerable line broadening of the associated Mössbauer spectrum, so even slow translatory or rotational motion and very low relaxation times can be measured and quantified by this method.

Preparation

Several polyacrylamide (PAAm) hydrogels with different amounts of methylenebisacrylamide (MBA) as crosslinker were prepared, containing acicular hematite (α-Fe_2O_3) nanoparticles with an average length of 390 nm and an average diameter of 85 nm [1].
The hydrogel samples were mounted on a self-constructed sample holder with an integrated Peltier cooling-element. This setup allowed us to perform Mössbauer spectroscopy measurements in the 'liquid' as well as the 'solid' hydrogel state at tunable temperatures down to 245K. Mössbauer spectra were recorded up to velocities of about 200 mm/s by the combination of a laser interferometer used for calibration and a high-velocity Mössbauer driving-unit, which is essential to measure spectra with distinct line broadening.

Results

We observed static and sharp sextet spectra at temperatures up to 265K, corresponding to the frozen state without nanoparticular motion. A moderate increase of the linewidth Γ indicated beginning movement at about 270K before reaching the liquid state, while linewidths up to 30 mm/s were measured above the water melting point.
This reveals that, contrary to expectations, embedded nanoparticles are not completely immobilized even in strong crosslinked hydrogel networks. We can quantify those effects of Brownian motion by Mössbauer spectroscopy.

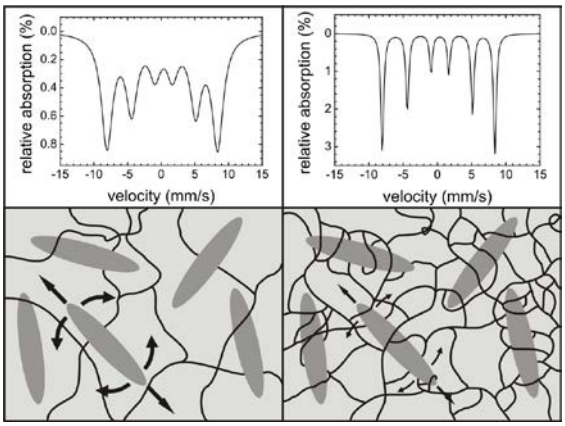

Figure 1: Hydrogel networks with different degrees of cross-linkage. Associated Mössbauer spectra (simulated, same temperature) illustrate the effect of reduced particle motion.

Theoretical calculations result in a temperature dependent effective microviscosity $\eta(T)$ estimated from $\Gamma(T)$ [2], which exceeds η_{H2O} by far and is correlated to the amount of MBA crosslinker.

Acknowledgments

This work was supported by DFG WE2623/7-1, SPP 1681. The authors are grateful to U. von Hörsten for his expert technical assistance.

References

[1] L. Roeder, P. Bender, A. Tschöpe, R. Birringer, A. M. Schmidt, *J. Polym. Sci. Part B: Polym. Phys.,* **50(24)**, 1772-1781 (2012).

[2] P. Fornal and J. Stanek, *Acta Phy*s. *Pol., A,* **114**, 1667-1673 (2008).

List of Participants

Sebastian Altmeyer
Institute of Science and Technology Austria
sebastian_altmeyer@t-online.de

Ingo Appel
Karlsruher Institut für Technologie
ingo.appel@kit.edu

Abdolhamid Attaran
Technische Universität Dresden
abdolhamid.attaran@tu-dresden.de

Günter Auernhammer
Max-Planck-Institut für Polymerforschung
auhammer@mpip-mainz.mpg.de

Sebastian Backes
Technische Universität Berlin
sebastian.backes@tu-berlin.de

Daniel Baumgarten
Technische Universität Ilmenau
daniel.baumgarten@tu-ilmenau.de

Philipp Bender
Universität des Saarlandes
p.bender@mx.uni-saarland.de

Valter Böhm
Technische Universität Ilmenau
valter.boehm@tu-ilmenau.de

Helmut Rainer Brand
Universität Bayreuth
brand@uni-bayreuth.de

Norbert Buske
MagneticFluids
n.buske@magneticfluids.de

Thorsten M. Buzug
Universität Luebeck
buzug@imt.uni-luebeck.de

Iwona Cicha
Universitätsklinikum Erlangen
iwona.cicha@uk-erlangen.de

Joachim Clement
Universitätsklinikum Jena
joachim.clement@med.uni-jena.de

Peet Cremer
Heinrich-Heine-Universität Düsseldorf
pcremer@thphy.uni-duesseldorf.de

Sabrina Disch
Universität zu Köln
sabrina.disch@uni-koeln.de

Joe Donaldson
Universität Wien
joe.donaldson@univie.ac.at

Silvio Dutz
Technische Universität Ilmenau
silvio.dutz@tu-ilmenau.de

Alexey Eremin
Otto-von-Guericke-Universität Magdeburg
alexey.eremin@ovgu.de

Dagmar Fischer
Friedrich-Schiller-Universität Jena
dagmar.fischer@uni-jena.de

Ralf Friedrich
HNO-Klinik Erlangen - SEON
ralf.friedrich@uk-erlangen.de

Christine Gräfe
Universitätsklinikum Jena
christine.graefe@med.uni-jena.de

Thomas Gundermann
Technische Universität Dresden
thomas.gundermann@tu-dresden.de

Jens Haueisen
Technische Universität Ilmenau
gabi.hey@tu-ilmenau.de

Dirk Heinrich
Technische Universität Berlin
dhein@physik.tu-berlin.de

Ingrid Hilger
Universitätsklinikum Jena
Ingrid.Hilger@med.uni-jena.de

Shilin Huang
Max-Planck-Institut für Polymerforschung
huangs@mpip-mainz.mpg.de

Sofia Kantorovich
Universität Wien
sofia.kantorovich@univie.ac.at

Markus Kästner
Technische Universität Dresden
markus.kaestner@tu-dresden.de

Tobias Kaufhold
Technische Universität Ilmenau
tobias.kaufhold@tu-ilmenau.de

Santa Kolay
IFW Dresden
s.kolay@ifw-dresden.de

Florian Krämer
Universität des Saarlandes
email@kraemer-florian.de

Maria Krautz
IFW Dresden
m.krautz@ifw-dresden.de

Christian Kuhlmann
Technische Universität Braunschweig
c.kuhlmann@tu-bs.de

Joachim Landers
Universität Duisburg-Essen
joachim.landers@uni-due.de

Julia Linke
Technische Universität Dresden
julia.linke@tu-dresden.de

Gisella Lucero
Technische Universität Ilmenau
gisella-liliana.lucero-lucas@tu-ilmenau.de

Frank Ludwig
Technische Universität Braunschweig, EMG
f.ludwig@tu-bs.de

Stefan Lyer
HNO-Klinik Erlangen, SEON
stefan.lyer@uk-erlangen.de

Nina Matoussevitch
Karlsruher Institut für Technologie
matoussevitch@web.de

Sarah Kristina Metzke
Technische Universität Berlin
sarah_metzke@yahoo.com

Olaf Mollenhauer
TETRA Gesellschaft für Sensorik, Robotik und Automation mbH
olaf.mollenhauer@tetra-ilmenau.de

Robert Müller
Leibniz-Institut für Photonische Technologien
robert.mueller@ipht-jena.de

Annemarie Nack
Universität Rostock
annemarie.nack@uni-rostock.de

Johannes Nowak
Technische Universität Dresden
johannes.nowak@tu-dresden.de

Stefan Odenbach
Technische Universität Dresden
stefan.odenbach@tu-dresden.de

Stavros Peroukidis
Technische Universität Berlin
peroukid@upatras.gr

Nadine Pömpner
Universitätsklinikum Jena
nadine.poempner@med.uni-jena.de

Jana Popp
Thüringisches Institut für Textil- und Kunststoff-Forschung e.V.
jana.popp@tu-ilmenau.de

Sylvain Prévost
Technische Universität Berlin
prevost.sylvain@gmail.com

Pamela Quiroz
Technische Universität Ilmenau
pamela.quiroz-penaranda@tu-ilmenau.de

Patricia Radon
Physikalisch-Technische Bundesanstalt
patricia.radon@ptb.de

Ingo Rehberg
Universität Bayreuth
ingo.rehberg@uni-bayreuth.de

Reinhard Richter
Universität Bayreuth
reinhard.richter@uni-bayreuth.de

Ronny Rüger
Friedrich-Schiller-Universität Jena
ronny.rueger@uni-jena.de

Pedro A. Sánchez
Universität Wien
pedro.sanchez@univie.ac.at

Annette Schmidt
Universität zu Köln
annette.schmidt@uni-koeln.de

Daniel Schmidt
Physikalisch-Technische Bundesanstalt
daniel.schmidt@ptb.de

Johannes Schönke
Max-Planck-Institut für Dynamik und Selbstorganisation
johannes.schoenke@ds.mpg.de

Joerg Schotter
Austrian Institute of Technology
joerg.schotter@ait.ac.at

Mario Schrödner
Thüringisches Institut für Textil- und Kunststoff-Forschung e.V.
schroedner@titk.de

Jörg Schumacher
Technische Universität Ilmenau
joerg.schumacher@tu-ilmenau.de

Malte Schümann
Technische Universität Dresden
malte.schuemann@tu-dresden.de

Martin Silge
Technische Universität Ilmenau
martin.silge@tu-ilmenau.de

Christian Spieler
Technische Universität Dresden
christian.spieler@tu-dresden.de

Uwe Steinhoff
Physikalisch-Technische Bundesanstalt
uwe.steinhoff@ptb.de

Christian Stötzel
Friedrich-Schiller-Universität Jena
01797458624@o2online.de

Thomas Stürzel
Technische Universität Ilmenau
thomas.stuerzel@tu-ilmenau.de

Felix Theska
Technische Universität Ilmenau
felix.theska@tu-ilmenau.de

Anja Theumer
Universitätsklinikum Jena
anja.theumer@med.uni-jena.de

Rainer Tietze
Universitätsklinikum Erlangen
rainer.tietze@uk-erlangen.de

Lutz Trahms
Physikalisch-Technische Bundesanstalt Berlin
lutz.trahms@ptb.de

Andreas Tschöpe
Universität des Saarlandes
antsch@mx.uni-saarland.de

Harald Unterweger
Universitätsklinikum Erlangen
harald.unterweger@uk-erlangen.de

Tatiana Volkova
Technische Universität Ilmenau
tatiana.volkova@tu-ilmenau.de

Joachim Wagner
Universität Rostock
joachim.wagner@uni-rostock.de

Anja Waske
IFW Dresden
a.waske@ifw-dresden.de

Rudolf Weeber
Universität Stuttgart
weeber@icp.uni-stuttgart.de

Andreas Weidner
Technische Universität Ilmenau
andreas.weidner@tu-ilmenau.de

Frank Wiekhorst
Physikalisch-Technische Bundesanstalt
frank.wiekhorst@ptb.de

Marcus Witt
Technische Universität Berlin
m.witt@tu-berlin.de

Sascha Wulff
Capsulution Pharma AG
sashn132ers@hotmail.de

Jan Zaloga
Universitätsklinikum Erlangen
jan.zaloga@uk-erlangen.de

Klaus Zimmermann
Technische Universität Ilmenau
klaus.zimmermann@tu-ilmenau

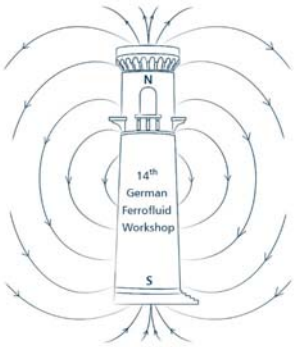
N
14th
German
Ferrofluid
Workshop
S

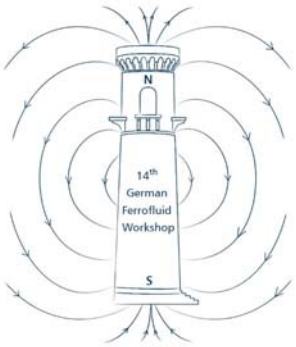
N
14th
German
Ferrofluid
Workshop
S

The 14th German Ferrofluid Workshop, Ilmenau 2014, is sponserded by: